A theoretical and experimental study including design, construction, and test is achieved for a solar-powered continuous flow absorption refrigeration system. The experimental system is tested under Iraqi weather conditions at Babylon province at 32.39N latitudes and 44.39E longitudes. The system consists of a compound parabolic concentrator (CPC), generator, condenser, absorber and evaporator units, storage tank, and set of pumps. The amount of beam solar radiation, diffuse solar radiation, total solar radiation as well as direct solar radiation incident on a fixed, or tilted the surface is calculated during the year and compared with the pyranometer measurements.

Sabah Auda AbdulAmeer, Babylon, Iraq,

978-3-659-76681-7

Dissertation (Ph.D)

Sabah Auda AbdulAmeer
Haroun Abdul-kadhim Shahad

# Experimental and Theoretical Study of (ACS)with Solar Collector

Renewable Energy

LAP LAMBERT Academic Publishing

AbdulAmeer, Shahad

**Sabah Auda AbdulAmeer**
**Haroun Abdul-kadhim Shahad**

# Experimental and Theoretical Study of (ACS)with Solar Collector

Sabah Auda AbdulAmeer
Haroun Abdul-kadhim Shahad

# Experimental and Theoretical Study of (ACS)with Solar Collector

## Renewable Energy

LAP LAMBERT Academic Publishing

**Imprint**
Any brand names and product names mentioned in this book are subject to trademark, brand or patent protection and are trademarks or registered trademarks of their respective holders. The use of brand names, product names, common names, trade names, product descriptions etc. even without a particular marking in this work is in no way to be construed to mean that such names may be regarded as unrestricted in respect of trademark and brand protection legislation and could thus be used by anyone.

Cover image: www.ingimage.com

Publisher:
LAP LAMBERT Academic Publishing
is a trademark of
International Book Market Service Ltd., member of OmniScriptum Publishing Group
17 Meldrum Street, Beau Bassin 71504, Mauritius

Printed at: see last page
**ISBN: 978-3-659-76681-7**

Zugl. / Approved by: Babylon,University of Babylon,Diss.,2018

# Abstract

A theoretical and experimental study including design, construction and test is achieved for a solar-powered continuous flow absorption refrigeration system. The experimental system is tested under Iraqi weather conditions at Babylon province at 32.39° N latitudes and 44.39° E longitudes.

The system consists of a compound parabolic concentrator (CPC), generator, condenser, absorber and evaporator units, storage tank, and set of pumps. The amount of beam solar radiation, diffuse solar radiation, total solar radiation as well as direct solar radiation incident on a fixed, or tilted surface is calculated during the year and compared with the pyranometer measurements.

The maximum computed value of normal direct solar radiation is 894-944 W/$m^2$ in the summer season at time 12:00 pm and the solar global pyranometer measurement is 1031 W/$m^2$. The solar angles are, also calculated such as elevation angle ($\alpha$), sun azimuth angle ($\psi$) and zenith angle($\theta_z$). The maximum elevation angle is 80.99 in 21$^{st}$ June month at 12:00 pm and 34.1° in 21$^{th}$ December at 12:00 pm. The value of Solar Azimuth Angle (deg. CW from N) is the range between 76.285° at 7:00 am and 282.75 ° at 17:00 pm on 21$^{st}$ June, while Azimuth angle in December starts at 117.5° at 7:00 am and ends 242.3 ° at 17:00 pm.

The incident angle ($\theta$) must take the optimum value for maximum irradiation that would be gained from the direct normal solar radiation. The value of the solar incident angle is 24.1°- 32° on 21$^{th}$ of April, May, June, July, and August from 12:00 pm, while it is 42°-67.35° in 21$^{th}$ of September, October November, December, January, February, and March. The increasing in the solar incident angle led to an increasing in the solar radiation losses due to the decreasing in cosine of the incident angle. The (CPC) has an absorber plate with (0.2*2.5m) an aperture area of (0.9*2.5m).

The CPC (reflector) is made from stainless steel to reflect the solar radiation on to absorber unit. A serpentine copper tube is fixed on the absorber plate and coated with selective black paint. The maximum receiver temperature is recorded in August which is 148°C and 120°C with and without glazing. While the reflector temperature is 69°C, and aperture glazing temperature is 43°C.

Experimental results showed that maximum thermal efficiency at 12:00 pm at 21$^{st}$ for each month from (0.48-0.67) when the flow rate is 0.0277 kg/s while the thermal efficiency becomes (0.5-0.69) when the mass flow rate of water is 0.0377 kg/s. The temperature of hot water at mass flow rate 0.0277kg/s is 98°C while at mass flow rate 0.0377kg/s is 94°C.

A theoretical model of the collector is developed and tested under the same weather conditions. Thermal efficiency (0.67-0.73) at the total flow rate (0.0277 kg /s) for a concentration ratio of 4.5 at 12:00 pm at 21$^{st}$ per month. Two pairs of working fluid are tested namely, lithium bromide-water and diethyl ether-ethanol. The system is charged with 16 L lithium bromide solution with 50% concentration in first part of the experimental program. In the second part of the program the system is charged with 16 L of diethyl ether-ethanol with different concentrations (40%, 50%, and 60%). The measured temperatures of the generator are 98$^{o}$C, 70$^{o}$C for lithium bromide-water and diethyl ether-ethanol absorption systems respectively at summer season.

The measured (high and low) pressure of absorption system for (lithium bromide-water and diethyl ether-ethanol) are (7 kPa and 1.45 kPa) and (300 kPa and 37.5 kPa) respectively. The predicted (high and low) pressure of absorption system for (lithium bromide-water and diethyl ether-ethanol) are (7.54 kPa and 0.72 kPa) and (347 kPa and 29.8 kPa) respectively.

The measured (high and low) temperature of absorption system for (lithium bromide-water and diethyl ether-ethanol) are (92$^{o}$C and 67$^{o}$C), respectively. The theoretical and experimental coefficient of performance of the absorption system for two pairs and at different solution concentrations are ((0.31-0.72) for lithium bromide/water while (0.6-.82) for Diethyl Ether/Ethanol).

The steady-state model and dynamic model are analyzed by using linking between Matlab software and EES program. Energy and mass balance achieved on absorption system to predict some parameters such as temperature, pressure, (ECOP) and (COP) to compare it with the measured parameters. The results of the model satisfied the experimental results for temperatures and pressure as well as the coefficient of performance.

# NOMENCLATURES

## Latin Symbols

| Symbol | Description | Units |
|---|---|---|
| $A_a$ | Aperture area | $m^2$ |
| $A_{con}$ | Concentrator area | $m^2$ |
| b | Absorber width | m |
| C | Optical concentration ratio | …. |
| $C_p$ | Specific heat at constant pressure | kJ/kg.K |
| *f* | Focal length | m |
| f | Darcy friction factor | .... |
| f | Fouling factor | $m^2$.K/W |
| $F'$ | Collector efficiency factor | …… |
| $F_R$ | Removal efficiency factor | …… |
| H | Height of concentrator | m |
| h | Convection heat transfer coefficient | $W/m^2$.K |
| $h_{fg}$ | Latent heat of evaporation | kJ/kg |
| $I_{beam}$ | Beam solar radiation | $W/m^2$ |
| $I_{diffuse}$ | Diffuse solar radiation | $W/m^2$ |
| $I_{DN}$ | Direct normal beam radiation | $W/m^2$ |
| $I_T$ | Total solar radiation | $W/m^2$ |
| k | Thermal conductivity | W/m.K |
| *L* | Length | m |
| L | Reflector arc length | m |
| *m* | Mass | kg |
| n | Number of reflection | …. |
| Qu | Useful heat | $W/m^2$ |
| *T* | Temperature | $^oC$, K |
| t | time | sec |
| u | Velocity | m/s |
| $U_L$ | Overall heat loss coefficient | $W/m^2$. K |
| $U_o$ | Overall heat transfer coefficient | $W/m^2$. K |
| W | Aperture width | m |
| w | Hour angle | Degree |

## Greek Symbols

| Symbol | Description | Units |
|---|---|---|
| $\alpha$ | Elevation angle | degree |
| $\alpha_a$ | Absorptivity | …. |
| $\beta$ | Tilt angle | degree |
| $\delta$ | Declination angle | degree |
| $\varepsilon$ | Emissivity | ..... |
| $\eta$ | Efficiency | |
| $\theta_c$ | Half acceptance angle | degree |
| $\theta$ | Incident angel | degree |
| $\gamma$ | Correction factor for diffuse | ….. |
| $\mu$ | Dynamic viscosity | kg/m-s |
| $\rho$ | Density | $kg/m^3$ |
| $\tau_{cpc}$ | Effective transmissivity | ..... |
| $\psi$ | Solar azimuth angle | Degree |
| $\Gamma$ | Mass flow rate of falling film per unit perimeter | kg/s/m |

## Dimensionless Group

| Symbol | Description | Equation |
|---|---|---|
| Gr | Grashof Number | $g\beta q_w d^4/kv^4$ |
| Nu | Nusselt number | h.D/k |
| Pr | Prandtle number | $\mu cp/k$ |
| Ra | Rayliegh number | $Gr*P_r$ |
| Re | Reynolds number | $uD/\upsilon$ |

## Subscripts

| Symbol | Description |
|---|---|
| a | absorber |
| r | receiver |
| C | Condenser |
| Con. | concentrator |
| e | Evaporator |
| g | generator |
| i | Inlet |
| o | Outlet |
| sat | saturated |
| HX | Heat exchanger |
| ss | Strong solution |
| w | water |
| ws | Weak solution |
| DN | Direct Normal irradiance |

## Abbreviations

| | |
|---|---|
| CPC | Compound Parabolic Concentrator |
| AST | Apparent solar time |
| COP | Coefficient of performance |
| ECOP | Exergy Coefficient of performance |
| LMTD | Log mean temperature difference |
| LST | Local solar time |
| am | ante meridiem (before midday) |
| pm | post meridiem ( past midday) |
| HX | Heat exchanger effectiveness |
| Sc | Solar constant |
| EES | Engineering Equation Solver |
| PVC | Panel Photo voltage Cell |

# TABLE OF CONTENTS

# CHAPTER ONE
# INTRODUCTION

## 1.1 Renewable Energy

The renewable energy refers to energy that is produced from a natural resource having the characteristics of inexhaustibility over time and natural renewability. The sources of renewable energy include hydropower, wind, biomass, geothermal, tidal, wave and solar energy **Hassan and Mohamad [1]**. The numerous efforts were undertaken by developed countries to implement different renewable energy technologies. The use of wind energy has dramatically increased over the last few years; for example, the Netherlands and Germany are using wind turbines to the north and west for producing electricity **Lucas and Raoult [2]**, and some Asian countries, such as India and Malaysia, have constructed wind turbine power plants to generate electricity. In Mangal City, there are numerous wind turbines, and in northwestern Iran, mineral materials are used for the production of geothermal energy **Balaras et al. [3]**. In Iceland, seventy percent (70%) of their factories utilize geothermal energy for industrial purposes, **Abu Hamdeh and Al-Muhtaseb. [4]**.The renewable energy is cost-effective and pollution-free compared to fossil fuels **Afshar et al. [5]**. **Figure. (1.1)** shows the energy of the renewable source all over the world. Among all these environmentally friendly and naturally available sources, solar energy stands out on the list of renewables **Mirasgedis et al [6].**

## 1.2 Solar Energy

Solar energy is the flow of energy from the sun. The main forms of solar energy are heat and light. Sunlight and heat are converted and absorbed by the environment in many ways. Some of these transformations lead to renewables flows such as biomass, wind, and waves. Earth receives 174 PW of solar radiation in the upper atmosphere. While, traveling through the atmosphere, 6% of incoming solar radiation (insolation) is reflected,

and 16% is absorbed. Average atmospheric conditions (clouds, dust, pollutants) reduce the insolation rate by 20% by reflection and 3% by absorption.

Convection absorbs solar energy in the atmosphere, evaporation, and condensation of water vapor (latent heat transfer) drive of the wind and the water cycle. Weather conditions not only reduce the amount of solar radiation that reaches the Earth's surface but also affects the quality of the sun before diffusing approximately 20% of incoming light and changing its spectrum. After passing through the Earth's atmosphere, nearly half the insolation in the visible electromagnetic spectrum with other half is mostly in the infrared and ultraviolet spectrum **[7].**

The radiation influx of solar energy, which is called "solar constant, Sc." **Choudhury et al. [8]** calculated a mean solar constant value, which equals to 1368 $W/m^2$. Most countries now accept that solar power has enormous potential because of its cleanliness, low price, and natural availability. For example, it is used commercially in solar energy plants. Sweden has been operating a solar power plant since 2001. In addition, **Turanjanin et al. [9]** described a solar powered solar plant located in the rural areas of Iran. In their study, they also observed solar radiation in Belgrade for a full year and concluded that the maximum radiation occurred from May to September. In recent years, many countries have faced difficulties with the issue of refrigeration systems; especially the demand for air conditioning for both commercial and residential purposes during the hot season is ever-increasing **Kalkan et al. [10]**. Three technologies can be implemented to make use of solar energy 1-Converting solar energy into thermal energy for heating purposes. 2-Converting solar power into electrical energy by using (PVC). 3-Using solar absorption/adsorption system for cooling purposes.

## 1.3 CPC Technology

The abbreviation **CPC** stands for "**C**ompound **P**arabolic **C**oncentrator" and a **CPC** is a type of non-imaging concentrators. Imaging optics form an image of the source on the receiver, a non-imaging concentrator does not form an image of the source, but transfers the radiation from source to receiver over a larger distance. **Winston et al [11].**

The three most important components in a **CPC** are the receiver, the reflector and the cover. High absorptance of the receiver is very important in order to absorb as much solar radiation as possible. As seen in **Figure (1.2)**, a **CPC** consists of two parabolic reflectors. Reflectors for solar concentrators should have the highest reflectance as possible. Its function is to focus beam-solar radiation onto the receiver **Mansi et al [12].**

The incident angle of the sun to the collector surface is constantly changing through the motion of the earth. Therefore, the majority of the suns rays fall obliquely on the collector. Collectors with CPC technology have the great advantage that the rays above of the sun can be very well utilized.

The main use of CPC´s in solar applications is for use in thermal collectors or together with PV cells. In thermal collectors, the use of CPC technology reduces the absorber area relative to the aperture area, and this can reduce the overall heat loss coefficient since the absorber area is reduced **Winston et al. [11]**. On the other hand, the use of CPC in thermal collectors reduces the optical efficiency due to increased reflector losses, and the optimal use of CPC reflectors in thermal collectors is the tradeoff between these two parameters.

### 1.3.1 Collector Configurations

The concentrator uses to increase the flux of the radiation on the receivers. The receivers much smaller than the aperture (the plane opening of the concentrator through which the solar radiation passes) are effective only on direct radiation. The angle of incidence of the beam radiation on

the concentrator is important, and that sun tracking will be postulated for these collectors. A variety of orienting mechanisms have been designed to move focusing collectors so that the incident beam radiation will always be reflected the receiver **Winston et al. [11].**

### 1.3.2 Classification of Optical Concentrators

There are different types of concentrator designs. They are classified into two major optical categories: (I) Imaging optics concentrators. (II) Non-imaging optic concentrators.

The imaging optic concentrators is concerned with the image formed by the optical concentrator on the receiver, so that the receiver must be small enough to attain some homogeneity in the distribution of the formed image (focus). Thus, the imaging optic concentrators have their advantage that they have a high value of concentration **Abdulameer and Shahad [13]**. On the other hand, the non-imaging optics is not concerned with forming an image, and thus the receiver may be large with the homogeneity of the radiation on the receiver, but its concentration is smaller than that of imaging optic concentrators. **Auda and Shahad [14]**

### 1.3.3 Applications of Concentrators

There are several potential fields of application of solar thermal energy in the temperature range of 60°C to 180°C, like heat production for industrial processes in the food, textile, wine and chemical industries, solar cooling and air conditioning, solar drying and seawater desalination, thermal detoxification of drinking water, and small power generation and water pumping through medium temperature Rankine cycle systems.

An overview of the potential of solar industrial process heat in the food industry is presented below **Kalogirou Soteris [15]**.

Worldwide energy consumption for cooling and air-conditioning is rising rapidly and the market potential for solar thermal cooling is very large. Solar energy has the advantage that cooling is generally required when solar radiation is available. This is the main reason for sustained

research into solar cooling devices for at least three decades. These studies include solar energy technologies operating with absorption, adsorption, and desiccant cycles to produce cooling and refrigeration using medium to high-temperature solar technologies (from 80°C to 250°C) However, the market is still very much at an initial stage, with only around 500 solar cooling systems installed globally, and has been largely dominated by Europe so far **David [16].**

## 1.4 The Vapor Absorption Systems

Vapor absorption systems are in the technology class of heat pumps. Heat pumps are machines used to transfer heat from a low-temperature source to a high-temperature sink. This direction of heat flow requires a significant amount of work input into the heat pump as per the second law of thermodynamics. Whereas this work input is accomplished by the supply of electricity to the compressor in the vapor compression heat pump, it is by contrast achieved by the supply of heat in vapor-absorption heat pumps. **Figure (1.3)** is a primary vapor absorption cycle using $H_2O$-LiBr as the working pair in which $H_2O$ is the refrigerant and LiBr the absorbent. The cycle is a single-stage or single-effect type. It can be visualized as a combination of two cycles, i.e., the work producing cycle (red dotted box) and a refrigeration cycle (black dotted box). When the cycle is in operation, a significant amount of heat $Q_g$ is supplied at a temperature $T_g$ whereby $T_g > T_c >= T_a > T_e$. The cycle is then able to cause a cooling effect at a temperature $T_e$ by drawing heat $Q_e$ from the medium being cooled. This, in addition to the heat of condensation of refrigerant and the heat of mixing of refrigerant and absorbent, i.e. $(Q_c + Q_a)$ is rejected to the environment. The work input WP into the pump is the only electrical supply to the cycle and is very small compared to the heat input **Muhumuza and Strachan [17].** The cycle in **Figure (1.3)** can be shown on a T-s diagram in which the work producing cycle is combined with a refrigeration cycle as shown in **Figure (1.4).** It is assumed that the processes in both cycles are reversible.

## 1.5 Solar Absorption Cooling

Solar cooling engages a system where solar energy is used for cooling purposes. Implement solar cooling system can save the Mediterranean countries approximately 50% of their energy costs **Balaras et al. [3]**. Solar cooling has become more important for cooling purposes today due to the use of desiccant gases, such as (lithium chloride) and (lithium bromide), or water instead of harmful Freon gas **Thirugnanasambandam et al. [18]**. Cooling can be achieved through two primary methods. The first is a PV (Photovoltaic) based solar energy system, where solar energy is converted into electrical power and used for cooling much like conventional methods. The second one employs a solar thermal cooling system, where the solar collector directly warms the chillers through assembly tubes instead of using solar electrical energy **Saidur et al. [19]**. An absorption cooling system is a heat-operated device based on two factors, which produce a cooling effect; these are

**One-**A primary liquid that boils at low temperatures

**Two-**A secondary fluid absorbs the primary liquid that has been evaporated in the evaporator

When the system uses a mechanical pump to circulate the absorbent-cooling solution, a small amount of work input will be required. The heat source may be steam or another hot fluid. There are two main types of absorption systems: the aqueous lithium bromide system and the aqua ammonia system. Other absorbent-refrigerant combinations have recently been considered **Dalichaouch [20]**. Solar energy operates the majority of modern absorption refrigeration units currently in use.

### 1.5.1 Cooling and Vapor Absorption

The purpose of cooling is to provide a cooling or chilling effect. This cooling effect is realized through the introduction of an energy sink that is at a temperature lower than the stream, object or space to be cooled. However, a low-temperature energy sink is not always available due to the

geographical limitations, seasonal variation or daily fluctuation in temperature. The differences between refrigeration by vapor compression and vapor absorption are briefly discussed in **Appendix A**

Vapor absorption systems require both thermal and electrical sources of energy that are supplied to the vapor generation and electrical components respectively. However, it is essential to see that thermal energy needs dwarf the electric power requirements of a vapor absorption system. Due to this significant discrepancy between the thermal and electrical requirements, it is not uncommon for the coefficient of performance (COP) of a vapor absorption system to be calculated without the inclusion of the electrical power for pumping requirements and control related components. Concerning the heating stream, the viable temperature ranges for this stream that is fed to the vapor absorption system can, dependent on system configuration, be between 70°C and 250°C. This entire temperature range is not feasible for use in any single type of vapor absorption system but is viable for some different physical configurations. Three of these configurations are referred to as the single, double and triple effect vapor absorption cycles, and the typical temperature of the heating stream as well as the associated COP values for these system configurations can be seen in Table (1.1)**, Srikhirin et al. [21]** and **Labus et al. [22].**

## 1.6 The Aims of the Present Work

The immediate work goals to design, fabricate, and test of an appropriate solar absorption cooling system. Also, model of a solar powered absorption cooling system will be developed for validity and feasibility of the unit in the weather of Iraq. Therefore, this work is an attempt to test a compound parabolic concentrator solar collector (CPC) to reach maximum temperature and pressure in collector loop. Continuous absorption process principle will be used the running of the unit. The generator, condenser, absorber and evaporator components will be constructed. All parts of the fabricated test rig must resist high pressure and

temperature and should be corrosion resistant. The design of solar collector and absorption system has the following features different absorption pairs will be tested to study the system performance namely LiBr-Water and Ethanol-Diethyl ether

**1.** The water refrigerant fluid has high latent heat and zero or above zero evaporation temperature.

**2.** The water fluid and diethyl ethers are zero ozone depletion and zero global warming potential (GWP).

**3.** The location and orientation of any solar unit is an important parameter to gain the maximum radiation and minimum losses.

In the present work, the detailed calculations, and prediction for the orientation direction and solar angles are investigated to optimize location for manual seasonal adjustment during the year. The measurements include the pressure and temperature at different locations of the unit to predict the coefficient of the performance (COP) = cooling capacity obtained at evaporator divided by heat input for the generator + work input for the pump. The work input for the pump is negligible relative to the heat input at the generator. Therefore, the pump work is often neglected for the purposes of analysis. The theoretical is based on energy and mass balance principle as a mathematical model and dynamic model. The validation of the numerical model will be achieved by a comparison with the experimental results.

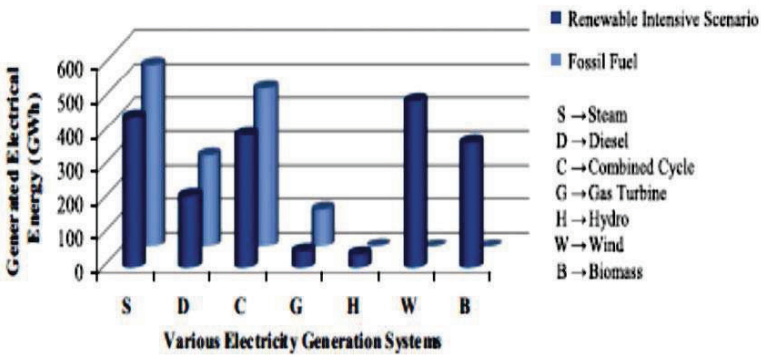


**Figure. (1.1) Electricity generation in Cretein2005 Mirasgedis et al [6].**

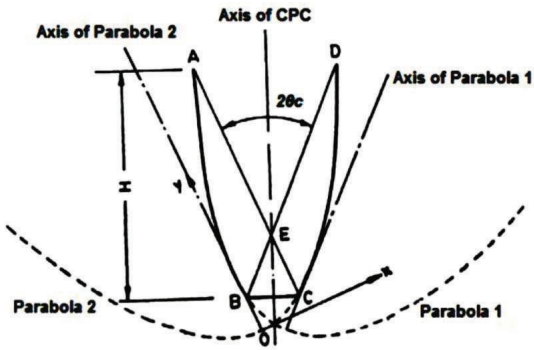


**Figure (1.2): Cross section of a symmetrical non-truncated CPC Winston et al [11].**

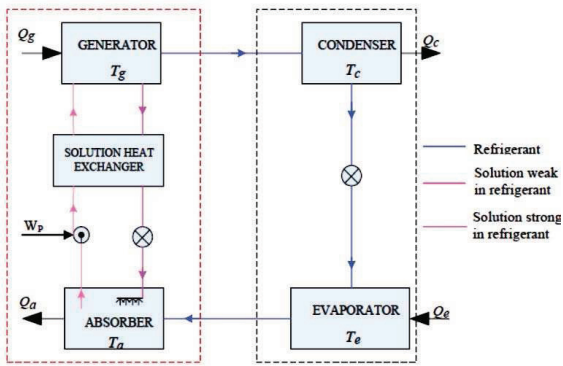


**Figure (1.3): Single vapor $H_2O$-LiBr absorption cycle**

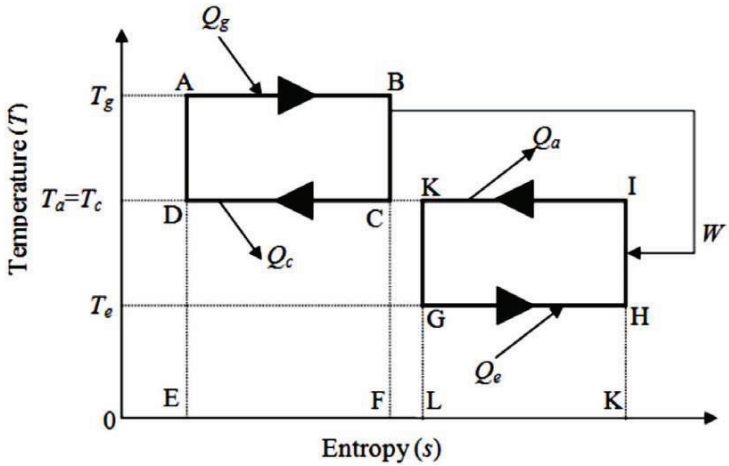


**Figure (1.4): Vapor absorption system Muhumuza and Strachan [17].**

| Configuration | Heating Stream Temperature Range (°C) | COP |
|---|---|---|
| Single Effect | 70 - 150 | 0.5 -0.75 |
| Double Effect | 120 - 170 | 0.8 - 1.2 |
| Triple Effect | 200 -250 | 1.4 - 1.7 |

**Table (1.1) Comparison of vapor absorption COP values Labus et al. [22].**

# CHAPTER TWO
# LITERATURES REVIEW

The goal for this chapter of the thesis is to review and discuss available literatures related to vapor absorption and optical concentrators as well as topics related to it in a manner that is accessible and informative. Other topics will also be discussed in this section which includes the history of vapor absorption, the possible working fluids, and the operation of a vapor absorption cycle.

## 2.1 The Vapor Absorption Studies

The earliest reference to the principle of vapor absorption can be traced to the 1750s when William Cullen used diethyl ether to produce a small quantity of ice **Labus et al. [22]**. In 1810, Sir John Leslie made use of the manner in which sulphuric acid absorbs water vapor to produce ice **Gosney [23].** Machines making use of Leslie's method were implemented to chill wine but required periodic recharging of the sulphuric acid. In 1824, Michael Faraday made use of a combination of silver chloride and ammonia to produce a chilling effect **Marsh and Olivo [24]**. In Leslie's method, sulphuric acid was the absorbent and water was the refrigerant while in Faraday's apparatus silver /chloride was the absorbent and ammonia the refrigerant. Although both of these methods successfully implemented the principle of vapor absorption, more significant developments in vapor absorption were still to come in decades to follow. In 1859, Ferdinand Carré developed an absorption system that made use of a combination of ammonia and water, where ammonia was the refrigerant and water was the absorbent **Gosney [23]**. A significant advantage that this system had at the time of its development is that it could operate continuously to produce refrigeration at low temperatures. The ammonia/water system developed by Carré was used for many years and formed the foundation for future progress in the field of refrigeration **Gosney [23]**. In the early 1920s, Baltzar von Platen and Carl

Munters invented what is referred to as the Platen-Munters absorption system that makes use of water, ammonia, and hydrogen. The purpose behind the inclusion of an additional substance, in this case, hydrogen, was to operate the system at a single pressure and by operating at a single pressure level, notwithstanding slight pressure differences due to changes in height, the electrical pump and pressure reducing components were no longer necessary for the operation of the system. Two attractive aspects of a Platen-Munters system are that it operates silently and does not require an electrical input for a pump. A company called AB Arctic manufactured these systems and in 1925, Electrolux purchased this company **[25]**. By 1936 Electrolux had manufactured its one-millionth absorption refrigerator **Grant [26]**. The silent operation has made this type of refrigeration system attractive for use as a hotel room refrigerator. Caravans, motor-homes, and recreational vehicles typically have no access to electricity, making the utilization of a Platen-Munters system attractive. Another single pressure absorption system is the Einstein Cycle, invented by Einstein and Szilard in the 1920s and patented in 1930 **Einstein and Szilard [27]**. This system made use of butane, water, and ammonia to operate at only pressure. This type of single pressure vapor absorption system was at times referred to as a diffusion absorption system. An absorption system that made use of a solution of water and lithium bromide was introduced in the 1930s **Srikhirin et al. [21].** In this type of system, water was used as the refrigerant and lithium bromide as the absorbent. Like the ammonia/water system, the water/lithium-bromide system can operate continuously. One disadvantage of a water/lithium-bromide system in comparison with the ammonia/water system is that due to water being the refrigerant, the system can only supply refrigeration at temperatures above 0°C.While absorption refrigeration gained popularity in the early 1900s, the technology was overshadowed by the successes and subsequent popularity of vapor compression cycles. Due to the, absorption

technologies were neglected in the west until the 1930s **Jordan and Priester [28]**, when large-scale absorption refrigeration plants were implemented. However, the portion of global sales that originated in the United States (US) decreased significantly from the1970s to 1990. This decline of interest in vapor absorption resulted in the US vapor absorption industry falling behind concerning the technological developments made by the Japanese vapor absorption manufacturers **Garland et al. [29]**.

**Srikhirin et al. [21]** discussed some improvements that have been made in the field of vapor absorption. A few of these improvements include the addition of heat exchangers to the ammonia/water system to improve the performance, the introduction of various refrigeration cycle stages that operate at multiple pressures and the replacement of hydrogen with helium for safety in the Platen-Munters system.

## 2.2 The Fundamentals of a Vapor Absorption Cycle

This section gives the background literature related to the operating principles upon which a vapor absorption refrigeration cycle works. It is essentially a summary of the known information **Srikhirin et al. [21]**, **Marsh and Olivo [24]**, and **King [30]**. Vapor absorption is a process by which a solution can attract and absorb the vapor in its vicinity. Particular solution compositions are required in vapor absorption applications where the solution is composed of a refrigerant and absorbent.

This refrigerant/absorbent solution can be manipulated with a cooling or heating effect to absorb or release refrigerant respectively. The principle of vapor absorption can be applied in some applications, as discussed by **Ziegler [31]**. Two examples will be used to explain the operation of a primary vapor absorption refrigeration cycle. For the first example consider a pair of vessels that are linked together, but initially separated, where the first vessel contains a refrigerant and the second container contains a refrigerant/absorbent solution. Once the vapor space became common

between the two vessels and provided that the conditions be appropriate the refrigerant vapor that is exposed to the liquid solution will be absorbed by it, as seen in **Figure (2.1)**.The effect of this absorption on the solution is that the temperature of the solution will increase, due to the nature of the process, and the mass fraction of the absorbent present in the solution will decrease as the solution contains additional refrigerant.

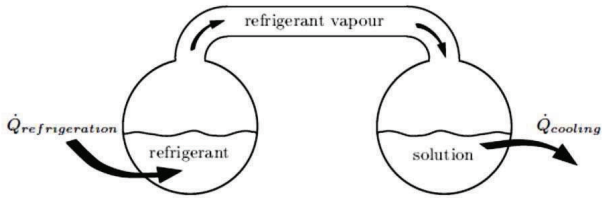


**Figure (2.1): Absorption principle, part one absorption of vapor Dawood [32]**

For the second example consider once again a situation where two vessels are linked together. As in the previous example, one container contains refrigerant, in liquid and vapor form, and the other holds a two-part refrigerant/absorbent solution. However, the difference is that for this example the liquid in the solution vessel is heated and the vapor in the refrigerant vessel is cooled. This configuration can be seen in **Figure (2.2).** Heating the solution will promote the separation of refrigerant vapor from the solution. While this is taking place, the cooling of the vapor in the refrigerant vessel will be provided that the conditions are conducive, because the refrigerant vapor to condense and drip into the refrigerant liquid pool.

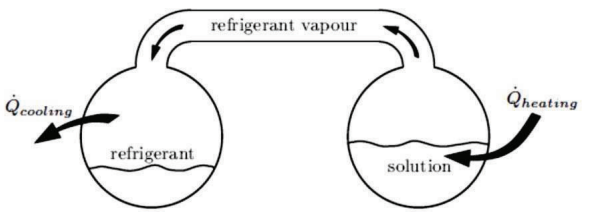


**Figure (2.2): Absorption principle, part two generation of vapor Dawood [32]**

**Figure (2.3)** shows a component configuration that combines two processes with the addition of a pump and two throttling devices, the two previously discussed examples. This component configuration forms the first continuous vapor absorption cycle. While this configuration will function, as it contains the essential components that form a vapor absorption system, there are typically many additional components that are included in an economic vapor absorption cycle. In this configuration, the previously discussed examples for the absorption of vapor and the generation of vapor are operated at two different pressure levels. The high-pressure components will be referred to as the condenser and the generator while the low-pressure components will be referred to as the evaporator and the absorber. Starting from the absorber, the solution is pumped to the generator where it is heated, and a portion of the refrigerant is separated from the solution.

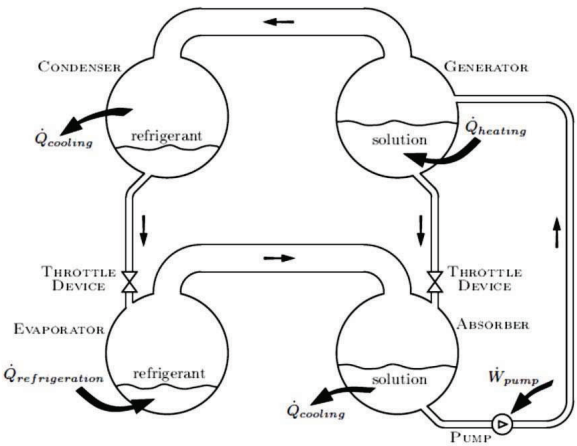


**Figure (2.3): Absorption principle, part three absorption and generation of vapor combined for a complete cycle Dawood [32]**

Two streams leave the generator the first of which is the refrigerant vapor going to the condenser and the second is the solution, now with a higher concentration of absorbent that returns to the absorber. The refrigerant vapor entering the condenser is cooled and condensed, this condensate then passes

through throttling device before entering the evaporator as a stream of low-temperature refrigerant liquid that contains a tiny percentage of vapor. The liquid portion of this refrigerant entering the evaporator is used to provide a refrigeration effect on an external space or stream. The solution leaving the generator also passes through a throttling device before going into the absorber. Once in the absorber, the solution has to be cooled to help facilitate the absorption of the vapor leaving the evaporator and maintain a low temperature. Once the refrigerant has been absorbed into the solution, thereby decreasing the concentration of absorbent, it can once again be pumped up to the generator which will complete the cycle.

**2.3 Solar Absorption Cooling System**

Nowadays, the need for thermal comfort in housing and office buildings generate a sharp increase in energy demand, especially during summertime. Air conditioning systems are mechanical vapor compression types, use high-grade electric power generated in the authority stations using fossil fuels. This situation presents a very serious handicap in isolated areas with the non-interconnected electrical grid. For this reason, renewable energies are excellent alternatives. The Absorption cooling systems are one of the ways to produce air conditioning and refrigeration by using the solar thermal source as driving energy. In the Water-Lithium bromide absorption systems, the solution is first heated in the desorbed (generator), and the obtained superheated water vapor (refrigerant) flows to the condenser where heat is transferred to the environment. The liquid is moved through the expansion valve and enters to the evaporator, where the liquid refrigerant evaporates by absorbing the heat from the refrigerated space. The weak liquid in the absorber absorbs the vapor leaving the evaporator and heat is transferred from the mixture. The enriched refrigerant- the solution is pumped to the pressure level in the generator, where the weak solution returns to the absorber by transferring heat to the strong solution by way of the intercooler

(heat exchanger). Many works were done to evaluate the performance of a solar cooling system working on water-lithium bromide pair, **Sury et al. [33]** and **Darkwa et al. [34]**. **Darkwa et al. [34]** evaluated the performance of a solar-assisted 70 kW single effect LiBr-Water chiller located in Spain and achieved a maximum COP of 0.6.

**Florides et al. [35]** described the performance of a 1.5-ton solar cooling unit. The unit comprises a 14 $m^2$ flat plate solar collector system and five shell and tube heat exchangers. The unit was tested in April and May in Jordan. The maximum value obtained for the actual coefficient of performance was 0.85. **Gomri [36]** studied the global modeling of an absorption system working with $LiBr/H_2O$ powered by solar energy. It satisfied the air-conditioning necessities of a classroom in an educational center in Puerto Lumbreras, Murcia, Spain. The absorption system used a set of solar collectors to meet the thermal needs of the vapor generator.

## 2.4 Design and Performance of Absorption Cooling Systems

The operating principles of absorption refrigeration have been described **[37- 43]** in numerous publications.

**Neely [44]** reviewed the published thermodynamic properties of aqueous solutions of lithium bromide and the data supplied by the major manufacturers of lithium bromide absorption equipment. The data have been reduced to equations for use in computer programs. New equilibrium chart, diagrams and tables were presented.

**Rozenfel'd, and Shmuilov [45]** examined the design refinements of the principal components of large capacity absorption chillers.

Little information was given on diffusivities of concentrated solutions. Most of the data were related to very dilute solutions at about atmospheric pressures.

The effect of pressure on liquid diffusivity has received little attention. If low-pressure diffusion coefficient data can be used in conjunction with a

correction factor to estimate high-pressure coefficients, no method has been proposed to connect diffusion coefficients to vacuum pressures. The conditions prevailing in the aqueous lithium bromide absorption refrigeration system are such that the solution concentration is between 50% and 60%, the operating pressures are relatively high vacuum pressures, and the effect of latent heat is necessary.

Mass transfer in the absorption of water vapor by the aqueous lithium bromide solution is accompanied by a significant release of heat. Mass transfer coefficients are determined experimentally **Gosh and Gupta [46].**

**Nakotyakov et al**. **[47, 48]** obtained approximate solutions of the problem of the non-isothermal absorption of water vapor by films of aqueous lithium bromide. Dimensionless correlations were provided for heat and mass transfer coefficients in simple models.

**Chang [49] and Sheridan [50]** using commercial machines without modifications for the solar experiments performed the pioneer work on the operation of the aqueous lithium bromide cycles with solar energy.

A significant amount of work on research and development of solar-operated chillers has been carried out. Discussion on this subject is available in some publications **Kettle borough [51], Dickinson and Cheremisinoff [52], and Chinnappa [53].** The most common systems used for absorption refrigeration are the solar supplemented systems in which solar energy supplies part of the required thermal load, the rest being furnished by an auxiliary source. However, an aqueous lithium bromide absorption refrigeration system working with solar energy alone has been analyzed and designed **Gosh and Gupta [46].** The thermodynamic analysis of this system has been made using the first law based-mass and energy balance equations. Simulation methods of solar absorption cooling have been used extensively in the study of performance and design of the components of the physical

system, and several sophisticated programs were published **Klein et al [54], Winn et al. [55]**, **Holm stead [56] and [57]**. The TRNSYS and SIMSHAC programs are more useful as analysis tools than design tools because they are expensive to use and require expertise in programming. The transient system simulation program or TRNSYS and the simulation program for solar heating and cooling of buildings or SIMSHAC both consist of some subroutines for modeling system components. The user can simulate the performance of a particular system using an executive program that calls the subroutines according to the description of the system. User-written subroutines can be added to the programs. The main objective in the development of the TRNSYS and SIMSHAC programs was to develop a dynamic point design performance analysis of simple models as well as of more complex models.

**Winn et al [55]** discussed and compared several computer simulation programs. The f-chart programmer **lein and Beckman [58]**, based on correlations to the TRNSYS results, was developed and served as a design tool that is easy and inexpensive to use. It consists primarily of a set of three algebraic correlations that can be used to predict the monthly solar fraction of standard system configurations for space and domestic hot water heating with daily storage. The f-chart correlation for domestic hot-water systems is applicable only when the inlet water temperature is between 5°C and 20°C, and the upper hot water temperature is between 50°C and 70°C.

The phi bar-f chart method, a generalized version of the f-chart procedure, presented by **Duffie and Beckman [59]** is typically applicable to solar absorption systems. No restrictions are imposed on the temperature limits of the heated fluid in the solar thermal system. The phi bar-f chart method was developed for solar systems with the auxiliary heater in parallel.

A modified empirical correlation similar to that of the original phi bar-f chart method was proposed for systems with the auxiliary heater in series.

Both approaches assume a constant and uniform thermal load over each day and for at least a month. The phi bar-f chart method also requires that the thermal energy supplied to the load must be above a minimum temperature. It yields values of monthly solar fractions for one set of variable parameters specifying the size of the system components. The calculation should be repeated for each of the twelve months and also for different sets of parameters.

Comparisons with TRNSYS program **Klein et al. [54]** have shown that the prediction accuracy of the phi bar-f chart method is excellent on an annual basis and is satisfactory for most months.

The phi bar-f chart procedure requires little climatic data. It is simple and convenient to use but its application is limited to closed-loop system configuration and to the range of parameters for which it has been constructed.

**El sayed et al. [60]** proposed a simple technique to develop a simulation program for a solar-operated lithium bromide-water cooling unit.

**Anand et al. [61]** investigated the modeling of the dynamic performance and the transient behavior during start-up and shutdown of a water-cooled aqueous lithium bromide chiller.

**Wilbur and Mitchell [62]** compared theoretically single-stage, lithium bromide-water absorption cooling system heated from flat-plate solar collector to an ammonia-water system, and the lithium bromide system was preferred. It was shown that it required smaller cooling towers than the conventional one. **Li and Sumathy [63-64]** experimentally studied a solar-powered absorption air conditioning system of lithium bromide-water solution as the refrigerant fluid. Their experimental results showed that using a partitioned hot-water storage tank is necessary to enhance the reliability of the system and achieve a continuous process operation. **Florides et al. [65]** numerically studied a solar absorption cooling system with TRNSYS

simulation program for the weather conditions of Nicosia, Cyprus. A system optimization was carried out in order to select the appropriate type of collector, the optimum size of the storage tank, collector slope and area under the two most favorable thermostats setting of the auxiliary boiler. The final optimized system consisted of a 15 $m^2$ trough parabolic solar collector tilted by $30^o$ from the horizontal and a 0.6$m^3$ hot water storage tank. **Atmaca and Yigit [66]** developed a modular computer program for a solar-powered single-stage absorption cooling system using the lithium bromide-water solution as their working refrigerant. They examined various cycle configurations and solar energy parameters at Antalya, Turkey. The effects of hot water inlet temperatures on the coefficient of performance (COP) and the surface area of the absorption cooling components were studied. The minimum allowable hot water inlet temperatures or reference temperature effects on the coefficient of performance were examined as part of their research. Their results showed that the increment of reference temperature decreases the absorber and solution heat exchanger surface area, and increases the system COP, while the size of the other components remains unchanged. **Atmaca and Yigit [66]** showed that evacuated, selective surface solar collector is the best option for the effective operation of their solar-power absorption cooling system. Their results showed that solar power absorption cooling system requires a high performance collector. **Florides et al. [67]** presented a method to evaluate the characteristics and performance of a single stage LiBr-water absorption machine. The heat and mass transfer equations including the appropriate equations of the working fluid properties were employed in a computer program as part of their research. The sensitivity analysis results showed that the greater difference between inlet and outlet concentrations of the LiBr-water solution at the absorber will reduce the mass flow rate. **Florides et al. [67]** determined the cost for a domestic size absorber cooler, and concluded that despite the high price of

the LiBr–water absorption cooling system in comparison with an electrical chiller of similar capacity, the absorption system remained favorable due to the use of renewable energy sources and waste heat, whereas the electric chiller uses electrical power that is produced from fossil fuels and has harmful effects on the environment. **Assilzadeh et al. [68]** studied a solar absorption cooling system that has been designed for Malaysia climate and similar tropical regions using TRNSYS numerical simulations. They used evacuated tube solar collector for energy input to the absorption cooling system and Lithium bromide-water mixture as the working fluid. They proved that evacuated tube solar collector provides high cooling performance at high temperature due to its high efficiency under this weather condition. The results showed that the cooling capacity of the system is large during periods of high solar radiation energy. The authors suggested a 0.8 $m^3$ hot water storage tank in order to increase the reliability of the system and to achieve continuous operation for a 3.5 kW (1 refrigeration ton) system consists of 35 $m^2$ evacuated tubes solar collector sloped by 20$^o$ as an optimum system at Malaysia's weather condition. **Mittal et al. [69]** performed numerical simulations of a solar-powered single-stage absorption cooling system using a flat-plate solar collector and LiBr-water solution. A modular computer program was developed for the absorption system to simulate various cycle configurations with the help of weather data of Bahal village, district of Bhiwani on the western fringe of Haryana, India. The authors studied the effects of hot-water inlet temperatures on the coefficient of performance and the surface area of the absorption cooling component. Their results showed that the increment of the hot-water inlet temperature decreases the absorber and solution heat exchanger surface area, while the sizes of the other components remain the same. **Sayegh [70]** investigated an absorption cooling system powered with solar energy with the use of a thermal storage tank, auxiliary heater and flat plate solar collector for the

weather conditions of Aleppo, Syria. Lithium bromide-water is used as a working fluid for the system. A computational program is prepared to investigate the effect of varying the generator temperature between 80 to 100$^{o}$C, and the evaporator temperature between 5-15$^{o}$C on the coefficient of performance (COP) and solar useful heat gain of the absorption cooling system. Their results show that higher COP values are obtained by the increment of the generator temperature and the temperature drop of the evaporator. In addition, **Sayegh [70]** recommend the installation of seasonal thermal storage tank to decrease the AC load differences, which must be supplied by an auxiliary heater. **Balghouthi et al. [71]** assessed the feasibility of solar-powered absorption cooling system under Tunisian weather conditions. They used TRNSYS and EES software is including a meteorological year data file containing the climatic condition of Tunis, the capital of Tunisia, in order to select size of the different components of the solar system to be installed. Their system was optimized for a typical building of 150m$^2$ and water lithium bromide absorption chiller with a capacity of 11 kW, and 30m$^2$ flat plate solar collector area tilted by 35$^{o}$ from the horizontal and a 0.8m$^3$ hot-water storage tank. The simulation results showed that solar-power absorption cooling system is suitable under Tunisian conditions. The potential of integrated solar absorption cooling and heating systems for building applications were evaluated by **Mateus** and **Oliveira [72].**

### 2.4.1 Additives for Enhancing an Absorption System

The operation of an absorption system can be improved through the inclusion of small quantities of additional chemicals or additives. Various additives can be included in both water/lithium-bromide and ammonia/water systems for corrosion mitigation as well as the improvement of the heat and mass transfer characteristics. In addition to this, there are also additives that can be included in water/lithium-bromide systems in order to reduce the

likelihood of encountering crystallization of the solution. **Herold et al. [73]** discussed the reduction of corrosion rates in water/lithium- bromide cycles through the inclusion of some possible lithium salts such as lithium chromate, lithium molybdate, and lithium nitrate and lithium hydroxide.

**Agrawal, Hindin [74], Mansfeld, and Sun [75]** discussed the use of some possible additives for corrosion mitigation in ammonia/water vapor absorption cycles including sodium silicate, sodium chromate, sodium dichromate and cerium chloride. **Kulankara and Herold [76]** presented a paper on the manner in which additives can reduce the surface tension of water/lithium-bromide solutions. This reduction in surface tension improves the vapor absorption process and is referred to as the vapor surfactant theory.

**Möller and Knoche [77]** investigated the effect of the inclusion of a surfactant on surface tension and mass transfer of ammonia/water.

The likelihood of crystallization can be reduced by the inclusion of heat and mass transfer additives as these additives will improve system performance thereby avoiding undesired operating conditions.

**Wang and Chua [78]** discussed the use of cesium chloride as a means through which the crystallization characteristics can be improved.

**Wang et al. [79]** discussed the research and development of chemical additives, such as pyro phosphoric acid, as well as absorbent combinations such as lithium bromide and potassium format

### 2.5 Absorption System Studies

A vast amount of research has been performed towards the goal of understanding and improving the operation of vapor absorption technologies. This section discusses a selection of research from the field of vapor absorption that is of relevance to the project at hand.

#### 2.5.1 Simulation Focused Studies

The simulation of vapor absorption systems has been approached through steady state solutions, transient solutions as well as dynamic responses. These various approaches for simulations can provide insight into different

aspects of a vapor absorption system. In the case of a steady state simulation the resulting effect of altering operating conditions can be assessed. Transient simulations can be used to investigate the startup behavior and control of a vapor absorption system. Lastly, dynamic simulations can be used to examine the response that the simulation would have to an external disturbance. In addition to the different types of simulations, the literature that was found regarding the simulation of a vapor absorption system showed that a number of different software packages could be used for the steady state simulations. This section will continue to present a number of articles that document the simulation of vapor absorption systems. **Herold et al. [73]** showed how the Engineering Equation Solver (EES) could be used to simultaneously solve the heat transfer rates, heat transfer surface areas and cycle temperatures from supplied external cycle temperature in combination with the values for the overall heat transfer coefficient values in a steady state scenario. EES is also used in an extension of this example to maximize the refrigeration potential that can be obtained from the cycle specifications. **Grossman and Zaltash [80]** discussed the development and usage of the **AB**sorption **SIM**ulation program (ABSIM).

This simulation program was made for the sole purpose of steady state simulation of vapor absorption cycles and makes use of a graphical user interface that allows a user to configure the cycle components that are to be simulated. ABSIM is capable of simulating expansive vapor absorption cycles and includes the property functions for a number of vapor absorption working pairs. **Somers et al. [81]** made use of ASPEN Plus (**A**utomatic **S**ystem for **P**erformance **E**valuation of the **N**etwork) a chemical process package, to simulate both a single effect and a double effect vapor absorption cycle.

The results of this simulation compared well with the results obtained from a similar simulation that was performed with EES. **Bakhtiari et al. [82]**

developed a model to assess the steady state behavior of a single effect water/lithium-bromide cycle. The external streams were used as the user specifications for this steady state simulation. Results from an experimental apparatus were used for verification of the model and the results were favorable. **Kohlenbach and Ziegler [83]** combined the use of a steady state solution with a transient model in order to examine the dynamic response of a water/lithium-bromide cycle. A finite difference Jacobian method was used to solve the equations via MATLAB.

**Kim and Park [84]** implemented differential equations in order to describe the transient behavior and dynamic response of a single effect ammonia/water absorption chiller. A Runge-Kutta Merson technique was used to simultaneously solve the equations. The behavior of the simulated cycle during transient start-up as well as during a dynamic response to a change in the fuel supply of the cycle was discussed.

### 2.5.2 Experimental Investigations

The majority of articles that were found during the literature survey that referred to experimental investigations regarding the operation of a vapor absorption system. A further distinction could be made in order to categorize these articles according to similar directions of investigation. The investigation of the steady state performance of a vapor absorption system when the operating conditions were altered and the performance of a solar-driven absorption system.

**Asdrubali and Grignaffini [85]** made use of a Yazaki water/lithium bromide absorption chiller as part of an experimental plant. This experimental plant was used to assess the steady state performance of the absorption chiller at various operating conditions. **Agyenim et al. [86]** discussed the use of a small capacity commercial absorption system as the cooling apparatus for a solar powered refrigeration installation. This installation made use of a solar collector to indirectly fuel the absorption

chiller. A cold water tank was used as a buffer between the chiller outlet stream and the fan coil unit that was used for the space cooling. The operation and performance of the installation was further discussed with the conclusion being made that as far as electrical consumption is concerned the system as a whole compare well with mechanical air conditioning systems. **Kalogirou et al. [87]** discussed the design and construction of a 1 kW water/lithium-bromide vapor absorption chiller. The desired cycle output was used as the design point around which the heat exchangers of the apparatus were sized according to the heat exchanger requirements and the available theory for the heat transfer coefficients. Heat exchangers for the generator, absorber and evaporator were submerged in their respective liquid sections. In addition to this, the length of the generator heat exchanger was varied in order to determine viable lengths of piping for different inlet temperatures.

**2.6 Contribution of the Present Work**

It is clear from the previews cited survey that the most researcher focused on design and fabrication of solar absorption system. They used the evacuated tube and flat plate receiver. Also, the most researchers used LiBr-$H_2O$ and $NH_3$-$H_2O$ as working pairs.

In the present study, a serpentine copper tube fixed on a flat plate will be used on the solar receiver, which is not adapted perversely.

New working fluid pair will be used which Diethyl ether-ethanol $(C_2H_5)_2O$-$C_2H_5OH$.The performance of the absorption system will be studied using the two modification and compared with previews studies.

# CHAPTER THREE

# EXPERIMENTAL WORK

The design and fabrication of a **C**ompound **P**arabolic **C**oncentrator (CPC) cooling system to convert incoming solar radiation into thermal energy is illustrated in this chapter. It consists of (CPC) a detailed explanation of how the individual components of the system work. The design, working, and testing of the system is carried out at Babylon University, Babylon province, Iraq. Lithium bromide-water and ethanol-diethyl ether are chosen and tested as working pairs.

## 3.1 Solar Absorption Cooling System Components

The size and dimension of the different components of the system depends on the cooling capacity required (cooling load) and the thermodynamics properties of the working fluid pair. Components of the solar absorption cooling system are:

1. Compound Parabolic Concentrator (CPC)
2. Generator
3. Condenser
4. Evaporator
5. Absorber
6. Heat Exchanger
7. Capillary Tube
8. Storage Tank
9. Pumps

The goal of this work is to obtain a cooling effect by using the solar absorption system. A continuous solar absorption cooling system is designed and fabricated to achieve this purpose. The operation and performance of the system is tested using two pairs of working fluid, namely Water-LiBr and Diethyl ether-ethanol. Water and Diethyl ether are the refrigerant and LiBr

and ethanol are the sorbent. The solar absorption cooling system consists of many components, which are explained in the following subsection. The components of a solar absorption cooling system are shown schematically in **Fig. (3.1)**

### 3.1.1 Compound Parabolic Concentrator (CPC)

A CPC receives solar radiation during a during day hours without the need for tracking the sun, besides, it is capable to collect some diffuse radiation. The basic design concept of the **C**ompound **P**arabolic **C**oncentrator (CPC) is shown in **Fig. (3.2).** It has a large acceptance angle and requires only intermittent tracking. **[88]** Noted the usefulness of the geometry of the CPC for solar energy collection**.**

#### 3.1.1.1 CPC Geometry

The design procedures and the calculation of the features of the inverter segments are explained below. The two dimensional compound, parabolic collector consists of the main three parts

1- Reflector: Two reflectors in the shape of parabolas are made of stainless steel mirror image sheets.

2-Reciever: It is the component of the compound parabolic collector, which receives the reflected radiation from the reflectors and absorbs the heat. It is made of the serpentine copper tube fixed on a flat plat MS (16 gauge). The copper tube and the flat plate are black coated (selective surface).

3- Aperture cover: The aperture and the side openings of the collector are closed with a toughened glass of 4 mm thickness. A two dimensional CPC as shown in **Fig. (3.2)** consist of two distinct parabolic segments placed in such a manner that the focus of one parabola fells on the profile of the other. The slope of the parabolic reflector surface at the entrance aperture is parallel to the CPC optical axis. Thus, the solar rays entering the concentrator at the maximum acceptance angle are reflected tangentially to the surface of the

absorber. For the simple geometry, it can be shown in **Fig. (3.2)** **[89]**:

$$\tan\theta_C = \frac{W + b}{2H} \tag{3.1}$$

Where **W** is the aperture width, **b** is the receiver width and **H** the height of concentrator of CPC:

$$\frac{W}{b} = CR = \frac{1}{\sin\theta_C} \tag{3.2}$$

Using above equations

$$H = \frac{W(1 + \sin\theta_C)}{2\tan\theta_C} \tag{3.3}$$

The area of the concentrator or reflector, $\mathbf{A_{con}}$, is related to the area of the apertures $\mathbf{A_a}$, as **[89]**

$$A_{con} = A_a(1 + \sin\theta_C)\left[\frac{\cos\theta_C}{\sin^2\theta_C} + \ln\left\{\frac{(1 + \sin\theta_C)(1 + \cos\theta_C)}{\sin\theta_C\left\{\cos\theta_C + (2 + 2\sin\theta_C)^{\frac{1}{2}}\right\}}\right\} - \frac{\sqrt{2}\cos\theta_C}{(1 + \sin\theta_C)^{\frac{3}{2}}}\right] \tag{3.4}$$

The average number of reflection, n**,** passing through a CPC inside is acceptance angle is given a **[89]**

$$n = \frac{1}{2\sin\theta_C}\left(\frac{A_{con}}{A_a}\right) - \frac{(1+2\sin\theta_C)(1-\sin\theta_C)}{2\sin^2\theta_C} \tag{3.5}$$

The effective transmissivity of CPC **($\tau_{cpc}$)**, accounting for the reflection loss inside the CPC depends on the specular reflectivity, (ρ), of CPC wall and the average number of reflections, **n,** and is given as **[89]:**

$$\tau_{CPC} = \rho^{n} \tag{3.6}$$

The XY coordinate system is shown in **Fig. (3.2)**, at the vertex of parabola right, it is easy to show that the equation for parabola right is

$$Y = \frac{X^2}{2b(1+\sin\theta_C)} \tag{3.7}$$

The focal length is shown below

$$\text{focal length} = \frac{b}{2}(1+\sin\theta_C) \tag{3.8}$$

The coordinates of the endpoints of the part CD are as follows:

Point C:

$$x = b\cos\theta_C \tag{3.9}$$

$$y = \frac{b}{2}(1-\sin\theta_C) \tag{3.10}$$

Point D

$$x = (b+W)\cos\theta_C \tag{3.11}$$

$$y = \frac{b}{2}(1-\sin\theta_C)\left(1+\frac{1}{\sin\theta_C}\right)^2 \tag{3.12}$$

The ratio of height to the aperture of (CPC) is given by:

$$\frac{H}{W} = \frac{1}{2}\left(1+\frac{1}{\sin\theta_C}\right)\cos\theta_C = \frac{1}{2}(1+C)\left(1-\frac{1}{C^2}\right)^{\frac{1}{2}} \tag{3.13}$$

The surface area of the concentration is obtained by integrating parabolic arc. The ratio of the surface area of the concentrator to the area of the aperture is calculated using the following reflector arc length (L) expression: **[89]**

$$L = b(1+\sin\theta_C)\left[\frac{\cos\theta_C}{\sin^2\theta_C} + \ln\left\{\frac{(1+\sin\theta_C)(1+\cos\theta_C)}{\sin\theta_C\left\{\cos\theta_C + (2+2\sin\theta_C)^{\frac{1}{2}}\right\}}\right\} - \frac{\sqrt{2}\cos\theta_C}{(1+\sin\theta_C)^{\frac{3}{2}}}\right] \quad (3.14)$$

Aperture Area = W* $L_{axial}$

Absorber Area = b * $L_{axial}$

The reflector is constructed for half an acceptance angle of ($\theta_C$=11.55°). This angle covers the declination of the sun from summer to winter solstices **[89]**. The distance between AB and CD is the full height of the CPC, as in **Fig (3.2).** The receiver BC is flat plate type. Part of the solar radiation falls on the receiver directly while the other reaches the receiver via the reflector. The second law of thermodynamics implies that for maximum possible concentration the concentration ratio should be given regarding half acceptance angle **[89]**.

It can be set $\frac{w}{b} = (\frac{1}{\sin\theta_C})$ and that this concentration ratio is the maximum possible for the acceptance angle $2\theta_C$ **[89].**

The coordinates of points C and D are used to draw a curve, which represents the right hand parabola. The mirror image gives the left hand parabola, those results in two-dimensional compound parabolic concentrator. The upper part of the CPC can be removed (truncated) with little loss in performance see **Fig. (3.3)** and **Fig. (3.4).**

The CPC is usually truncated by about $\left(\frac{2}{3}\right)$ of its height to prevent interception of solar radiation in the upper part of the reflector. The cost of the truncated CPC is reduced without affecting its performance, with only a little loss in CR (Concentration Ratio). Also, truncation reduces the shadowing effect. The modified CR is given by:

$$\text{CR} = \frac{\text{Aperture width after truncation}}{\text{Width of the absorber}} \quad (3.15)$$

Truncation is finished by drawing a flat line over the reflector at chose stature ($\frac{2}{3}$ of as curtained tallness). The truncation does not affect the acceptance angle. The benefit of this sort of CPC is that it does not require a consistent following when installed in the east-west direction. When concentration ratio is (2 to 10) small tilt adjustment times is required throughout the year. From the above equations the dimensions of the CPC before and after truncation as given below.

The focal length of the CPC is 12 cm; also, the Arc length of the reflector is 105 cm. The number of reflection is 0.86.The reflectivity of the reflector is 0.92 and $\tau_{CPC} = 0.93$. The collector capacity is equal the average of minimum heat collection in the winter season at 21st December from 9:00 am to 15:00 pm is equal 8.38 MJ/m$^2$ per day. The required energy for heating 15 kg of water at 25ºC to 100ºC

$$\text{Q}_{\text{for heating water}} = \dot{\text{m}} * \text{cp} * \Delta\text{T} \quad (3.16)$$

$$\text{cp} = 4.2 \frac{\text{kJ}}{\text{kg °C}}$$

$$\Delta\text{T} = 75\ °\text{C}$$

$$\text{Q}_{\text{for heating water}} = 4.725 \frac{\text{MJ}}{\text{day}}$$

$$\text{Receiver area} = \frac{4.725}{8.38} = 0.56\text{m}^2$$

Therefore, the receiver area for the CPC assumed to be the width of (0.2m) and length (2.5m). From the above information, the length of the serpentine copper tube is 10 m. The required area of the serpentine copper tube fixed on the flat plate absorber is 0.8977m$^2$ .The diameter of the tube is 28.575 mm and the number of passes equals four. The aperture glass cover has high transitivity (0.92) so it transmits most radiation on to the reflector and the absorber plate surface. Both the reflector surfaces reflect the

radiation to the receiver surface, which has an absorptivity of (0.92) as indicated by the manufacturer. The flat plate and the serpentine tube are coated black color to increase the absorptivity as shown in **Fig. (3.5)** and **Fig. (3.6).** the figures also, show the serpentine tube is fixed on flat plate with positions of thermocouples.

**Table (3.1) Dimensions of CPC**

| Dimensions of CPC | Before Truncated | After Truncated |
|---|---|---|
| Height of CPC | 294cm | 98 cm |
| Receiver width | 20 cm is selected | 20 cm |
| Aperture width | 100 cm | 90 cm |
| Axial length | 250 cm | 250 cm |
| Concentration Ratio | 5 is selected | 4.5 |

### 3.1.1.2 CPC Construction

The reflector shape is drawn on a large size paper for full scale. Two stainless steel sheets of the specified dimensions are used. The reflector according to the calculated dimension in section (3.1.1.1) surfaces. Welding technique is used to fix the absorber plate with reflector.

The aperture area keeps constant, the top distance between the two reflectors is held constant by riveting these mirrors to an individual frame. A serpentine copper tube of 28.575 mm diameter is fixed on the mild steel flat plate receiver. A 4 mm glass sheet closes the aperture opening. The collector is constructed so that it can be tilted by the required angle in opposite directions see **Figs. (3.7, 3.8, 3.9, 3.10).**

## 3.2 Absorption System Design

The thermodynamic design of water-lithium bromide absorption cooling system assumes the steady-state operating conditions based on the first law. System cooling capacity is assumed (0.526 kW). Rates of heat added to or rejected from the system are found from equations of mass and energy

balances; Heat transfer areas are determined from appropriate correlations of heat transfer coefficients.

The lower condenser and absorber temperatures increase cycle efficiency; they should be chosen as low as possible However, in practice, they are more or less fixed by the cooling water available. In this study, a condenser temperature of 40°C and an absorber temperature of 34°C are selected.

The low temperature in the evaporator is designed at 4°C to satisfy both practical requirements and needs of higher second law efficiency Nevertheless, in this design of a laboratory model, an evaporator temperature of 4°C is selected.

This is due to two reasons. The first is that operation at very low evaporator temperatures implies relatively high vacuum working pressures that need rigid standards of vacuum integrity to be maintained. The second reason is that for an evaporator temperature of 4°C and for an absorber temperature of 34°C, the weak solution concentration in the absorber will be typical of concentrations used in small lithium bromide-water cooling units.

The saturation pressure of refrigerant, water vapor at 4°C is equal to 0.81 kPa. Assuming a small pressure difference of 0.133 kPa between evaporator and absorber, the pressure in the absorber will be 0.676 kPa. The saturation pressure of water vapor at 40°C in the condenser is 7.346 kPa. Assuming a small pressure difference of 3% between condenser and generator the pressure in the generator becomes equal to 7.567 kPa. The generator temperature is selected, a value of the solution heat exchanger effectiveness HX is necessary.

By definition of HX, higher values mean lower exit temperatures have cooled strong solution in the heat exchanger. However, under some conditions of operation the solution is so strong, leaving the generator that it would crystallize if cooled below a certain temperature. Besides, assumed

values of heat, exchanger effectiveness should result in acceptable temperature approaches for the cold-end of the solution heat exchanger. Assume a heat exchanger effectiveness of 36% in this design. A generator temperature of 80°C can be selected to give higher values of efficiency and to be sufficiently higher than the minimum generator temperature of 74.9°C for better operation. By using the mass and energy balance, principle the rates of heat transfer have been evaluated as in **Fig. (3.1)**

$$\dot{Q}_G = \dot{m}_7 h_7 + \dot{m}_1 h_1 - \dot{m}_6 h_6 \quad (3.17)$$

$$\dot{m}_1 = \dot{m}_2 = \dot{m}_3 = \dot{m}_{SS} \quad (3.18)$$

$$\dot{m}_4 = \dot{m}_5 = \dot{m}_6 = \dot{m}_{WS} \quad (3.19)$$

$$\dot{m}_7 = \dot{m}_8 = \dot{m}_9 = m_W \quad (3.20)$$

$$\dot{Q}_C = \dot{m}_r(h_7 - h_8) \quad (3.21)$$

$$\dot{Q}_a = \dot{m}_3 h_3 + \dot{m}_{10} h_{10} - \dot{m}_4 h_4 \quad (3.22)$$

Where

$h_1$=h ($T_1$, Xss) strong solution

$h_6$=h ($T_6$, $X_{ws}$) weak solution

$h_7$=h ($T_7$) superheated vapor

$T_G$=$T_1$=$T_7$

$h_8$=h ($T_8$) Saturated water liquid

$T_C$=$T_8$

$h_8$=$h_9$ throttling process

$h_9$=h ($T_9$) Saturated water liquid

$h_{10}$=h ($T_{10}$) Saturated vapor

$T_E$=$T_{10}$

$h_3$=$h_2$ throttling process

$h_2$=h ($T_2$, $X_{ss}$)

$h_3$=h ($T_3$, $X_{ss}$)

$h_4$=h ($T_4$, $X_{ws}$) saturated weak solution

$T_a$=$T_4$

Thus

$\dot{Q}_g = 0.932$ kW

$\dot{Q}_a = 0.902$ kW

$\dot{Q}_C = 0.555$ kW

With mass flow rate of refrigerant $\dot{m}_r$=0.0002kg/s, mass flow rate of strong solution $\dot{m}_{ss}$=0.0052kg/s and mass flow rate of weak solution $\dot{m}_{ws}$=0.00541kg/s. The exit temperature of the weak solution in heat exchanger is found equal to 49.4°C.The heat transfer rate in the heat exchanger is 0.17kWatt". The work input to the system in the pump is small and neglected in the calculation of COP and efficiency. However, in practice, it is usually estimated to size the driving motor

$$\dot{W}_P = \frac{\Delta P * \dot{\upsilon}}{\eta_p} \qquad \text{Watt} \qquad (3.23)$$

Where

$\dot{\upsilon}$ is the volume rate of flow in $m^3/s$,

$\Delta P$ the pump pressures difference in Pascal.

$\eta_p$ the pump efficiency

The work input calculated by EES software is ($\dot{W}_P$=0.000022kW)

**3.2.1 Design of Generator**

The generator unit of absorption cooling system is usually of the submerged type where the tubes carrying the hot water fluid are immersed in the cycle working solution. A generator of shell and coiled is designed in which hot water flows inside the tubes and solution is distributed over the tubes is shown in **Figs. (3.11, 3.12)**

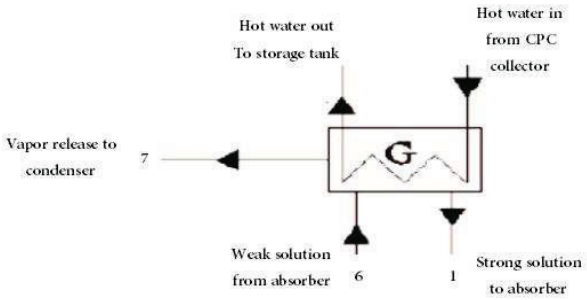


| **Input and output data to the generator** | | | | | | | | | | |
|---|---|---|---|---|---|---|---|---|---|---|
| $\dot{Q}_g$ kW | $\dot{m}_{ss}$ kg/s | $\dot{m}_{ws}$ kg/s | $T_{hot,i}$ °C | $T_{hot,o}$ °C | $T_{ss}$ °C | $T_{Ws}$ °C | $X_{ss}$ % | $X_{ws}$ % | $T_g$ °C | $\bar{T}$ °C |
| 0.932 | 0.0052 | 0.00541 | 90 | 85 | 80 | 49.4 | 58 | 55.8 | 80 | 87.5 |
| Properties of hot water at 87.5°C **[90]** | | | | | Properties of Libr-Water solution at 80°C and 58.2% **[38]** | | | | | |
| $\rho_w$ kg/m³ | $\mu_w$ kg/m.s | $k_w$ W/m.K | $Cp_w$ kJ/kg.K | $h_{fg}$ kJ/kg | $\rho_{ss}$ kg/m³ | $\mu_{ss}$ kg/m.s | $k_{ss}$ W/m.K **[91]** | $Cp_{ss}$ kJ/kg.K | | |
| 963.614 | 0.0003238 | 0.669 | 4.201 | 2289 | 1649.911 | 0.0024 | 0.4866 | 1.9728 | | |

$$\mathrm{Pr_w} = \frac{\mu_w \mathrm{Cp_w}}{\mathrm{k_w}} = 2.03 \qquad (3.24)$$

The inner heat transfer coefficient ($h_i$) for the hot water flow on the inside of the tubes is evaluated first. The hot water mass flow rate inside tubes is

$$\dot{m}_r = \frac{\dot{Q}_g}{\Delta T_w \mathrm{Cp_w}} = 0.0443 \frac{\mathrm{kg}}{\mathrm{s}} \qquad (3.25)$$

So Reynolds number is evaluated as

$$\mathrm{Re} = \frac{4\dot{m}_r}{\mu_w \pi \mathrm{D_i}} = 12841.542 \qquad (3.26)$$

Where $D_i$ the inside diameter of tubes. 15 mm nominal diameter tubes are used with following dimensions inside diameter $D_i$=13.562 mm, outside diameter $D_o$=14.962 mm and thickness 0.7 mm. Since the flow is turbulent, the Nusselt number for fluids flowing inside tubes is **[91]**

$$Nu = 0.023Re^{0.8}Pr^{n} \quad (3.27)$$

Where n =0.4 for heating and n=0.3 for cooling .

N=0.4

$$Nu = 55.064$$

And

$$Nu = \frac{D_i h_i}{k_w} \quad (3.28)$$

$$h_i = 2719.63 \frac{W}{m^{2}°C}$$

The outside heat transfer coefficient $h_o$ is calculated from a correlation **[92]** developed for predicting heat transfer by combined boiling and evaporation of falling liquid films on horizontal tubes. The average heat transfer coefficient over the tube circumferential length L is

$$h_o = h_b + h_d \frac{L_d}{L} + h_c \left(1 - \frac{L_d}{L}\right) \quad (3.29)$$

Where

$h_b$ is the nucleate boiling heat transfer,

$h_d$ the average heat transfer coefficient in the thermal developing region where the fluid is being superheated

$h_c$ the convective heat transfer coefficient due to evaporation of liquid films at the vapor-liquid interface

$L_d$ the thermal developing length .

$h_d$ is given by

$$h_d = \frac{3}{8} CP \frac{\Gamma}{L_d} \quad (3.30)$$

Where

$$\Gamma = \frac{\dot{m}}{2L_{tube}} \quad (3.31)$$

$$L_d = \frac{\Gamma^{\frac{4}{3}}}{4\pi\rho\alpha}\left(\frac{3\mu}{g\rho^2}\right)^{\frac{1}{2}} \quad (3.32)$$

α is the thermal diffusivity

$h_c$ is foundas follows

1-Laminer flow

$$h_c = 0.821\left(\frac{\upsilon^2}{k^3 g}\right)^{-0.33}\left(\frac{4\Gamma}{\mu}\right)^{-0.22} \quad (3.33)$$

2-Turbulent flow

$$h_c = 0.0038\left(\frac{\mu^2}{k^3 g}\right)^{0.33}\left(\frac{4 * \Gamma}{\mu}\right)^{0.4}\left(\frac{\upsilon}{\alpha}\right)^{0.65} \quad (3.34)$$

ν is the kinematic viscosity. Therefore, equation (3.29) is rewritten as

$$h_o = h_d \frac{L_d}{L} + h_c\left(1 - \frac{L_d}{L}\right) \quad (3.35)$$

Tube length of 0.30 m.

$$\Gamma = \frac{\dot{m}_{ss}}{2L_{tube}} = 8.667 * 10^{-3}\,\frac{kg}{ms}$$

$$\alpha_{ss} = \frac{k_{ss}}{\rho_{ss} cp_{ss}} = 1.495 * 10^{-7}\,\frac{m^2}{s} \quad (3.36)$$

$L_d$ =9.43*10$^{-6}$ m

$h_d$ =679879.1816 W/m$^2$ °C

The point of transition from equation (3.33) to (3.34) in calculating $h_c$ **[92]**

$$\left(\frac{4\Gamma}{\mu}\right)_{tr} = 5800\left(\frac{\nu}{\alpha}\right)^{-1.06} = 520.034$$

In this design,

$$\left(\frac{4\Gamma}{\mu}\right) = 14.445$$

So the correlation for the laminar case equation (3.33), may be used to give

$h_c$ =3669.848 W/m$^2$ °C

The external heat transfer coefficient can be evaluated from equation (3.35).

$h_o$ =3691.103 W/m$^2$.°C

The overall heat transfer coefficient $U_o$ depend on the outside area of the tubes is **[38]**

$$U_o = \left[\left(\frac{D_o}{D_i h_i}\right) + \left(\frac{D_o}{D_i}\right) f_o + \left(\frac{1}{h_o}\right) + \left(\frac{D_o}{2k} ln\left(\frac{D_o}{D_i}\right)\right)\right]^{-1} \quad (3.37)$$

Where

$f$ is the fouling factor for the hot water side at 52°C equal 0.0002 m$^2$*K/W **[93]**

k the thermal conductivity of copper tubes. For copper tubes k=390 W/m°C **[93]**

$$U_o = 1112.267 \frac{W}{m^{2\circ}C}$$

The logarithmic mean temperature difference LMTD is

$$LMTD = \frac{(T_g - T_{hot,o}) - (T_g - T_{hot,i})}{\ln\left(\frac{T_g - T_{hot,o}}{T_g - T_{hot,i}}\right)} = 7.213 \quad (3.38)$$

$$Q_g = U_o A \ LMTD \quad (3.39)$$

A=0.116m$^2$

$A = \pi D_o L$

Number of turns=6

L=2.9 m

### 3.2.2 Design of Condenser

The design of condenser unit is shell and coil, where water vapor is condensing inside the coil tube and cooling water at the outside

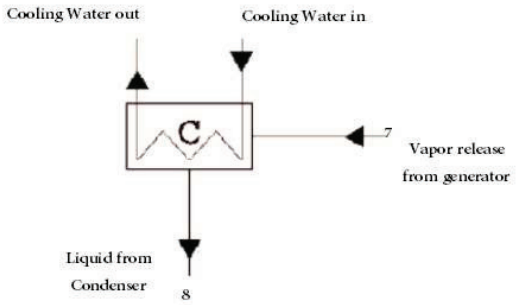


| Input And Output In Condenser | | | | | | Properties Of Cooling Water At 32.5°**[90]** | | | |
|---|---|---|---|---|---|---|---|---|---|
| $\dot{Q}_c$ kW | $\dot{m}_r$ kg/s | $T_{cw,i}$ °C | $T_{cw,o}$ °C | $T_c$ °C | $\bar{T}$ °C | $\rho_w$ kg/m$^3$ | $\mu_w$ kg/m.s | $k_w$ W/m.K | $Cp_w$ kJ/kg.K |
| 0.555 | 0.0002 | 30 | 35 | 39.9 | 32.5 | 995.024 | 0.7566E-03 | 0.6205 | 4.183 |

$$\mathrm{Pr_w} = \frac{\mu_w \mathrm{Cp_w}}{\mathrm{k_w}} = 5.1$$

Outside heat transfer coefficient is calculated in the case of natural convection on the cylindrical surface **[94]**

$$\left(\frac{\mathrm{h_o d_o}}{\mathrm{k}}\right)^{\frac{1}{2}} = 0.6 + 0.387\left[\frac{\mathrm{GrPr}}{\left(1+\left(\frac{0.559}{\mathrm{Pr}}\right)^{\frac{9}{16}}\right)^{\frac{16}{9}}}\right]^{\frac{1}{6}} \quad (3.40)$$

$$\mathrm{Gr} = \frac{\mathrm{g\beta(T_w - T_\infty)d_o^3}}{\left(\frac{\mu}{\rho}\right)^2} \quad (3.41)$$

Assume the $\mathrm{T_w} = 38°\mathrm{C}$ and $\mathrm{T_\infty} = 32.5°\mathrm{C}$

$$\mathrm{T_f} = \frac{\mathrm{T_w} + \mathrm{T_\infty}}{2} = 35.25°\mathrm{C}$$

$$\beta = \frac{1}{T_f + 273} = 3.2441 * 10^{-3}\ K^{-1} \quad (3.42)$$

$$Gr = 1014596.148$$

$$Ra = GrPr = 5174440.353$$

$$h_o = 1174.2056 \frac{W}{m^{2}°C}$$

The Inside heat transfer coefficient is

$$h_i = 0.725 \left[\frac{\rho_l g h_{fg} k^3 (\rho_l - \rho_v)}{\mu d_i \Delta T}\right]^{\frac{1}{4}} \quad (3.43)$$

**Table (3.2) properties of water at 39.9°C**

| $\rho_l$ kg/m³ | $\mu$ kg/m.s | $k$ W/m.K | $Cp$ kJ/kg.K | $\rho_v$ kg/m³ |
|---|---|---|---|---|
| 992.063 | 0.654E-03 | 0.629 | 4.181 | 0.05124 |

$$\Delta T = T_C - T_w = 40 - 38 = 2°C$$

$$h_i = 3082.443\ \frac{W}{m^2 * °C}$$

$$U_o = 698.297 \frac{W}{m^2 * °C}$$

$$LMTD = 7.213$$

$$Q_c = U_o\ A\ LMTD$$

Number of turns=5

L=2.76 m

### 3.2.3 Design of Evaporator

A shell and coil evaporator is used

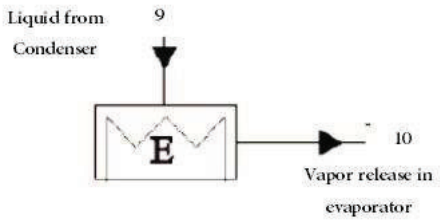


The cooling load $Q_e$=0.526kW

Refrigerant mass flow rate =0.0002 kg/s

Inner diameter=0.01356 m

Outer diameter=0.01496 m

Temperature of evaporator=4°C at 0.81kPa evaporator pressure

Water temperature=45°C

The properties of saturated water at film temperature

The temperature inters to the evaporator =4°C

The temperature leaves the evaporator =30°C

The properties at film temperature

Dynamic viscosity $\mu$=1.003E-03 kg/m.s

Vapor density $\rho_v$ =0.0173 kg/m$^3$

Liquid density $\rho_L$ =998 kg/m$^3$

Latent heat of vaporization $h_{fg}$=2454 kJ/kg

Acceleration g=9.81 m/s$^2$

Prandtl number Pr=7.0

Thermal conductivity k=0.598 W/m$^{2.}$ K

From the above information the inner heat transfer coefficient

$$h_i = 0.725\left[\frac{\rho_l g h_{fg} k^3(\rho_l - \rho_v)}{\mu d_i \Delta T}\right]^{\frac{1}{4}} = \frac{1429.046W}{m^2K} \qquad (3.44)$$

For outer heat transfer coefficient

$$\left(\frac{h_o * d_o}{k}\right)^{\frac{1}{2}} = 0.6 + 0.387\left[\frac{GrPr}{\left(1+\left(\frac{0.559}{Pr}\right)^{\frac{9}{16}}\right)^{\frac{16}{9}}}\right]^{\frac{1}{6}} \quad (3.45)$$

$$Gr = \frac{g\beta\Delta T d_o^3}{\left(\frac{\mu}{\rho}\right)^2}$$

Assume the $T_{intial} = 45°C$ and $T_{final} = 5°C$

The properties at the film temperature

Dynamic viscosity $\mu$=0.891E-03 kg/m. s

Vapor density $\rho_v$ =0.0231 kg/m$^3$

Liquid density $\rho_L$ =997 kg/m$^3$

Latent heat of vaporization $h_{fg}$=2442 kJ/kg

Acceleration g=9.81 m/s$^2$

Prandtl number Pr=6.14

Thermal conductivity k=0.607 W/m$^2$K

$Gr = 333000.56$

Rayleigh Number Ra=Pr*Gr=2044623.43

$h_o$ =946.21 W/m$^2$ .K

$$U_o = 488\frac{W}{m^2°C}$$

$LMTD = 9.1$

$Q_e = U_o\ A\ LMTD$

Number of turns=6

L=3 m

### 3.2.4 Design of Absorber

The absorber unit is shell and coil. The falling film type is used the solution flows through the tubes and the cooling water inside pipes

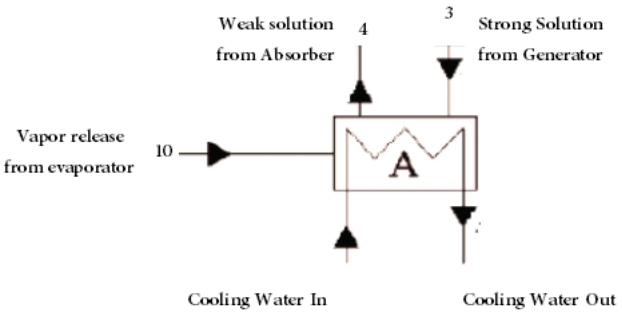


| **Input And Output In Absorber** | | | | | | | | | | |
|---|---|---|---|---|---|---|---|---|---|---|
| $\dot{Q}_a$ kW | $\dot{m}_{ss}$ kg/s | $\dot{m}_{ws}$ kg/s | $T_{cw,i}$ °C | $T_{cw,o}$ °C | $T_{ss}$ °C | $T_{Ws}$ °C | $X_{ss}$ % | $X_{ws}$ % | $T_a$ °C | $\bar{T}$ °C |
| 0.902 | 0.0052 | 0.00541 | 30 | 32 | 63.4 | 34 | 58.2 | 55.8 | 34 | 31 |
| Properties of Cooling Water At $\bar{T}$ =31°C | | | | | Properties of Solution At $\bar{T}$ =48.7°C And $\bar{X}$ =57% | | | | | |
| $\rho_w$ kg/m³ | $\mu_w$ kg/m.s | $k_w$ W/m.K | $Cp_w$ kJ/kg.K | $P_r$ | $\rho_{ss}$ kg/m³ | $\mu_{ss}$ kg/m.s | $k_{ss}$ W/m.K **[125]** | $Cp_{ss}$ kJ/kg.K | | |
| 996.015 | 0.0007806 | 0.61858 | 4.183 | 5.278 | 1648.31 | 0.0035 | 0.4619 | 2.0043 | | |

The mass flow rate of cooling water is

$$\dot{m}_{cw} = \frac{\dot{Q}_a}{cp\Delta T} = \frac{902}{2 * 4183} = 0.1078 \frac{kg}{s}$$

$$A_{cross-section} = 1.44 * 10^{-4}\ m^2$$

$$V = 0.75 \frac{m}{s}$$

$$\mathrm{Re} = 12964.1$$

$$\mathrm{Nu} = 0.023\mathrm{Re}^{0.8}\mathrm{Pr}^{0.4}$$

$$\mathrm{Nu} = 87.27$$

$$h_i = 3980.021\frac{W}{m^2K}$$

The outside heat transfer coefficient is evaluated from the following conditions **[38]**

for $\frac{4\Gamma}{\mu} < 2100$

$$h_o = 0.5\left[\frac{k^2\rho^{\frac{4}{3}}cpg^{\frac{2}{3}}}{\frac{\pi d_o}{2}\mu^{\frac{1}{3}}}\right]^{\frac{1}{3}}\left[\frac{\mu}{\mu_{wall}}\right]^{\frac{1}{4}}\left[\frac{4\Gamma}{\mu}\right]^{\frac{1}{9}} \quad (3.46)$$

With all properties evaluated at mean bulk temperature except $\mu_{wall}$ at the wall temperature

for $\frac{4\Gamma}{\mu} > 2100$

$$h_o = 0.01\left[\frac{k^3\rho^2 g}{\mu^2}\right]^{\frac{1}{3}}\left[\frac{\mu cp}{k}\right]^{\frac{1}{3}}\left[\frac{4\Gamma}{\mu}\right]^{\frac{1}{3}} \quad (3.47)$$

In this design

$$\Gamma = \frac{\dot{m}}{2L_{tube}} = 8.666 * 10^{-3}\frac{kg}{m.s}$$

And

$$\frac{4\Gamma}{\mu} = 9.904 < 2100$$

Assume $T_w$ =32°C

$$\mu_{wall} = 0.0048\frac{kg}{m\,s}$$

$$h_o = 1302.186\frac{W}{m^2\,K}$$

$$U_o = 788.92\,\frac{W}{m^2\,K}$$

$\text{LMTD} = 13.29$

$Q_a = U_o \, A \, \text{LMTD}$

Number of turns=4.5

L= 2 m

### 3.2.5 Solution Heat Exchanger Design

For small capacity lithium bromide-water cooling units, solution heat exchanger is usually formed of strictly double pipe of copper. Such a heat exchanger is designed in this section with a hot strong solution in inner space and cold, weak solution in outer space.

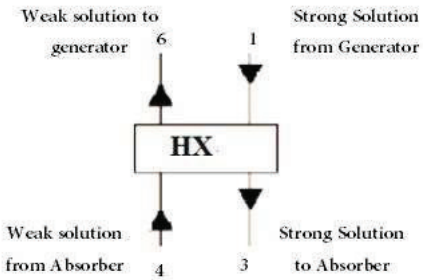

| Input And Output In Heat Exchanger | | | | | | | | | | |
|---|---|---|---|---|---|---|---|---|---|---|
| $\dot{Q}_{HX}$ kW | $\dot{m}_{ss}$ kg/s | $\dot{m}_{ws}$ kg/s | $T_{ss,i}$ °C | $T_{ss,e}$ °C | $T_{Ws,i}$ °C | $T_{ws,o}$ °C | $X_{ss}$ % | $X_{ws}$ % | $\bar{T}_{ss}$ °C | $\bar{T}_{ws}$ °C |
| 0.17 | 0.0052 | 0.00541 | 80 | 63.4 | 34 | 49.9 | 58.2 | 55.8 | 71.7 | 41.7 |
| Properties Of Strong Solution At 71.7°C **[38]** | | | | Properties at $\bar{T}_{Ws} = 41.7$°C And $X_{Ws} = 55.8\%$ | | | | | | |
| $\rho_{ss}$ kg/m³ | $\mu_{ss}$ kg/m.s | $k_{ss}$ W/m.K **[125]** | $Cp_{ss}$ kJ/kg.K | $\rho_{ws}$ kg/m³ | $\mu_{ws}$ kg/m.s | $k_{ws}$ W/m.K **[125]** | $Cp_{ws}$ kJ/kg.K | | | |
| 1655.4 | 0.0027 | 0.4784 | 1.9728 | 1630.8 | 0.0036 | 0.4595 | 2.0361 | | | |

The inside and outside heat transfer coefficients are evaluated. The outer and inner diameter are (28.575, 15.875) mm respectively.

$\mathrm{Re} = 154.467$

For laminar flow Nu=3.66

$h_i = 110.295 \frac{W}{m^2 K}$

$\mathrm{Re} = 150.66$

For laminar flow Nu=3.66 and $h_o$=132.42 W/m² *°C

$$U_o = 66.815 \frac{W}{m^2 K}$$

$$\mathrm{LMTD} = \frac{(T_{ss,i} - T_{ws,e}) - (T_{ss,e} - T_{ws,i})}{\ln\left(\frac{T_{ss,i} - T_{ws,e}}{T_{ss,e} - T_{ws,i}}\right)} = 29.99$$

$Q = U_o A \, \mathrm{LMTD}$

$A = 0.0848 \ m^2$

$L = 0.944 m$

### 3.2.6. The Storage Tank

The storage tank is used to store the hot water in the collector loop. The diameter and length of the storage tank are 35 cm, 50 cm respectively. The capacity of the storage tank is 48 liters. Hot water exits from CPC collector loop and enters to the generator and return to the storage tank. The container is sealed. The tank is fabricated from steel, which can withstand a pressure up to (4 bar) and corrosion resistance.

### 3.2.7. Capillary Tube

A capillary tube is used between the condenser outlet and evaporator inlet of a domestic refrigerator working as a simple expansion device in the vapor compression cooling system (VCRS) to reduce the pressure and the corresponding saturation temperature of refrigerant from condenser condition to the evaporator condition. The liquid refrigerant from the condenser flows through the capillary tube, causes an expansion following the flash vaporization due to the drop of internal energy and hence enthalpy, also with the change of other state properties **[94].** The basic theory of capillary design depends on fluid friction Darcy pressure drop relationship. Higher-pressure drop can be achieved with decreasing diameter and increasing length of the capillary tube. Since the capillary tube is available in only specified diameters, so their actual design emphasizes on the determination of lengths for a given cooling effect see in **Fig. (3.13).**

#### 3.2.7.1. Calculations Procedure

The capillary tube length design calculations

Follows the following steps **[94].** See **Fig (3.14).**

1-The expansion of the liquid refrigerant is assumed to be isenthalpic along the line ks- k'-1-2-3 on P-h- chart and the momentum gain is due to the pressure drop of the enthalpy. Here ks is the point of sub cooling of condensate from the outlet point k of the condenser. So at any $i^{th}$ node enthalpy = h**i** = $h_{k'}$. (Neglect sub cooled).

2-At nodes (1, 2, and 3) quality of the refrigerant is wet vapor, hence: -

$$x_i = \frac{\left(h_{k'} - h_{fi}\right)}{h_{fg}} \tag{3.48}$$

Where $h_{fi}$ = saturated liquid enthalpy, $h_{fg}$ = Enthalpy of vaporization.

3-Specific volume of the refrigerant at these nodes is

$$v_i = v_{fi} + x_i\left(v_{gi} - v_{fi}\right) \tag{3.49}$$

4-Mass flow rate of refrigerant in the capillary is

$$\dot{m} = \frac{\dot{Q}_r}{h_{g3} - h_3} \tag{3.50}$$

Where $\dot{Q}_r$ = cooling effect in kW

5-Mass flux: -

$$G = \frac{4\dot{m}}{\pi d^2}$$

6- Flow velocity of the refrigerant

$$u_i = G v_i$$

**3.2.7.2. Design Procedures**

One important parameter of the capillary design is the determination of mass flow rate through a suitable available diameter of the capillary tube for some specific cooling effect as determined by using equation (3.52). Here using water as refrigerant in 1 mm diameter capillary tube for 0.526 kW cooling capacity and is explained below.

1. The whole temperature and pressure drops from the capillary tube inlet to the outlet is divided into suitable elementary steps of intermediate nodes, such as 40°C, 30°C, 20°C, 10°C, 6°C at their corresponding saturation pressures as shown in **Table (3.3).**

2. First the expansion is assumed isenthalpic with simultaneous frictional pressure drop, flash vaporization, change of refrigerant properties and momentum gain without considering the internal mechanism. The expansion

is shown by process line ks-k'-1-2-3 on P-h plot **Fig. (3.14)** and the saturation pressure, refrigerant properties like liquid enthalpy, phase change enthalpy and specific volume are noted from the property table corresponding to the nodal saturation temperatures.

3. Some parameters will be determined first on the isenthalpic line using above relations.

At $T_C$=40ºC

Saturated pressure=7.3851 kPa

$h_3 = h_{fk}$ =167.53 kJ/kg

$h_{g3}$ =2512 kJ/kg at $T_3$ =6°C

$\dot{Q}_r$ =0.526 kW

d=1mm

$$\dot{m} = 2.0117 * 10^{-4} \frac{kg}{s}$$

G=254.647 kg/ ($m^2$ s)

**3.2.7.3. Friction Factor**

The analysis of frictional pressure drop of the refrigerant as it flows through the pipe or capillary tube incorporates friction factor "f" that can be determined on several theoretical and experimental relations. For capillary tube design of refrigerators, a standard relation frequently used is the Blasius (1911) relation as following.

$$F = \frac{0.32}{Re^{\frac{1}{4}}} \tag{3.51}$$

Where

$$Re = \frac{\rho u d}{\mu} \tag{3.52}$$

At different nodes the refrigerant properties vary in the vapor-liquid mixture and the coefficient of dynamic viscosity is determined according to the relation:

$$\mu_i = \mu_{fi} + x_i(\mu_{gi} - \mu_{fi}) \tag{3.53}$$

### 3.2.7.4. Capillary Tube Length

Actually, the wall friction of the capillary tube causes the gradual pressure drop of the refrigerant flow, which results in the drop of corresponding saturation temperature, internal energy and enthalpy but increase of specific volume and kinetic energy with adiabatic flash vaporization using its own enthalpy. The pressure drop and its corresponding increase in specific volume keep the term (PV) nearly constant **[94].** In addition, the actual pressure drop has no share contribution towards the gain of kinetic energy through phase change and hence the momentum gains pressure drop share (ΔPm) is zero. Therefore, the actual total pressure drop (ΔP) is nearly equals to the frictional pressure drop, $\Delta P_F$. Now taking $\Delta P_F = \Delta P_i$, as actual drop for every elementary length of the capillary tube between two adjacent temperature nodes, the following relations (Darcy–**Weisbach equation 1845)** are used to determine the required length of capillary tube:

$$\Delta P_F = \frac{\rho F \Delta L u^2}{2d} \tag{3.54}$$

The total length is about 1.257 m made of copper material. **Table (3.3)** shows all **values for capillary tube calculations.**

**Table (3.3). Values of different parameters for capillary tube design**

| Node | $T_c$(C) | P(pa) | $h_f$(kJ/kg) | $h_{fg}$(kJ/kg) | x | v(m³/kg) | u(m/s) | Δp(pa) | (kg/m.s) $\mu$ | Re | f | ΔL |
|---|---|---|---|---|---|---|---|---|---|---|---|---|
| ks | 40 | 7400 | 167.53 | subcooled | 0 | 0.001008 | 0.258 | ------ | $0.65*10^{-3}$ | ---- | --- | --- |
| K· | 30 | 4300 | 125.74 | 2430 | 0 | 0.001004 | 0.257 | 3100 | $0.798*10^{-3}$ | 320.8 | 0.075 | 1.256 |
| 1 | 20 | 2330 | 83.9 | 2454 | 0.017 | 0.982 | 251.1 | 1970 | $0.985*10^{-3}$ | 259.6 | 0.079 | $0.776*10^{-3}$ |
| 2 | 10 | 1230 | 42 | 2477 | 0.033 | 3.5 | 895.6 | 1100 | $1.26*10^{-3}$ | 203.1 | 0.084 | $0.114*10^{-3}$ |
| 3 | 6 | 930 | 25 | 2486 | 0.04 | 5.2 | 1330.57 | 300 | $1.45*10^{-3}$ | 175.5 | 0.087 | $0.02027*10^{-3}$ |
| Total length of capillary tube | | | | | | | | | | | | 1.257 m |

### 3.3. Pumps

In the solar absorption, cooling system divided into two loops. The first loop is called collector loop while the second is absorption-cooling loop. A hot water pump is used to circulate hot water in the collector loop. The hot water pump is set up on the storage tank. The flow meter is linked to the hot water pump. The second loop used a chemical pump. The chemical pump is used to circulate the weak solution and pumped to the generator passing through the heat exchanger . The cooling water is circulated between condenser and absorber unit by another water pump (25 W, 1000L/h, and maximum suction 1.8m)

### 3.4 Temperature Instrument

Temperature is the most important property in this experimental work. The measured temperatures at different locations are used to determine the state of refrigerant at any point in the cycle along with the corresponding pressure. Thermocouples are used to measure the temperature of receiver surface, the solution water vapor outlet, condenser outlet, environment, and evaporator. The thermocouples are of k type. The diameter of the wires is 0.4mm, with rubber insulation them . Each wire is skinned from both ends, and one end was spot-welded to form a 0.6mm diameter round head while the other end is connected to the recording device. A data logger is used to record the temperatures measured by the thermocouples. The data logger is programmed to record the temperature every 10 minutes. The type of the used data logger is (BTM-4208SD card-12 channels) as shown in **Fig. (3.15)** . A small hole is drilled at each location, and the thermocouple junction is inserted through this hole. These holes are then covered by a thermal silicon rubber to prevent any movement.

### 3.5. Pressure Measurements

Two pressure transducer sensors are used to measure the pressure inside generator and absorber.

### 3.5.1 Pressure Interface

An interface is used to connect the pressure sensor and the personal computer. The interface transforms the voltage (analog) signal from the sensors into a digital signal that can be read by a software program (DaLi08). A universal data logger (UDL100) is used. It has high accuracy and resolution, sampling period (750ms) and channels isolation voltage (400 volts). The pressure measurement is also essential for safety. Analogue pressure gauges and pressure transmitter (QP-83A) are used for this purpose. The purpose of the analogue indicator is for calibration and easy monitoring. The pressure transmitter transfers the reading to pressure data logger. The pressure is measured at two locations, the generator, and absorber. The range of pressure transmitter reading is (0-10) bar. This transmitter is high temperature and corrosion resistant.

## 3.6. Experimental Procedures for Absorption Test

The detailed steps of test procedures are as follows:

1. All the 10 points thermocouples, as well as 3 points for water coolant and environment temperature (Type K), are connected by plugs and connectors to the data logger.

2. All the two pressure transmitter (model: QP-83A) are connected to the data logger (as well as pressure gauges).

3. The whole system is evacuated (generator, absorber, condenser, evaporator, heat exchanger and piping system) by a vacuum pump to the minimum possible vacuum pressure (0.75-0.82 bar).

4. The lithium bromide-water solution (16 liters) for the experiment is charged to the unit by the charging valve. The solution concentration is 50% lithium bromide the concentration of the other pair, diethyl ether-ethanol, is varied in steps as (60%- 40%, 50%, 40%-60%) see **Fig. (3.16)**

5. The experiment starts at morning at a sunshine time. The axis of the orientation is into horizontal, and the angles of tracking are setting (tilt angle β, module azimuth angle γ). The tilt angle is measured in summer and winter season (43°in winter and 21°in summer). The module azimuth angle also measured in winter and summer season (90° in winter and 75° in summer) measured from North.

6- During the day, the water-lithium bromide solution in the generator is heated by the hot water from the collector until reach is saturation temperature when water starts evaporate. Due to the increase of the temperature and consequently of the pressure of the solution in the generator, the water vapor flows to the condenser, where cooling water condenses it, and then it is passed to the evaporator through the capillary tube where the cooling effect occurs . To know the amount of mass of evaporated water (refrigerant) two-sight glass are used, one the generator unit and the other on absorber unit, see **Fig. (3.17)**. the mean mass flow rate of refrigerant from the generator is calculated by measuring the drop of solution level in the sight glass of the generator during a specified period of the generator diameter . The mean flow rate is also regulated by using ultrasonic sensor type PT878, shown in **Fig. (3.18)**. Distilled water is produced by (GFL) Mono Water Stills model 2001/4. The Mono water still produces (2-4) liter/hour.

7. After the saturated water vaporized in the evaporator, the vapor went to the absorber when it is absorbed by the strong solution and pumped to the generator. The chemical pump is linked to the electrical control system (Twin Timer). The electrical system provides the power to the chemical pump at the specific time see **Fig. (3.19)**.

## 3.7 Instruments Calibration

### A- Flowmeter

The flowmeter is setup at the exit port of the storage tank to measure the flow rate of hot water in the collector loop . The operating range of the flow meter between (0.06-0.6) $m^3/h$ at 120°C. The calibration of the flowmeter is illustrated in **Fig (3.20)**

### B-Temperature Instrument

The calibration of the thermocouple is done in the heat transfer laboratory by comparing its readings with an already calibrated thermocouple of the same type (K) as shown in **Fig. (3.21)**. The figure shows that the error value is less than (0.25°C).

### C-Pressure Instrument

The pressure sensor and interface and data logger are used to measure in the absorption cooling system. The pressure gauge is set up to a location (generator and absorber). Manometer model calibrates the sensor device: PM-9107 with accuracy 2% FS, so the pressure gauges are calibrated with pressure sensor as shown in **Figs (3.22, 3.23, and 3.24).** The rig design is shown in **Fig. (3.25)**

| |
|---|
| Point 1=Strong Solution |
| Point 2= Strong Solution |
| Point 3= Strong Solution |
| Point 4=Weak Solution |
| Point 5=Weak Solution |
| Point 6=Weak Solution |
| Point 7=Superheated Vapor |
| Point 8=Saturated Liquid |
| Point 9= Saturated Liquid |
| Point 10= Saturated Vapor |
| TC1—TC13=Position of thermocouple |
| Two gauge pressure (High and Low )Pressure |

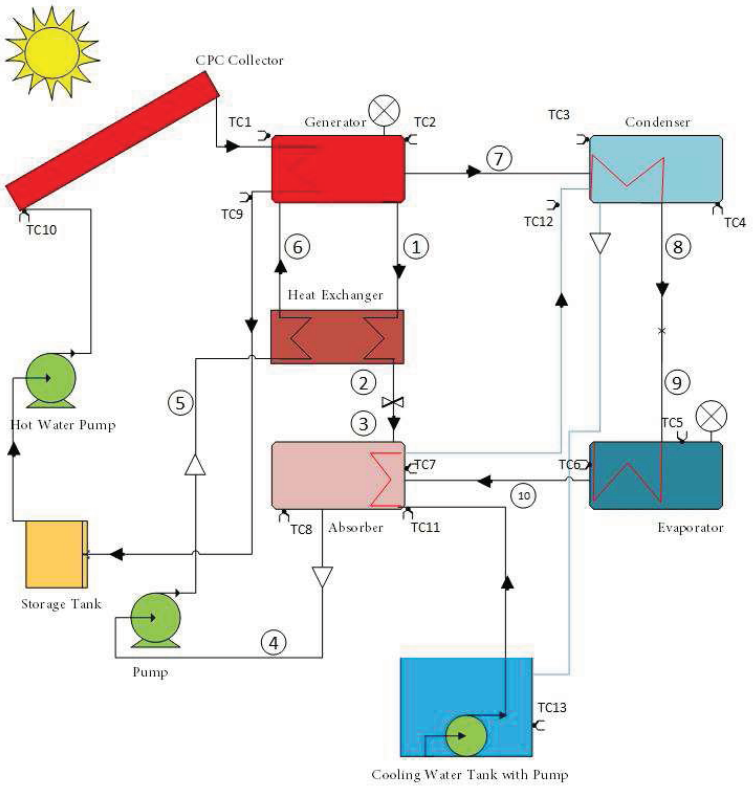


**Figure (3.1) Schematic Diagram of Solar Absorption Cooling System**

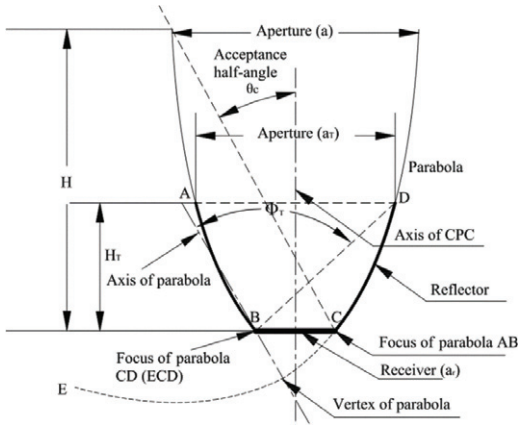


**Figure (3.2). Full Compound Parabolic Concentrator [94]**

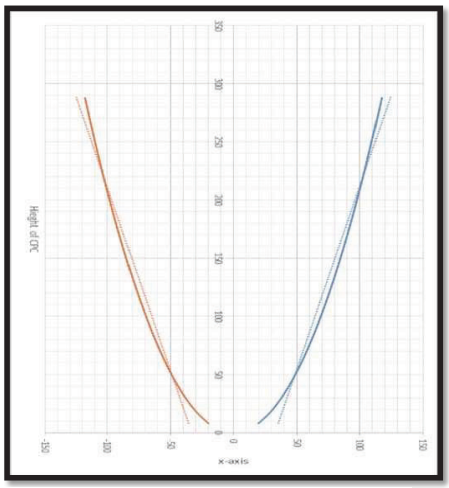


**Figure (3.3). Full Compound Parabolic Concentrator Dimension (cm)**

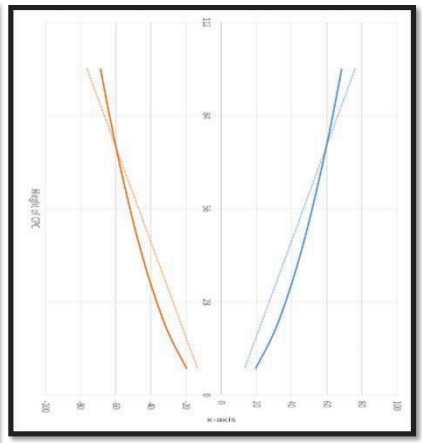


**Figure (3.4). Truncated Compound Parabolic Concentrator Dimension (cm)**


**Figure (3.5). Serpentine copper tube**

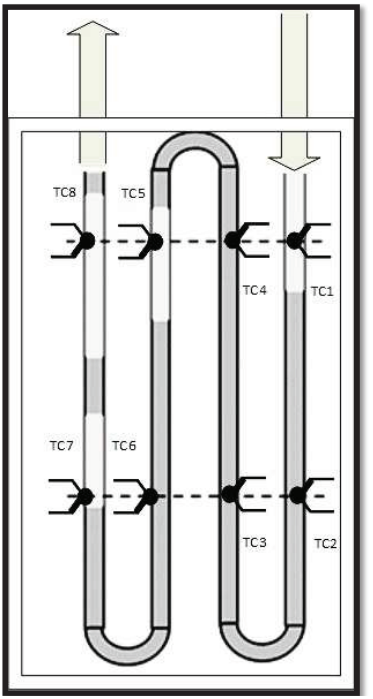


**Figure (3.6). Schematic Serpentine tube fixed on flat plate with thermocouple**

**Figure (3.7). Frame of collector and reflector shape**

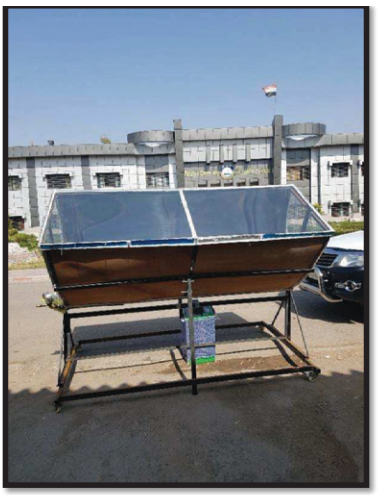

**Figure (3.8). Compound Parabolic Collector (CPC)**

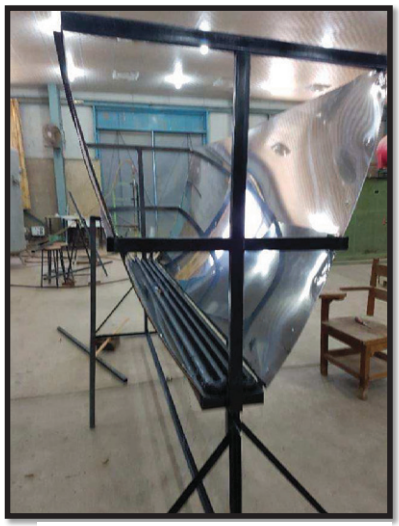

**Figure (3.9). Frame of collector**

**Figure (3.10). Flat plate receiver**

**Figure (3.11). Coil of copper**

**Figure (3.12). Coil setup in generator, absorber, evaporator and condenser**

**Figure (3.13). Capillary tube**

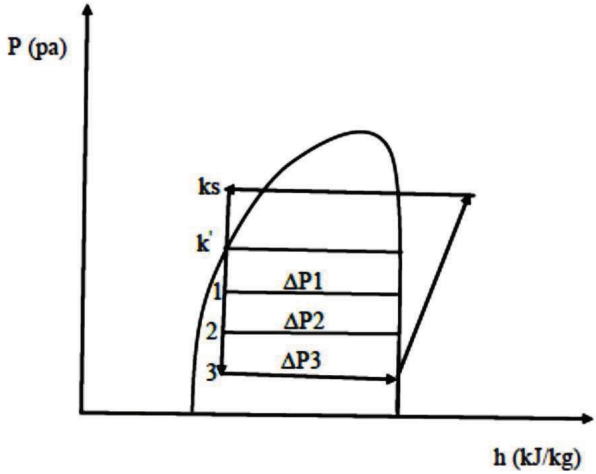


**Figure (3.14). P-h diagram of elementary length a long Isenthalpic Line.**


**Figure (3.15). The Temperature Recording Data Logger**


**Figure (3.16). Lithium bromide salt, diethyl ether and ethanol**

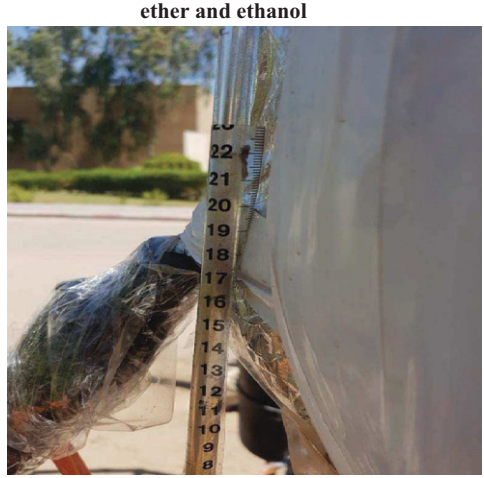

**Figure (3.17). Sight glass**

A


B


C

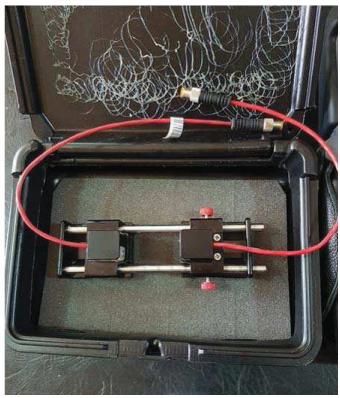

**Figure (3.18). A-Transport PT878 flowmeter indicator**
**B-Silicone grease**
**C-Transducer**

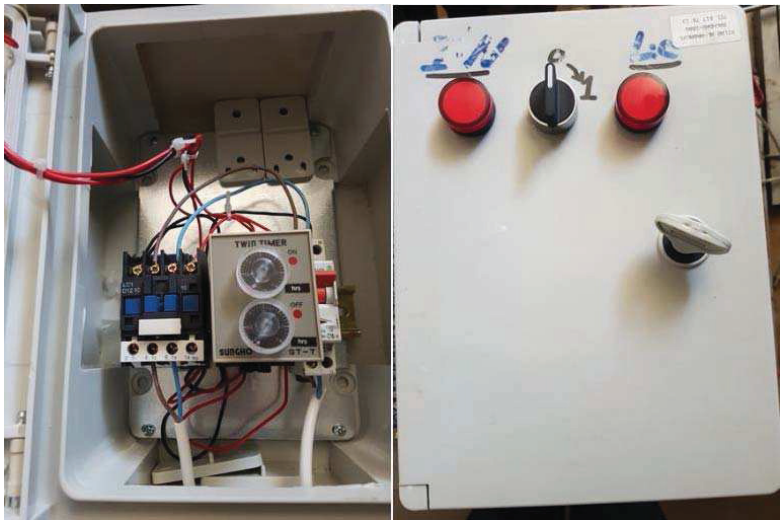


**Figure (3.19). Electrical control system (Twin Timer)**

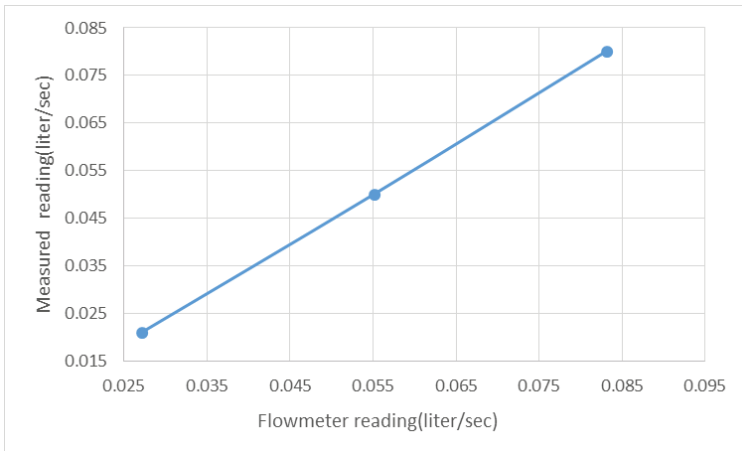


**Figure (3.20). Calibration of flowmeter**

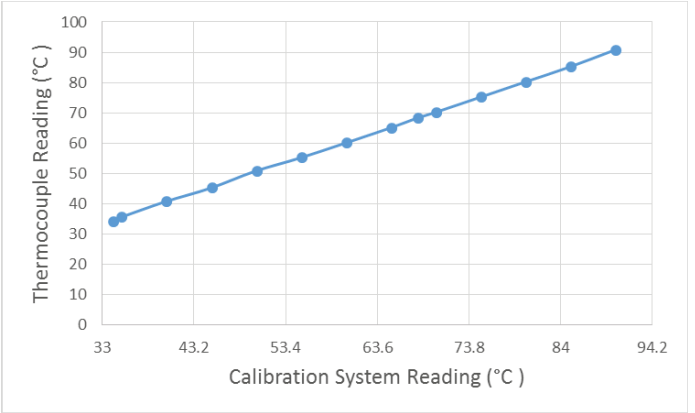


**Figure (3.21). Calibration of the Thermocouple**

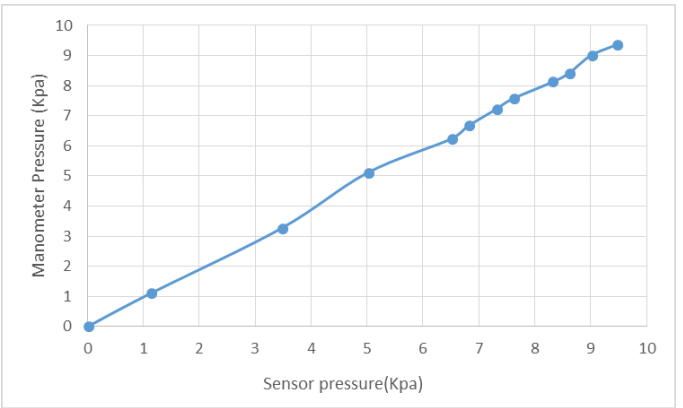


**Figure (3.22). Pressure calibration**

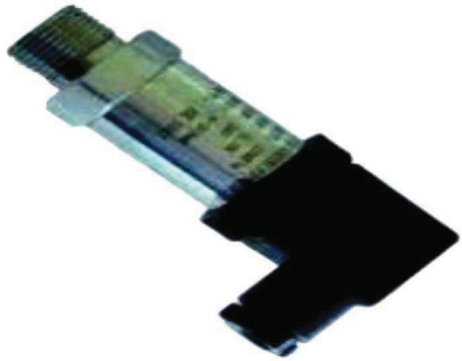

**Figure (3.23). Pressure sensor**


**Figure (3.24). Interface and data logger**


**Figure (3.25). Solar absorption cooling system**

**A- Solar Collector CPC**

**B- Condenser**

**C- Absorber**

**D- Evaporator**

**E-Chemical Pump**

**F- Storage Tank**

**G- Hot water pump**

**H-Generator**

**I-Capillary tube**

**J-Heat exchanger**

**K- Pressure sensor**

# CHAPTER FOUR

# THEORETICAL ANALYSIS

Theoretical design of compound parabolic solar collector (**CPC**) without tracking is presented in this chapter. The thermal efficiency of the collector is obtained. The total and diffused solar radiation are calculated for Babylon province by using theoretical equations.

The analysis and synthesis of absorption refrigeration systems require the application of principles of engineering thermodynamics and heat transfer. A parametric study of the steady state model and dynamic model of the cycle are undertaken for which two computer programs are implemented. As a result, considerable insight may be gained into the cycle performance. It is based on the conventional heat balance method derived from the first and second laws of thermodynamics.

## 4.1 Assumptions

1- The concentration ratio of (CPC) is (5) without need to tracking system

2- The amount of heat diffusion in the flow direction is negligible.

3- Neither the generator releases any heat to the surroundings nor does the evaporator receive any heat from the surroundings.

4- The refrigerant at the exit of the evaporator is assumed to be at the state of saturated vapor.

5- The refrigerant at the exit of the generator is assumed to be at the state of superheated vapor.

6- The concentration of solution leaving the generator and absorber is different from the concentration inside the generator and absorber respectively.

7- The input work of the pump is negligible.

8-There is no pressure loss in the pipes.

9- The fluid temperature at the exit of each component is the same as the temperature inside that component.

## 4.2 Compound Parabolic Collectors (CPC) Calculations

The CPC has the capability of reflecting nearly all of the incident radiation to the absorber. The necessity of moving the collector to accommodate the changing solar orientation is reduced by using a trough with two sections of parabolic sides facing each other, as shown in **Figure (4.1). [95]**

### 4.2.1 Calculation of Thermal Efficiency

The useful energy $Q_u$ can be calculated if we know the absorbed energy $I_a$ and $U_L$. The insolation, $I_{CPC}$ within the acceptance angle of CPC with concentration ratio, CR, is given as **[96]:**

$$I_{CPC} = I_T - \left(1 - \frac{1}{CR}\right) * I_d \quad (4.1)$$

Where $I_T$ and $I_d$ are the total and diffuse radiation respectively on the aperture plane. Now the absorbed radiation $I_a$ in terms of $I_{CPC}$ is **[96]**

$$I_a = I_{CPC}\tau_{cover}\tau_{CPC}\alpha_r$$

$$I_a = I_T\tau_{cover}\tau_{CPC}\alpha_r\gamma \quad (4.2)$$

$$\gamma = 1 - \left(1 - \frac{1}{C}\right)\frac{I_d}{I_T} \quad (4.3)$$

Where $\tau_{cover}$ = transmissivity of glass cover

$\tau_{CPC}$ =effective transmissivity of CPC

$\alpha_r$ = absorbtivity of receiver

$\gamma$ = correction factor for diffuse radiation.

The empirical expression of $U_L$ for a CPC with tubular absorber coated with selective coating and the entire collector covered with a transparent cover is given as **[97]:**

$$U_L = (0.18 + 16.95\varepsilon_r)[0.212 + 0.00255T_a + (0.00186 + 0.000012T_a)(T_r - T_a)] \quad (4.4)$$

Where

$U_L$= collector heat loss coefficient, W/m$^2$ K of receiver area.

$T_a$= ambient temperature, ºC

$T_r$= absorber temperature, ºC

εr = emissivity of absorber surface

A compound parabolic concentrating (CPC) collector is covered with a transparent cover and is tilted towards the south with the long axis in the East-West direction. CPC has tilted in such a fashion that it receives both beam radiations within the acceptance angle. Since in a CPC, the acceptance angle ($\theta_{max}$) is large it receives both beam and diffuse radiation. The receiver can be of any shape, but generally, tubes are used which are selectively coated and attached to the bottom The expression for the rate of useful energy collection is given as **[96]**:

$$Q_{u,th} = A_a F_R \left[ I_a - \left( \frac{U_L}{C} \right) (T_{fi} - T_a) \right] \quad (4.5)$$

Where, $A_a = D * L$

The heat removal efficiency factor is given as **[96]**:

$$F_R = \left( \frac{(\dot{m} C_f)}{(A_r U_L)} \right) \left[ 1 - \exp\left( - \frac{(A_r U_L \acute{F})}{(\dot{m} C_f)} \right) \right] \quad (4.6)$$

The collector efficiency factor is given as **[96]**:

$$\acute{F} = \frac{\left( \left( \frac{1}{U_L} \right) \right)}{\left( \left( \frac{1}{U_L} \right) + \left( \frac{(d * U_L)}{(N \pi D_{r,i} h_{ci})} \right) \right)} \quad (4.7)$$

Where, $h_{ci}$=heat transfer coefficient inside the tube which can be calculated from Nu **[96]**.

$$Nu = 0.023 Re^{0.8} Pr^{0.4} \quad (4.8)$$

$$Nu = \frac{h_{ci} D_{r,i}}{K} \quad (4.9)$$

The outlet fluid temperature is calculated from equation as:

$$T_{f,o} = T_{f,i} + \frac{Q_u}{\dot{m}C_f} \tag{4.10}$$

$$T_{f,m} = \frac{T_{f,i} + T_{f,o}}{2} \tag{4.11}$$

$$T_r = T_{f,m} + \frac{\dot{m}C_f\left(T_{f,o} - T_{f,i}\right)}{h_{ci}\pi D_{r,ext}L} \tag{4.12}$$

Finally, the efficiency of the collector can be calculated from equation as:

$$\eta_{th} = \frac{Q_{u,th}}{A_r I_{beam}} \tag{4.13}$$

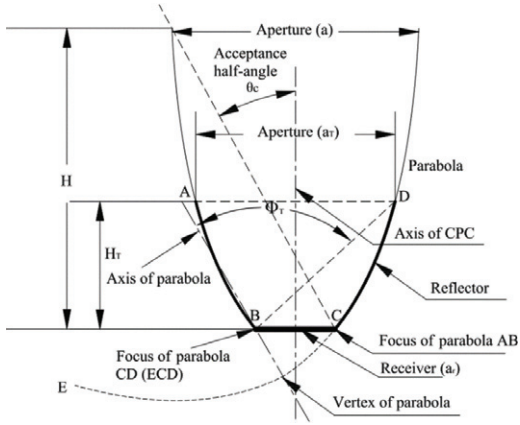


Figure (4.1): Schematic diagram of compound parabolic collector **[95]**

### 4.3 The Absorption Cycle

The absorption refrigeration cycle shown in **Figure (4.2)** is a closed cycle where the working fluid remains within the closed system, and the interface with the surroundings is at boundaries through which heat and work are transferred.

The working fluid for the absorption system is a solution of refrigerant and absorbent, which have a strong chemical affinity for each other. Heat from a high-temperature source is added to the solution in the generator; as

a result, a part of the refrigerant evaporates from the boiling solution (Point 7) which becomes stronger in absorbent concentration. Heat is removed from the refrigerant vapor as it is condensed in the condenser. The liquid refrigerant goes then to the evaporator via an expansion valve or a pressure restrictor in the feeding pipes (Points 8, 9).

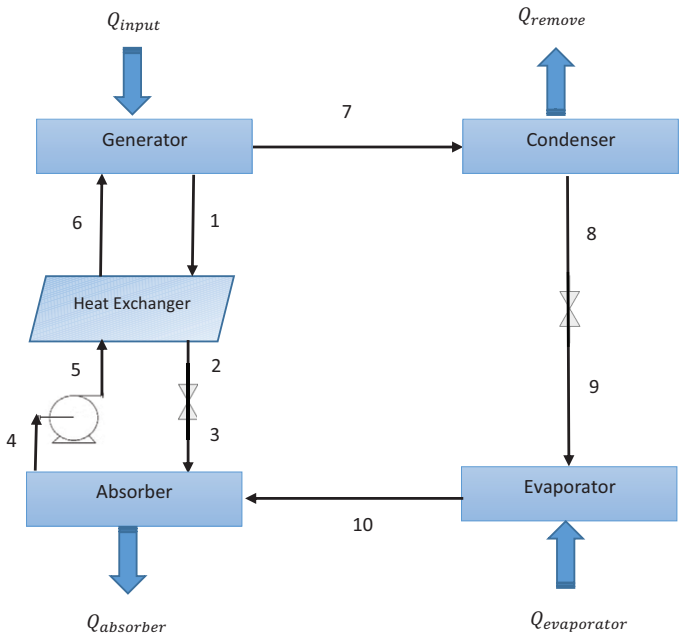


Fig. (4.2) Schematic of an absorption refrigeration process

In the cycle of absorption cooling system is using a pressure transducer to measure the small pressure difference between the high-pressure side of the system (generator and condenser) and the low-pressure side (evaporator and absorber).

Evaporation of the refrigerant liquid takes place in the evaporator. The solution draws vapor away from the refrigerant surface and causes the refrigerant temperature to fall until it can perform some useful refrigeration.

The vapor leaving the evaporator (Point 10) is mixed with a strong solution (Points 1, 2, 3) in the absorber, which comes from the generator through the heat exchanger and expansion valves. Since this process is exothermic, heat must be removed from the absorber to maintain its temperature at a sufficiently low value to assure a high chemical affinity between the refrigerant and the solution. The liquid solution, weak in its affinity for refrigerant, is now pumped to the generator through the heat exchanger so that the cycle can be continuous (Points 4, 5, 6). The heat exchanger placed in the solution circuit between the generator and absorber is used to minimize the sensible heat losses.

### 4.4 First Law Analysis

**Figure (4.3)** shows the energy transfers to and from the fluids of an absorption system. The rate of heat transfers to the refrigerant in the evaporator, denoted by $\mathbf{Q_e}$, is the refrigerating capacity. The system rejects heat $\mathbf{Q_o}$ to the environment cooling water or atmospheric air from the absorber and condenser. Heat $\mathbf{Q_g}$ is added in the generator and work $\mathbf{W_p}$ in the pump.

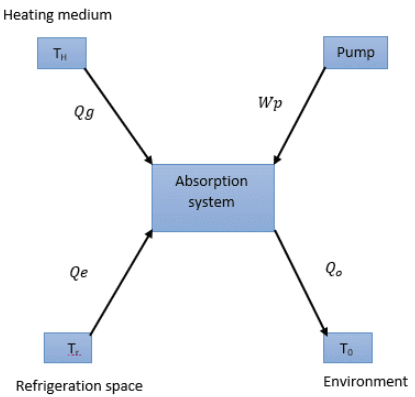


Fig. (4.3) External energy transfers for an absorption refrigeration system

The heat rejected to the environment is equal to the heat transfer $Q_a$ from the absorber plus the heat $Q_c$ from the condenser. Under steady conditions, the rate equation form of the first law for the whole system is :( Neglect K.E and P.E)

$$\dot{Q}_a + \dot{Q}_C = \dot{Q}_G + \dot{Q}_E + \dot{W}_P \tag{4.14}$$

The closed system is formed of a series of individual processes. Each process can be analyzed separately from the system by applying the first law to the component involved in the process. The steady state, steady flow energy equation is

$$\dot{Q} + \dot{W} = \dot{m}\left(h_e + \frac{V^2{}_e}{2} + gZ_e\right) - \dot{m}\left(h_i + \frac{V^2{}_i}{2} + gZ_i\right) \tag{4.15}$$

Where $\dot{Q}$ and $\dot{W}$ are the rates of heat and work transfer across the boundary of component.

$\dot{m}$- is the steady flow of mass in and out of the control volume

*h*- is the specific enthalpy

V -the velocity

*Z*- Elevation

*g*- The acceleration due to gravity.

The subscripts ***i*** and ***e*** denote the states of inlet and exit of the component. In refrigeration, the terms representing the kinetic and gravitational energy changes are usually neglected when considering a particular component. Equation (4.15) reduces to

$$\dot{Q} + \dot{W} = \dot{m}(h_e) - \dot{m}(h_i) \tag{4.16}$$

Energy losses of real absorption cooling cycles are observed in:

(i) Heat transfer through a finite temperature difference.

(ii) Mixing in the absorption process and throttling through the valves.

(iii) Boiling in the evaporator and generator.

(iv) Heat losses to the environment.

Neglecting the small work input to the solution pump, the coefficient of performance of absorption cycles is

$$\mathrm{COP} = \frac{\dot{Q}_E}{\dot{Q}_G} \tag{4.17}$$

The system performance is improved if the absorber and condenser are cooled in parallel streams instead of cooled in series. The parallel is better because of the more temperature difference and more heat exchange. The series is not as much temperature difference and hence less efficiency.

**4.5 Second Law Analysis**

The approach of lost work (or entropy production or irreversibility) is selected to analyze absorption refrigeration cycles mainly because it focuses more on thermodynamic systems and seems simpler to apply. Consider a closed system performing a thermodynamic cycle and in thermal contact with *n* heat reservoirs as shown in **Figure (4.4).**

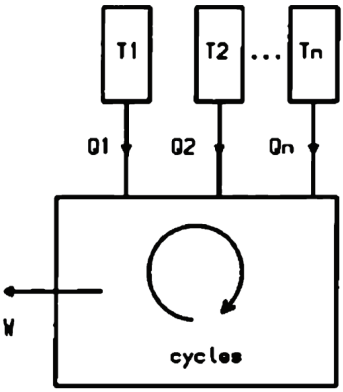


Fig. (4.4) Closed system in contact with *n* heat reservoirs **[20]**

W is the work done by the system, $Q_i$ the heat transfers across a portion i of the system boundary and $T_i$ is the corresponding temperature of that part of the boundary.

By the first law,

$$W = \sum_{i=1}^{n} Q_i \tag{4.18}$$

By the second law,

$$\Delta S_{system} + \Delta S_{heat\ recerviors} \geq 0 \tag{4.19}$$

For steady state operation of the closed system executing a cycle,

$\Delta S_{system} = 0$

For the surroundings;

$$\Delta S_{heat\ recerviors} = \sum_{i=1}^{n} \left( -\frac{\dot{Q}_i}{T_i} \right)$$

If equation (4.19) is written as an equality by introducing the term $S_{prod}$ for the irreversible entropy increase (or entropy production), then

$$\Delta S_{system} = \sum_{i=1}^{n} \left( \frac{Q_i}{T_i} \right) + S_{prod}$$

Or

$$S_{prod} = -\sum_{i=1}^{n} \left( \frac{Q_i}{T_i} \right) \geq 0 \tag{4.20}$$

Lost work LW is related to entropy production $S_{prod}$ by the expression

$LW = T_o\ S_{prod}$

Where $T_o$ is the absolute temperature of the infinite surroundings. The lost work of the considered closed system is

$$LW = -T_\circ \sum_{i=1}^{n} \left( \frac{Q_i}{T_i} \right) \tag{4.21}$$

Adding equations (4.31) and (4.34) produces

$$LW + W = \sum_{i=1}^{n} Q_i \left( 1 - \frac{T_\circ}{T_i} \right) \tag{4.22}$$

The sum of the lost work and the useful work done by the system is the work of a totally reversible system with heat exchange at the same temperature levels other than $T_o$.

$$W_{rev} = LW + W$$

Equation (4.22) may be obtained directly by using the general expression of the reversible work for open systems **[69],**

$$LW + W = \sum_j (mb)_j + \sum_j \left(1 - \frac{T_\circ}{T_i}\right) Q_i - \Delta[m(b - pv)]_{syst}$$

Where *m is* the mass flow across portions of the system boundary and *b* the availability function, b = h — $T_o$ S.

Application to a steady-state cycle exchanging heat with more than one reservoir gives the same result as by Equation (4.22).

The irreversibility concept has also been used **[61]** to develop the second law for the uniform state, uniform flow process. Appropriate simplifications yield the equation for the thermodynamic cycle exchanging heat with n reservoirs,

$$I = \sum_{i=1}^{n} Q_i \left(1 - \frac{T_\circ}{T_i}\right) - W$$

Where I**,** the irreversibility of the process, is defined as the difference between the reversible work that could theoretically be produced and the work that is actually produced.

For the absorption refrigeration process shown in **Figure (4.5)**, the cycle exchanges heat with four reservoirs as well as the surroundings.

From Equation (4.22),

$$(LW)_{cycle} = \sum_{i=1}^{5} Q_i \left(1 - \frac{T_\circ}{T_i}\right) - W_P$$

Or

$$(LW)_{cycle} = Q_G \left(1 - \frac{T_\circ}{T_H}\right) + Q_C \left(1 - \frac{T_\circ}{T_{cf,1}}\right) + Q_a \left(1 - \frac{T_\circ}{T_{cf,2}}\right) + Q_E \left(1 - \frac{T_\circ}{T_r}\right) - W_P \qquad (4.23)$$

Where $Q_G$, $Q_E$ are positive and $Q_C$, $Q_a$, W, are negative

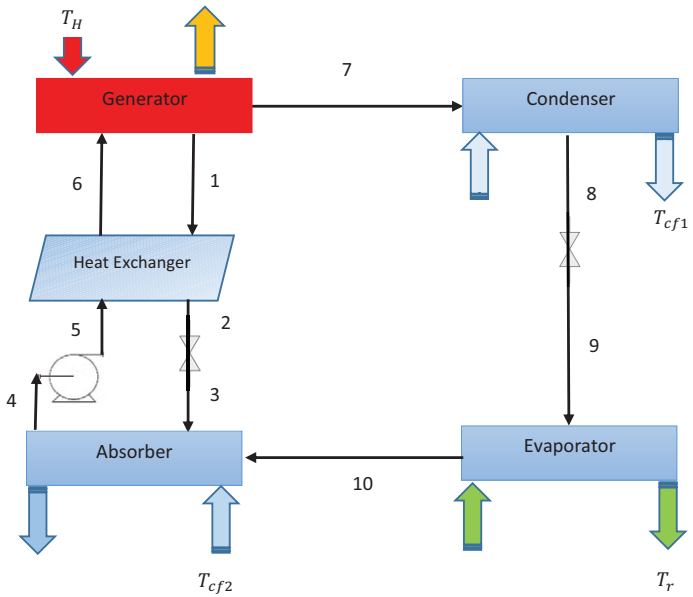


Fig. (4.5) Schematic of an absorption refrigeration process

The term for the heat transfer to the surroundings does not appear in Equation (4.23) because $T_i = T_o$. Similarly, if the temperatures of the cooling mediums are equal to $T_o$ (case of absorber and condenser cooled by atmospheric air), then

$$(LW)_{cycle} = Q_G\left(1 - \frac{T_o}{T_H}\right) + Q_E\left(1 - \frac{T_o}{T_r}\right) - W_P \qquad (4.24)$$

Small capacity absorption refrigeration systems can operate without mechanical pumps when the solution is circulated by use of vapor-lift pump. For such systems there is no work input or output (W=0). When a mechanical liquid pump is used, the work input is usually small.

There is however lost work in each individual component of the absorption cooling cycle, which must be taken into consideration. The overall cycle lost work is equal to the sum of the lost work of the individual

processes. Consider the steady-state operation of the open system of **Figure (4.6).**

From the first law,

$$W = \sum_j Q_j + Q_\circ + \sum m_i h_i - \sum m_e h_e$$

From the second law,

$$S_{prod} = -\sum_j \frac{Q_j}{T_j} - \frac{Q_\circ}{T_\circ} + \sum m_e S_e - \sum m_i S_i$$

And

$$LW = -Q_\circ - \sum_j Q_j \frac{T_\circ}{T_j} + \sum m_e T_\circ S_e - \sum m_i T_\circ S_i \qquad (4.25)$$

Applying equation (4.25) to each component of the absorption refrigeration system gives the expression of the lost work in each individual segment of the process. Referring to Figures (4.2) and (4.5) and taking the external fluids at the boundary of, but outside of, the system,

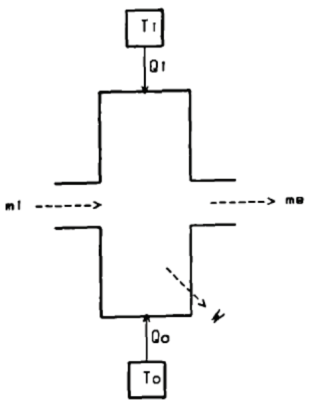


Fig. (4.6) Open system in thermal contact with *n* heat reservoirs **[20]**

$$LW_{\text{in generator}} = -Q_G \frac{T_\circ}{T_H} + m_7 T_\circ S_7 + m_1 T_\circ S_1 - m_6 T_\circ S_6 - Q_{\text{losses,gen}} \qquad (4.26)$$

$$LW_{\text{in condenser}} = -Q_c \frac{T_\circ}{T_{cf,1}} + m_2 T_\circ (S_8 - S_7) - Q_{\text{losses,cond}} \qquad (4.27)$$

$$LW_{\text{in evaporator}} = -Q_E \frac{T_\circ}{T_r} + m_{10} T_\circ (S_{10} - S_9) - Q_{\text{losses,evap}} \quad (4.28)$$

$$LW_{\text{in absorber}} = -Q_A \frac{T_\circ}{T_{cf,2}} + m_4 T_\circ S_4 - m_{10} T_\circ S_{10} - m_3 T_\circ S_3 - Q_{\text{losses,abs}} \quad (4.29)$$

$$LW_{\text{in pump}} = m_5 T_\circ (S_5 - S_4) - Q_{\text{losses,pump}} \quad (4.30)$$

$$LW_{\text{in heat ex}} = m_2 T_\circ S_2 + m_6 T_\circ S_6 - m_1 T_\circ S_1 - m_5 T_\circ S_5 - Q_{\text{losses,heat exch.}} \quad (4.31)$$

$$LW_{\text{i valves}} = m_9 T_\circ (S_9 - S_8) \quad and \quad m_3 T_\circ (S_3 - S_2) \quad (4.32)$$

The sum of the lost work for each individual segment should be equal to the overall cycle lost work as given by equation (4.23). The principal sources of lost work or irreversibility for the absorption refrigeration cycle are:

(i) Heat transfer through a finite temperature difference in the heat exchanging components.

(ii) Mixing in the absorber. The refrigerant vapor and the solution, that are mixed, differ with regard to temperature and to concentration.

(iii) Free expansion during the throttling process in the valves.

## 4.6 Thermodynamic Efficiency

One procedure of defining a second law-based thermodynamic efficiency of absorption refrigeration processes is to devise an ideal system that performs the same task as the actual system but in a reversible way and to form the ratio of the coefficient of performance of the two systems.

Consider an ideal absorption system (Figure 4.8) operating among a heat source temperature of $T_H$, a heat sink temperature of $T_o$ for heat rejection and a refrigerated medium temperature of $T_r$.

The ideal cycle operating with thermodynamically reversible processes between two temperatures is the Carnot cycle. From Figure (4.7) the ideal absorption cycle is a combination of a Carnot engine working between $T_H$ and $T_o$ and a Carnot refrigeration cycle operating between $T_r$, and $T_o$.

For the Carnot engine,

$$\frac{Q_G}{W} = \frac{T_H}{T_H - T_0}$$

For the refrigeration cycle,

$$\frac{Q_E}{W} = \frac{T_r}{T_0 - T_r}$$

The COP of the ideal cycle is

$$(COP)_{ideal} = \frac{Q_E}{Q_G} = \frac{T_r(T_H - T_0)}{T_H(T_0 - T_r)}$$

The maximum coefficient of performance for an absorption system is equal to the coefficient for a Carnot refrigeration cycle working between $T_r$ and $T_o$ multiplied by the thermal efficiency of a Carnot engine working between $T_H$ and $T_o$. In Figure (4.8), the COP of this ideal system is varied over ranges of operating Parameters**.** It can be seen that a higher COP can be obtained at lower heat source temperatures if the refrigerated medium is maintained at higher temperatures and the heat sink is maintained at lower temperatures.

$$Q_o = Q_G + Q_E + W_P$$

For the closed system performing cycles in steady state,

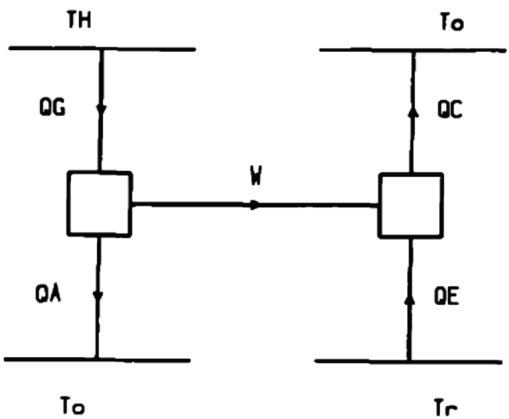


Fig. (4.7) Ideal absorption cycle **[20]**

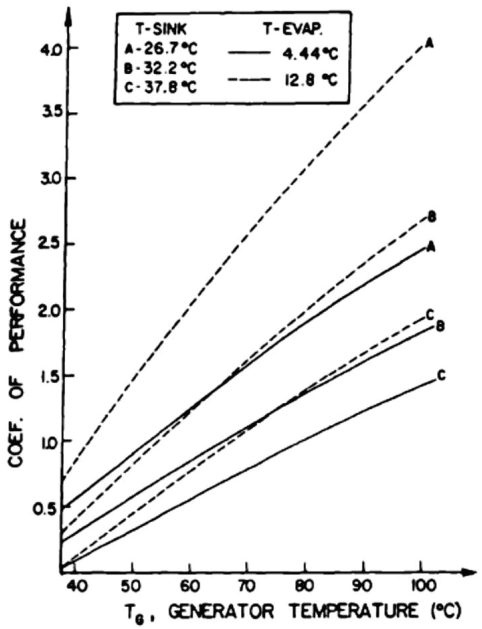


Fig. (4.8) System COP of an ideal absorption cycle **[20]**

$$(\Delta S)_{\text{system}} = 0$$

$$(\Delta S)_{\text{heat recerviors}} = \sum_i \left(-\frac{Q_i}{T_i}\right)$$

$$(\Delta S)_{\text{surroundings}} = +\frac{Q_0}{T_0}$$

By the second law,

$$(\Delta S)_{\text{total}} = -\frac{Q_G}{T_H} - \frac{Q_E}{T_r} + \frac{Q_0}{T_0} \geq 0$$

Rearranging the last equation,

$$\frac{Q_G(T_H - T_\circ)}{T_H} \geq \frac{Q_E(T_\circ - T_r)}{T_r} - W_P$$

or if we assume that Wp is negligible,

$$\mathrm{COP} = \frac{Q_E}{Q_G} \leq \frac{T_r(T_H - T_\circ)}{T_H(T_\circ - T_r)}$$

And for an ideal system,

$$\mathrm{COP}_{ideal} = \frac{T_r(T_H - T_\circ)}{T_H(T_\circ - T_r)}$$

The main task of an absorption cooling cycle is the removal of heat from the refrigerated medium. If the work input is small, the second law efficiency is

$$\eta = \frac{(Q_G)_{ideal}}{(Q_G)_{actual}}$$

$$\eta = \frac{\frac{Q_E}{(COP)_{ideal}}}{\frac{Q_E}{(COP)_{actual}}} = \frac{COP}{COP_{ideal}} \qquad (4.33)$$

And

$$\eta = \frac{Q_E\left(\frac{T_\circ - T_r}{T_r}\right)}{Q_G\left(\frac{T_H - T_\circ}{T_H}\right)} = -\frac{Q_E\left(1 - \frac{T_\circ}{T_r}\right)}{Q_G\left(1 - \frac{T_\circ}{T_H}\right)} \qquad (4.34)$$

Consider now the absorption cycle shown in Figure (4.6) where the system rejects heat to two reservoirs at $T_{cf,1}$ and $T_{cf,2}$. By equation (4.22),

$$W_{rev} = Q_G\left(1 - \frac{T_0}{T_H}\right) + Q_C\left(1 - \frac{T_0}{T_{cf,1}}\right) + Q_a\left(1 - \frac{T_0}{T_{cf,2}}\right) + Q_E\left(1 - \frac{T_0}{T_r}\right) \quad (4.35)$$

For the absorption cycle whose task is neither to produce work nor to consume work, it can be observed that the terms on the right side of equation (4.35) represent the possible accomplishments of the process plus the inputs necessary to perform them. A general definition of second law efficiency has been formulated as the ratio of the desired result to the inputs necessary to accomplish that result **[97].**

$$\eta = \frac{-Q_E\left(1 - \frac{T_\circ}{T_r}\right)}{Q_G\left(1 - \frac{T_\circ}{T_H}\right) + Q_C\left(1 - \frac{T_\circ}{T_{cf,1}}\right) + Q_A\left(1 - \frac{T_\circ}{T_{cf,2}}\right)} \qquad (4.36)$$

The minus sign appears because the two terms in the efficiency definition will have opposite algebraic signs due to thermodynamic conventions. If the temperatures $T_{cf,1}$ and $T_{cf,2}$ of the cooling mediums are equal to the ambient temperature $T_o$ then the efficiency expression reduces to the efficiency formulation of equation (4.34).

**4.7 Steady State Model**

The governing equations used to evaluate the irreversibility in each component follow.

$$m_{ws} = m_{ss} + m_w \tag{4.37}$$

LiBr, balance

$$m_{ws}X_{ws} = m_{ss}X_{ss} \tag{4.38}$$

Where $m_{ss}$, $m_{ws}$, $m_w$ are the mass flow of the strong solution, weak solution, and water refrigerant, and $X_{ss}$, $X_{ws}$ are the concentrations of LiBr, in the strong and weak solutions.

The concentration is defined as the ratio of the mass fraction of LiBr in a solution to the total mass of LiBr, and water contained in the solution.

$$X = \frac{\text{mass of } (L_iB_r)}{\text{mass of } (L_iB_r) + \text{mass } (H_2O)}$$

From equations (4.37) and (4.38)

$$\frac{m_{ws}}{m_w} = \frac{X_{ss}}{X_{ss} - X_{ws}} \tag{4.39}$$

$$\frac{m_{ss}}{m_w} = \frac{X_{ws}}{X_{ss} - X_{ws}} \tag{4.40}$$

To perform thermal calculations on the absorption refrigeration cycle, enthalpy data for the aqueous LiBr solution are needed. Enthalpy values are dependent upon the choice of standard state of the constituents. The enthalpy data that will be used for calculations in these investigations are based on a reference state of zero enthalpy at 0°C for each of the two constituents, water and lithium bromide.

The conventional steam tables can be used in conjunction with the enthalpy data of solutions since the reference state is also 0°C.

Using the notation of Figure 4.2, the steady state steady flow energy equation (4.16) will be applied to each component assuming equilibrium states and uniform temperatures.

(1) Generator: The rate of heat transfer to the solution is

$$\dot{Q}_G = \dot{m}_7 h_7 + \dot{m}_1 h_1 - \dot{m}_6 h_6$$

But

$$\dot{m}_1 = \dot{m}_2 = \dot{m}_3 = \dot{m}_{SS}$$

$$\dot{m}_4 = \dot{m}_5 = \dot{m}_6 = \dot{m}_{WS}$$

$$\dot{m}_7 = \dot{m}_8 = \dot{m}_9 = m_W$$

Or

$$\dot{Q}_G = \dot{m}_W h_7 + \dot{m}_{SS} h_1 - \dot{m}_{WS} h_6 \qquad (4.41)$$

Where

$h_1$=enthalpy of saturated strong solution at $T_1$ and $X_{ss}$

$h_6$ =enthalpy of weak solution at $T_6$ and $X_{ws}$

$h_7$ =enthalpy of saturated water vapor at $T_7$

Generator temperature= $T_1 = T_7 = T_G$

(2) Condenser: The rate of heat transfer from the condenser is

$$\dot{Q}_C = \dot{m}_W (h_7 - h_8) \qquad (4.42)$$

$h_8$ =enthalpy of saturated water liquid at $T_8$

Condenser temperature=$T_8$=$T_c$

(3) Water pressure restrictor:

$$h_9 = h_8$$

$h_9$= enthalpy of water liquid at $T_9$

(4) Evaporator: The rate of heat transfers to the evaporator i.e. the refrigerating capacity is

$$\dot{Q}_E = \dot{m}_W(h_{10} - h_9)$$

$$\dot{Q}_E = \dot{m}_W(h_{10} - h_8) \quad (4.43)$$

$h_{10}$=enthalpy of water vapor at $T_{10}$

Evaporator temperature=$T_{10}$=$T_E$

(5) Solution pressure restrictor:

$$h_3 = h_2$$

$h_2$ =enthalpy of solution at $T_2$ and $X_{SS}$

$h_3$ =enthalpy of solution at $T_3$ and $X_{ss}$

(6) Absorber: The rate of heat transfer from the absorber is

$$\dot{Q}_a = \dot{m}_3 h_3 + \dot{m}_{10} h_{10} - \dot{m}_4 h_4$$

$$\dot{Q}_G = \dot{m}_{SS} h_2 + \dot{m}_W h_{10} - \dot{m}_{WS} h_4 \quad (4.44)$$

$h_4$ =enthalpy of saturated weak solution at $T_4$ and $X_{ws}$

$h_{10}$=enthalpy of saturated water vapor at $T_E$

$T_4$=$T_a$=Absorber temperature

(7) Heat exchanger: Assuming that heat losses to the surroundings are negligible, the rate of heat transfer between the strong and weak solutions is

$$\dot{Q}_{HX} = \dot{m}_{SS}(h_1 - h_2) = \dot{m}_{WS}(h_6 - h_5) \quad (4.45)$$

(8) Solution pump: The power input to the pump is

$$\dot{W}_P = \dot{m}_{WS}(h_5 - h_4) \quad (4.46)$$

$h_5$ =enthalpy of weak solution at $T_5$ and $X_{ws}$.

The difference between $h_4$ and $h_5$ is not distinguished on the charts of specific enthalpy of LiBr-water solutions as the temperature is approximately the same.The coefficient of performance of the cycle is

$$COP = \frac{\dot{Q}_E}{\dot{Q}_G} = \frac{\dot{m}_W(h_{10} - h_8)}{\dot{m}_w h_7 + \dot{m}_{ss} h_1 - \dot{m}_{WS} h_6}$$

The second law efficiency of the cycle, given by equation 4.36, is

$$\eta = \frac{-Q_E\left(1-\frac{T_\circ}{T_r}\right)}{Q_G\left(1-\frac{T_\circ}{T_H}\right)+Q_C\left(1-\frac{T_\circ}{T_{cf,1}}\right)+Q_A\left(1-\frac{T_\circ}{T_{cf,2}}\right)}$$

Where

$T_r$= average temperature of cold and hot space

$T_H$= average temperature of hot water= $\frac{T_{HW,i}+T_{HW,e}}{2}$

$T_{cf1,\,i}$ = average temperature of cooling water= $\frac{T_{CW1,i}+T_{CW1,e}}{2}$

$T_{cf2,\,e}$= average temperature of cooling water = $\frac{T_{CW2,i}+T_{CW2,e}}{2}$

$T_o$= ambient temperature

Computer programs to be prepared, will examine the performance of LiBr, absorption cycles through the model. Suitable analytical expressions for the enthalpy of lithium bromide solutions and water refrigerant are needed.

The enthalpy of the binary solution is given **[43]** as a function of the solution temperature and concentration.

$$h = 2.326(a + b(1.8T + 32) + c(1.8T + 32)^2) \qquad (4.47)$$

Where

h is solution enthalpy in kJ/kg, T in °C,

a= -1015.07+ (79.5387) X-(2.358016) $X^2$+ (0.03031583) $X^3$-(1.400261E-4) $X^4$

b= 4.68108-(3.037676E-1) X+ (8.44845E-3) $X^2$-(1.047721E-4) $X^3$ + (4.80097E- 7) $X^4$

c= -4.9107E-3+ (3.83184E-4) X- (1.078963E-5) $X^2$ + (1.3152E-7) $X^3$ -(5.897E- 10) $X^4$

The equilibrium solution temperature is **[39]**

$$T = (a_o + a_1 X + a_2X^2 + a_3 X^3)\,\acute{T} + (b_\circ + b_1 X + b_2 X^2 + b_3 X^3) \qquad (4.48)$$

Where, $\acute{T}$ is the saturation temperature of water (°C)

$a_0$= - 2.00755 $b_o$ = 124.937

$a_1$= 0.16976 $b_1$= -7.7165

$a_2$= - 3.13336E-5 $b_2$= 0.152286

$a_3$ = 1.97668E-5 $b_3$= -7.9509E-4

Range: -20-≤ $\acute{T}$≤ 110°C

5-≤T≤ 180°C

$45\% < X < 70\%$

Where X is concentration

The enthalpy of water refrigerant is given **[23]** in simplified form. For water liquid

$$h_W = 4.19(T - T_0) \quad \frac{kJ}{kg} \tag{4.49}$$

T is the temperature and $T_o$ the datum temperature, 0°C.

For water vapor at low pressure

$$h_v = 2501 + 1.88(T - T_0) \quad \frac{kJ}{kg} \tag{4.50}$$

The absorber and evaporator are assumed at the same pressure at equilibrium though in actual processes a small pressure is necessary. Therefore, the evaporator pressure or temperature and the absorber temperature define the concentration, $X_{ws,}$ of the weak solution in the absorber.

Concentrations $X_{ws}$ at the absorber and evaporator temperatures of interest are taken from the available charts **[43]** and used as input for running performance tests.

The condenser and generator are assumed to work at the same pressure at equilibrium. The condenser temperature and concentration of the strong solution in the generator, $X_{ss}$, can determine the generator temperature using equation (4.48). The generator temperature may vary from a minimum to a maximum. The minimum is because the solution starts to boil and vapor is produced only above the saturation temperature of the solution.

The maximum value is due to crystallization of the solution. Different crystallization lines are given in the literature. For the purpose of this study the exact value of the strong solution concentration, Xss, at which the maximum generator temperature is calculated, is not critical. A maximum

concentration of 64.9% was taken using charts of equilibrium vapor pressure of aqueous solutions of lithium bromide **[43].**

The evaporator temperature varies from the theoretical value of 0°C (water solidifies at this temperature) to the highest practical limit of 10°C for a useful refrigeration effect.

The absorber and condenser temperatures depend on the cooling water conditions and are within the reasonable range of 20°C to 40°C.

While, the ambient temperature is taken as 25°C or 40°C, the heat exchanger is included in the study through its effectiveness. The heat exchanger effectiveness, HX, is defined as the ratio of the temperature drop of strong solution to the temperature difference of the strong and weak solutions entering the heat exchanger.

$$HX = \frac{T_G - T_2}{T_G - T_5}$$

But

$$T_5 = T_4 = T_a$$

So that

$$T_2 = (HX \,.\, T_a) + (1 - HX)T_G \qquad (4.51)$$

**4.8 Dynamic Model**

Lumped-parameter dynamic simulation of a single-effect LiBr-$H_2O$ absorption chiller. The model is used to solve simultaneous differential equations involving the continuity of species constituting the LiBr-$H_2O$ solution, momentum equations, and energy balances. This study deals with the dynamic analysis of a single-effect absorption chiller by considering the effect of quality on the solution concentration. Dynamic approach can be applied for controlling purposes. The fourth order Range-Kutta method is selected to solve the simultaneous equations deduced from continuity, momentum, and energy balances. The results inferred from the dynamic analysis are compared with the data from the steady-state condition.

Obtaining major parameters such as coefficient of performance, second law efficiency as a function of time.

### 4.8.1. Governing Equations

The schematic diagram of a single-effect LiBr-$H_2O$ absorption chiller is illustrated in **Fig. (4.5)**. Each main component is characterized by a single pressure, temperature, and concentration. The governing equations for the dynamic analysis are:

Mass continuity:

$$\frac{d(M_i)}{dt} = \dot{m}_{in} - \dot{m}_{out} \tag{4.52}$$

Continuity of LiBr and water species:

$$\frac{d(M_A Z_A)}{dt} = \dot{m}_3 X_1 - \dot{m}_4 X_4 \tag{4.53}$$

$$\frac{d(M_G Z_G)}{dt} = \dot{m}_6 X_4 - \dot{m}_1 X_1 \tag{4.54}$$

Momentum:

$$\frac{d\dot{m}_i}{dt} + \frac{1}{2} f_i \frac{\dot{m}_i |\dot{m}_i|}{\rho_i A_i D_i} = \frac{A_i}{L_i} (\Delta P) \tag{4.55}$$

Energy balance:

$$\frac{d(M_i h_i)}{dt} = \dot{m}_{in} h_{in} - \dot{m}_{out} h_{out} \mp Q_i \tag{4.56}$$

The concentration of solution at the exit of the absorber and generator is a function of the quality and solution concentration in the generator and absorber respectively:

$$X_1 = \frac{Z_G}{(1 - Qu_G)} \tag{4.57}$$

$$X_4 = \frac{Z_A}{(1 - Qu_A)} \tag{4.58}$$

Now, Equations (4.59) and (4.60) lead to

$$\frac{d(M_A Z_A)}{dt} = \dot{m}_3 \frac{Z_G}{(1 - Qu_G)} - \dot{m}_4 \frac{Z_A}{(1 - Qu_A)} \quad (4.59)$$

$$\frac{d(M_G Z_G)}{dt} = \dot{m}_6 \frac{Z_A}{(1 - Qu_A)} - \dot{m}_1 \frac{Z_G}{(1 - Qu_G)} \quad (4.60)$$

Z stands for the concentration of solution at the generator and absorber. X is the concentration of solution at the exit of the absorber and generator. As the quality approach zero, the amount of Z will become equal to X. The following equations can be applied for the expansion valve and the pump.

$$\frac{1}{2}\xi \frac{1}{\rho_i {A_V}^2} \dot{m}_i |\dot{m}_i| = {P_V}^{in} - {P_V}^{out} \quad (4.61)$$

$$\Delta P = a_0 + a_1 \dot{m}_i + a_2 {\dot{m}_i}^2 \quad (4.62)$$

Where $\xi$ is the expansion valve friction factor, which is assumed constant. $A_V$ is the smallest cross-sectional area of the expansion valve. $a_0$, $a_1$ and $a_2$ can be obtained from the characteristic curve of the pump. To solve the simultaneous differential equations, a trial and error process is needed to calculate the pressure, temperature, and quality of the main components. In the second stage, the properties at other state points of the cycle can be obtained from the initial conditions. These amounts are used to solve the simultaneous differential equations and the amounts of parameters at the next step can be calculated. This process is repeated until the convergence criterion is satisfied.

The exergic efficiency represents the reversible performance of the cycle and is defined as the ratio of total exergy taken from the system to the total exergy given in the system **[98].**

$$\eta_{second} = \frac{\Delta E_{taken}}{\Delta E_{given}} = 1 - \frac{\sum \Delta E_{loss}}{\sum \Delta E_{given}} \quad (4.63)$$

# CHAPTER FIVE

# RESULTS AND DISCUSSIONS

The results are divided into two parts for ease of presentation and discussion.

**A-The Experimental Study Results**

It is grouped into two parts

1-Solar radiation parameters, which includes incident radiation intensity and air temperature.

2-Solar absorption cooling system parameters which includes compound parabolic concentrator(CPC) with collector parameters, generator and evaporator pressure, the temperature at a different location in the cooling cycle, system coefficient of performance and effect of operating parameters on COP.

**B-The Theoretical Study Results**

A mathematical algorithm and a computer program are developed to solve the governing equations to predict all the above-mentioned parameters. The predicted results are compared with measured results to validate its correctness.

## 5.1 Experimental Results.

### 5.1.1 Total Solar Radiation

In this study, a WATCHDOG 2000 series weather station is used. The station is installed at Babylon University site on the roof of a two-story building so that no high structure or other possible obstacles affect the data accuracy especially wind speed and direction. The station collects the following metrological parameters (Solar radiation, Air temperature, wind speed, wind direction, wind gust, rain quantity and relative humidity). All of these data are collected immediately at the end of a pre-set period. The data are fed to a PC through an interface cable. In the present study, the data are collected at each 10 min period. The minimum instantaneous total solar

radiation is recorded in 21st December which is (572) W/m$^2$ and maximum recorded instantaneous total solar radiation are in 21st June which is (927) W/m$^2$ for year 2016 at 12:30pm. The maximum weather temperature is (50°C) on 29/6/2016 at 14:52.

**Figs. (5.1-5.4)** show the measured instantaneous total daily solar radiation and air temperature for the selected days during, June 21, September 21, December 21 and March 21, for the year 2016 as a sample of measured data. The maximum instantaneous total solar radiation is on June 21 corresponding 927 W/m$^2$. The maximum air temperature at this day is 43°C. The data of the incident radiation shows that at Hillah city in Iraq (32.4$^o$ latitude, 44.4$^o$ longitudinal) the climate features that the highest air temperature, and solar radiation occur during summer months, especially in May, June, July, and August. The results of March 21 and September 21 refer to the spring and fall equinox where the sunrays are perpendicular to the axis of daily rotation and the length of the days and nights everywhere are equal. Also, the Solstice occurs twice each year (June 21 and December 21). The figures show the maximum total solar radiation and air temperature are (927 W/m$^2$) for June 21 at 12:04 pm, (800W/m$^2$) for September 21 at 11:55 am. The maximum temperature of June 21 and September 21 are (43°C, 34°C) respectively. The figures also show the maximum instantaneous total solar radiation occur for 21-March,21-June,21-September, and 21-December are (12:09 pm,12:04 pm,11:55 am and 12:00 pm) respectively. The temperature of the air continues increasing even after the solar radiation reached its maximum value and starts decreasing temperatures. The rises gradually after sunrise, heating the surface of the earth and the amount of heat gained is higher than the amount of heat loss. Which is responsible for raising earth environment temperature and air temperature.

This situation continues until the balance is achieved at 2:00 pm, where the maximum temperatures are usually recorded. This balance occurs at

midday, i.e., at noon when the sun is in the sky, because the sun is close until 2:00 pm to the vertical state and still. The amount of heat gained by the earth is higher than the amount of heat loss.

After this time, the solar radiation energy is repduced by the deviation of the sun from the meridian line, and the radiation becomes very gradual and gradual. The amount of solar radiation gained by the earth increases as a result.

These Figs. show the maximum daily solar radiation occurs after mid-day in winter season, while in summer season occurs around noontime due to a long summer day. The figs. also show that the air temperature continues to increase even after the maximum daily solar radiation is reached.

**Fig. (5.5) s**hows a comparison between measured instantaneous total solar radiation on 21-June and 21-December 2016.The total solar radiation on 21-June is higher than 21-December because the declination angle is (23.28° and 0.637°) respectively. The day length on 21-June and 21-December are (14.14 and 9.58) Hours respectively.

**Fig. (5.6)** shows measured instantaneous total solar radiation and air temperature during the 21$^{th}$ for (March, June, September and December), 2016. The figure shows the maximum instantaneous total solar radiation, and air temperature occur at 21$^{st}$ June (927W/m$^2$ and 43°C), and minimum occur at 21$^{st}$ December (572 W/m$^2$ and 11.5°C). Also, the figure shows the time at which the maximum instantaneous solar radiation and maximum temperature of the air, which usually happens between 11:55 am and 12:15pm.

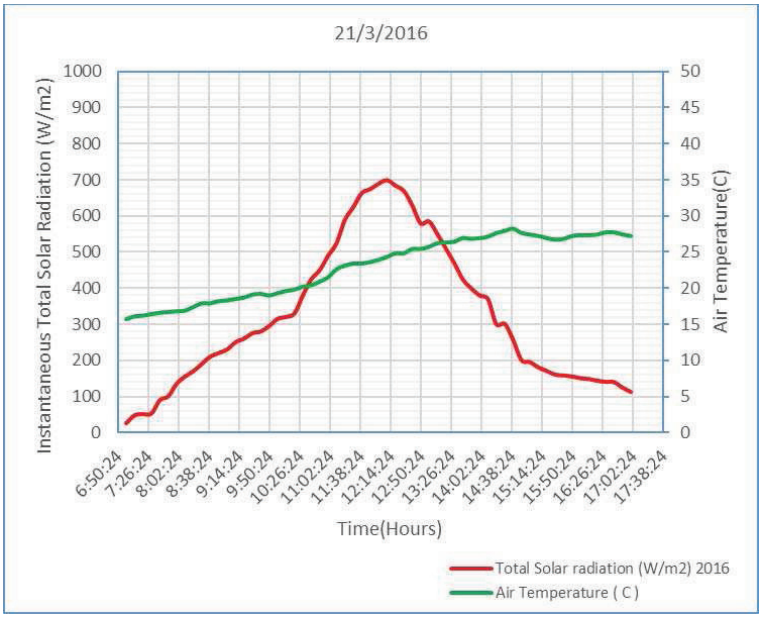


**Fig. (5.1) Measured total solar radiation and air temperature at 21st March-2016**

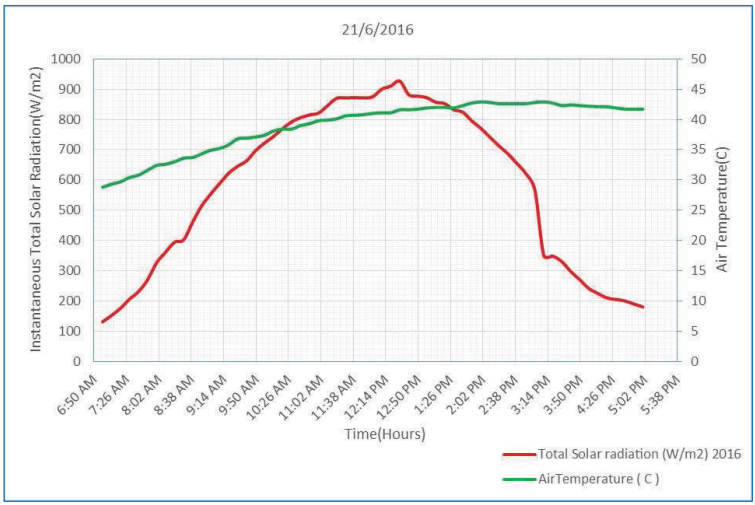


**Fig. (5.2) Measured total solar radiation and air temperature at 21st June-2016**

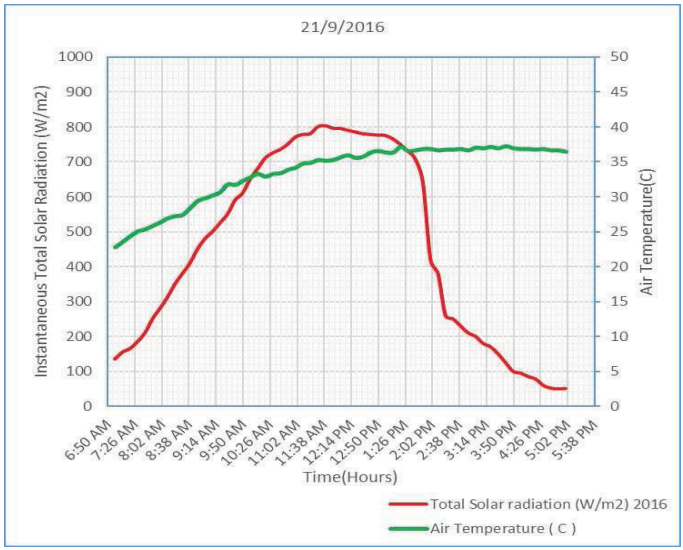


**Fig. (5.3) Measured total solar radiation and air temperature at 21st September-2016**

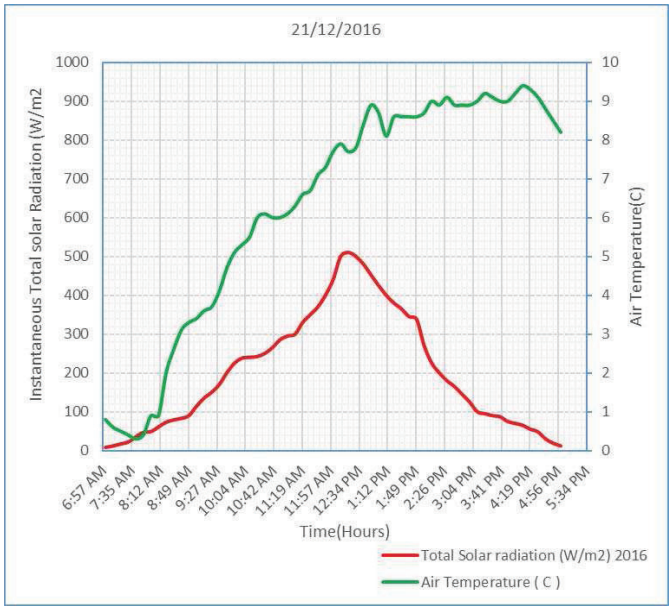


**Fig. (5.4) Measured total solar radiation and air temperature at 21stDecember-2016**

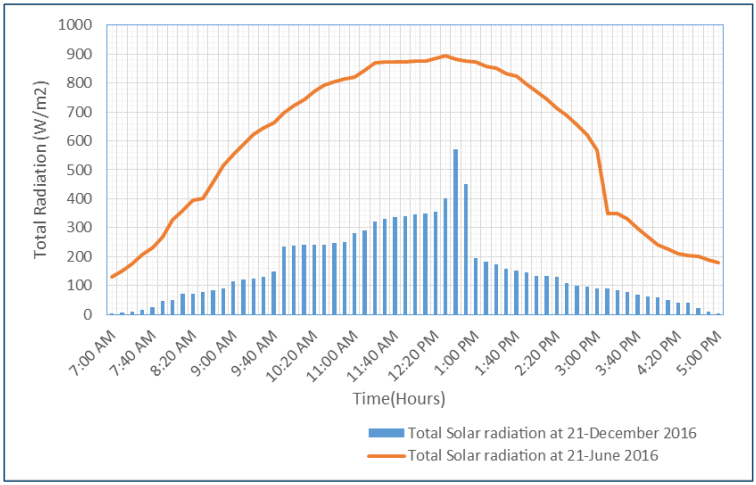


**Fig. (5.5) Comparison between measured instantaneous total solar radiation at 21-June and 21-December 2016**

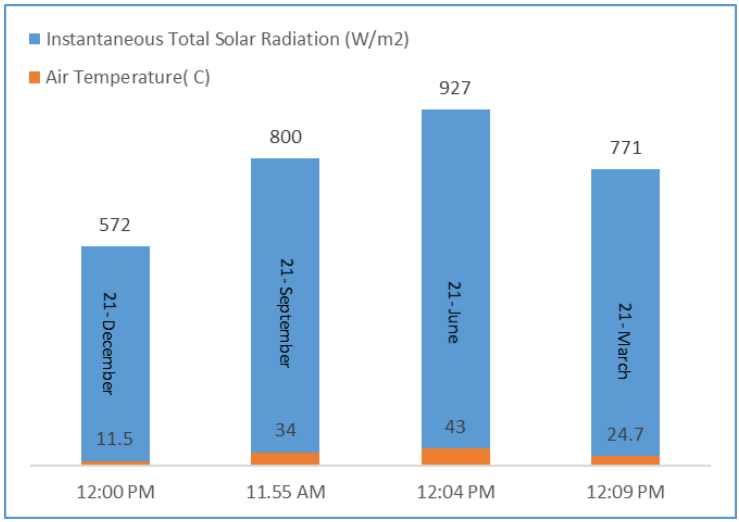


**Fig. (5.6).The measured instantaneous total solar radiation and air temperature at 21$^{th}$ for (March, June, September and December) with time, year 2016**

### 5.1.2 Collector Loop Performance (CPC)

The collector loop consists of the CPC, the flat plate receiver with the serpentine water pipes, the pump and the storage tank. The studied performance parameters include, receiver surface temperature, efficiency curve, exit water temperature and collector efficiency, the test are done with and without water circulation.

**Fig. (5.7)** shows the variation of receiver surface temperature from mooring to evening i.e. (8:00 am to 15:00 pm) at 21$^{th}$ for (March, June, September and December). The temperature in the morning increases gradually because of the increasing in the intensity of the radiation until the sun reaches its maximum peak at noon and the temperature is slowly decreasing after the back because of the lack of solar radiation throughout the day. The figure shows that the maximum collector receiver temperature occurs at 21-June at 13.17 pm after maximum solar radiation, which is (148°C). The higher temperature at this time is due to higher instantaneous solar radiation. Also, the minimum collector receiver temperature at 21-December at (13.12pm), after maximum solar radiation, which is (91°C)

**Fig. (5.8)** shows that the receiver temperature reaches its maximum value at about 13:00 pm. The receiver temperature peaks after the maximum solar radiation. It is obvious from a recorded temperature that there is a good feasibility of using solar energy in absorption cooling systems. The figure shows a comparison of the temperature of the receiver during the year 2016 with or without the circulation of hot water. Without the flow of hot water, the temperature of the solar receiver collector is about 148° C in 21-June.The temperature increase from (21-January to 21-July) because of increasing solar intensity. With the flow of hot water, the maximum receiver temperature about is 98° C.

**Fig. (5.9)** shows the collector performance curve which is the relation between experimental efficiency and operating point or efficiency function,

where the (y= -3.1667*X+0.67 with corresponding determination $R^2$ =0.9998), (UL = 3.25 W/$m^2$. k) and optical efficiency is 0.67. The overall loss coefficient (UL) is an indication of heat loss from the collector. The overall loss coefficient for the flat plate collector **[59]** is higher than CPC that refers to less heat loss from receiver plate and edges.

**Fig. (5.10)** illustrates the calculated efficiency of the solar collector in summer and winter seasons at a different mass flow rate (0.0277 kg/s and 0.0377 kg/s) and measured total solar radiation. The figure shows that the measured efficiency increase when increasing mass flow rate. The figure shows the increasing measured total solar radiation refer to increase the efficiency of collector. The efficiency increase from (0.48-0.63) at mass flow rate 0.0277kg/s and from (0.49-0.66) at 0.0377 kg/s.The maximum efficiency is during summer season.

**Fig (5.11)** demonstrates that it is possible to get hot water during winter season at a temperature of about 80°C, and during summer season, the water temperature could reach as high as 98°C, while the air temperature varies from about 20°C to 50°C. The figure illustrates that the increasing in instantaneous total solar radiation lead to increase the air temperature. The increasing in the instantaneous total solar radiation leads to increase absorption of radiation on the receiving surface refer to raises the temperature of the water in the loop of the solar collector.

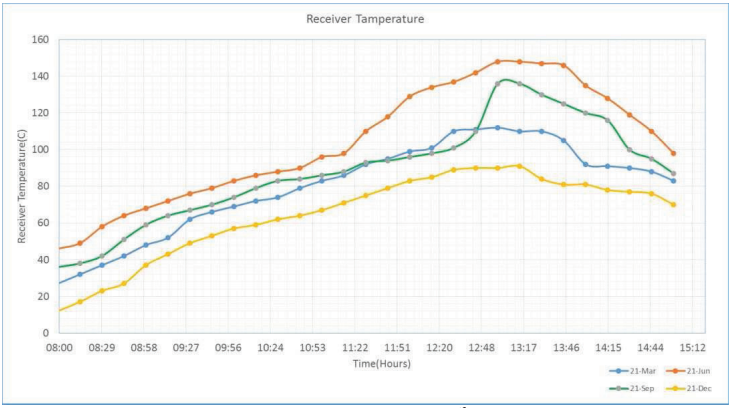


**Fig. (5.7). The collector receiver temperature at 21th for (March, June, September and December) with time, year 2016**

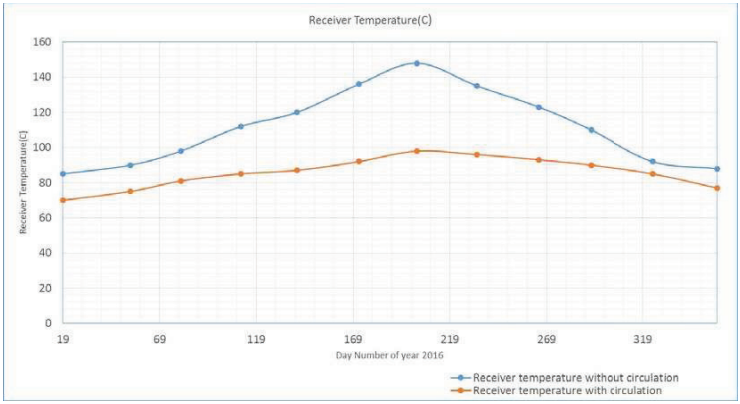


**Fig. (5.8). The collector receiver temperature at 21th of each month at 13:00 pm, with and without hot water circulation, year 2016**

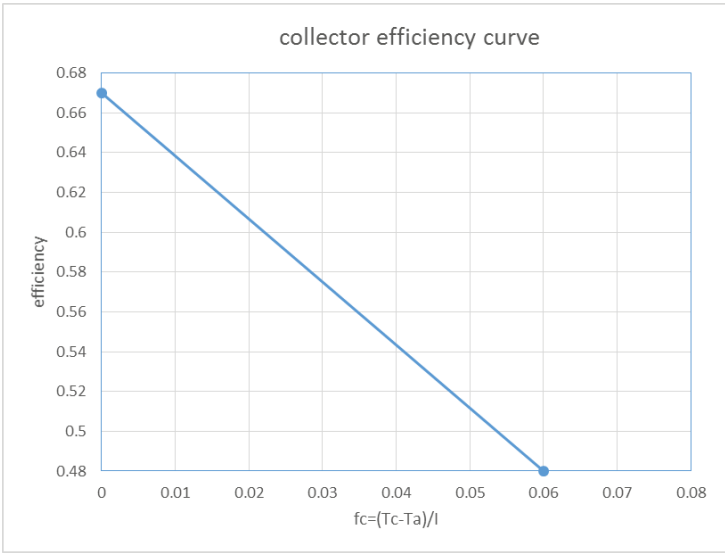


**Fig. (5.9). Experimental collector efficiency curve**

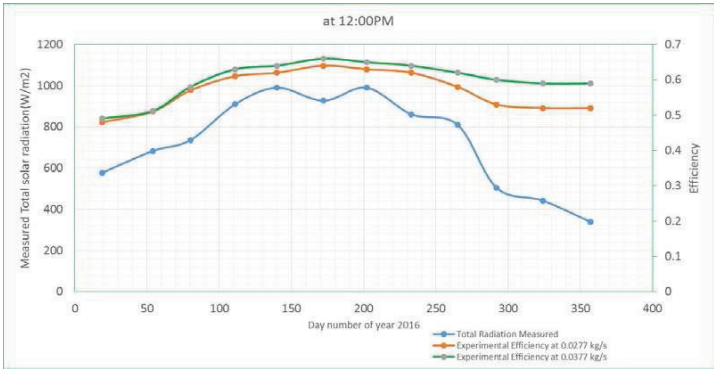


**Fig. (5.10). Efficiency of collector at different mass flow rates and measured total solar radiation at 21st for each month at 12:00 pm year 2016**

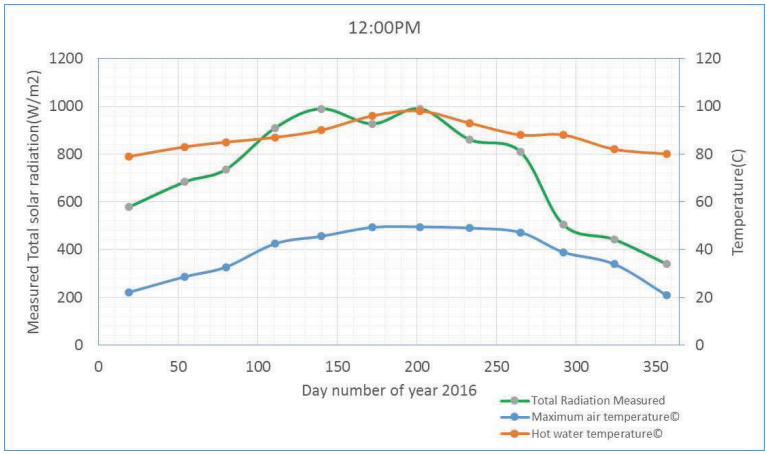


**Fig. (5.11). Measured instantaneous total solar radiation, ambient temperature and hot water temperature during year 2016**

### 5.1.3 Absorption Cooling System Loop

In this section the results of solar absorption cooling system tests are presented and discussed including both LiBr-water pairs and the diethyl ether-ethanol pairs

#### 5.1.3.1 Lithium Bromide-Water Solution Performance

The LiBr-water solution results are presented and discussed in this section. Water acts as the refrigerant and LiBr acts as the absorbent. The solution consists of 50% water and 50% LiBr by volume which means that the solution concentration is 50%. The Lithium bromide-water solution is prepared in the laboratory. The quantity required to be charged in the generator and part of the absorber unit and part of the heat exchanger is 16 liters. The solution concentration by weight is 12.8 kg, and the density of the solution is approximately 1600 kg/m$^3$. The concentration by volume is about 8 liters. The mixing process is done by mixing the lithium bromide in the distilled water with the continuous stirring during the preparation process. The lithium bromide dissolved instantaneously with slight stirring at normal condition. The process is accompanied by increase the solution temperature

is about 30 °C (exothermic reaction). The solution has been cooling to the lab temperature before charging to the generator.

**5.1.3.1.1 Variation of Temperatures and Pressures**

To evaluate the experimental solar cooling system performance with the amount of solution (lithium bromide-water) 16 liters with solution concentration 50%. During the experiments, the pressure and temperature are the main parameters, the pressure is logged every 60 seconds, and the temperature is recorded every 300 seconds. The temperatures, mass in (generator and condenser) and the pressure are measured.

**Figs. (5.12-5.14)** show that the water vapor temperature, pressure and mass within generator and condenser. The pressure and temperature of generator increase until reach the steady–state because continuous type system. The maximum pressure and temperature reach to over 7 kpa and 92°C respectively during the 21-June. Also, the maximum pressure and temperature reach to 6.6 kpa and 88°C respectively. The difference between the results of 21-June and 21-October due to the lower of solar radiation as well as the temperature of the air where the angle of declination on 21 -June is 23.45°, while on 21-October is -11.087°. The mass of the generator gradually decreases due to the process of evaporation within the generator while the mass within the condenser incrementally increases because of a condensation process. The evaporated mass is equal to the condensed mass of the condenser.

The condenser is cooled by water to increase the rate of condensation, the volumetric flow rate of cooling water (1000 L/h). The water cooling loop begins from absorber unit to the condenser unite to increase the rate of absorption in the absorber unit and the rate of condensation in a condenser unit to reach high coefficient of performance. The ambient temperature is measured at the site during the test hours. For the summer test days of the experimental part, higher temperatures are observed during

the daytime occurs between 10:30 am and 13:30 pm, since the higher measured solar radiation during the test period exhibited between 11:30 am and 13:30 pm with a peak occurring at about 11:00-12:00 o'clock. An increasing in outlet vapor temperature is noticed during early hours of the day until it reaches maximum values around solar noon when total solar radiation values are the highest. The temperature of the generator reaches 95$^{o}$C in June, July, August day, where the maximum recorded ambient temperature is 50$^{o}$C during the test. The evaporator temperature reaches 16$^{o}$C. It is noticed that the temperature inside the receiver increases as ambient temperature increases or when the solar intensity is abundant.

During the cold months as for December, January, February, the maximum pressure of released water vapor reaches to 6.5 kpa, and this value is good enough for the unit operation. Also, the temperature of the generator is more than the vapor solution temperature, since the generator represents the source of heating to the solution

**Fig. (5.15)** shows the variation of temperature difference across evaporator with daytime for the 21-June note that the process of evaporation gradually increases until it reaches its highest value at noon when the intensity of solar radiation increases and lead to raising the temperature of hot water into the generator, which leads to an increasing in cooling rate

**Fig. (5.16)** shows the increasing in generator temperature refers to the increasing the generator pressure, thus increasing the cooling rate in evaporator unit (decrease in the temperature of the evaporator). When increasing the generator temperature refers to increase the amount of water vapor release. The air temperature depends on the intensity of solar radiation, so the more solar radiation increased the temperature of the air and kept the temperature of the air high after the peak of solar radiation.

The pressure of generator, generator temperature and the evaporator temperature are (7.7 kpa, 96°C, and 16°C) respectively.

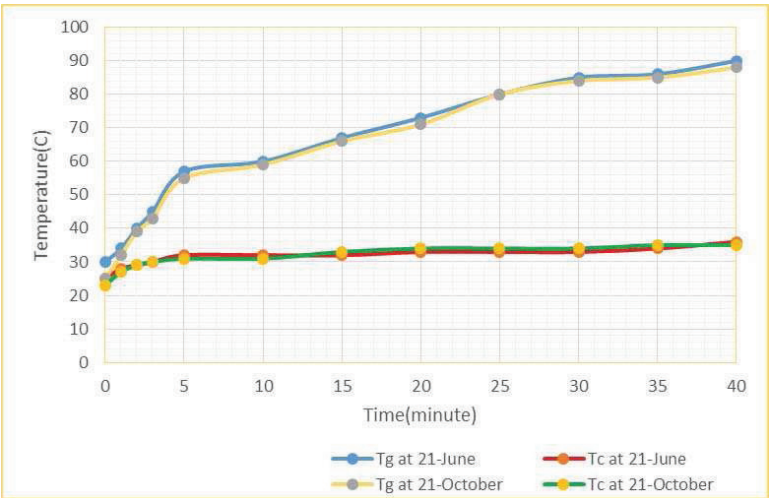


**Fig. (5.12). Measured variation of temperature of generator and condenser with time at 21th of June and October 2016**

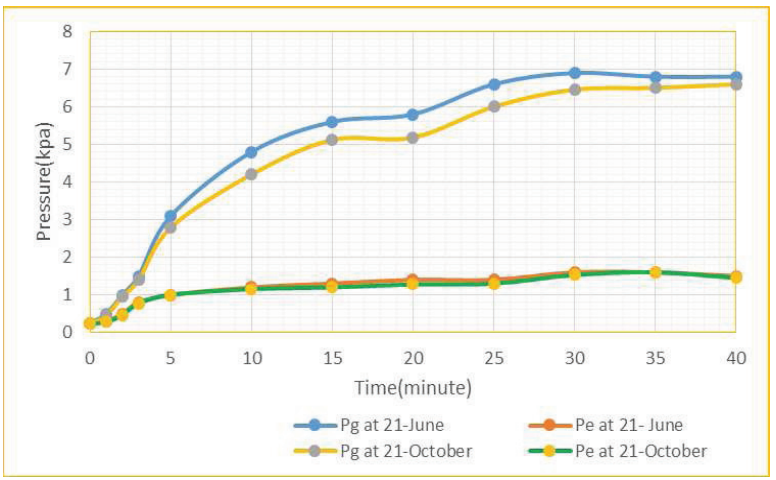


**Fig. (5.13). Measured variation of pressure of generator and evaporator with time at 21th of June and October 2016**

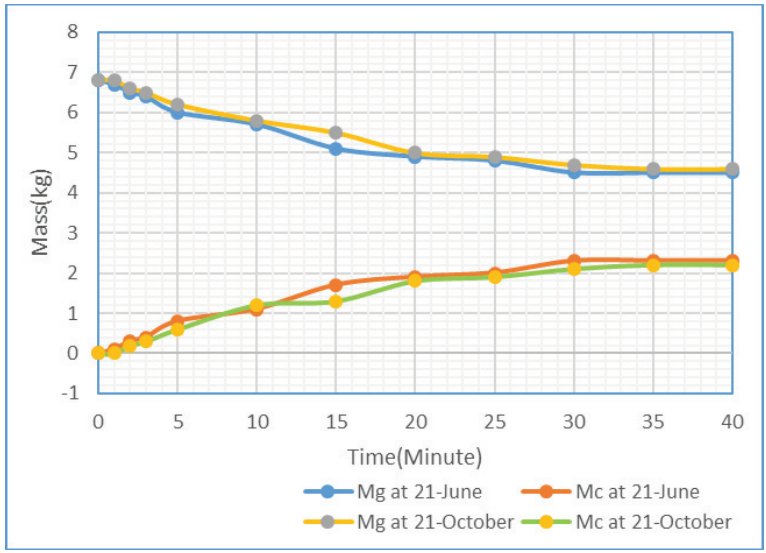


**Fig. (5.14). Measured variation of mass in generator and condenser with time at 21th of June and October 2016**

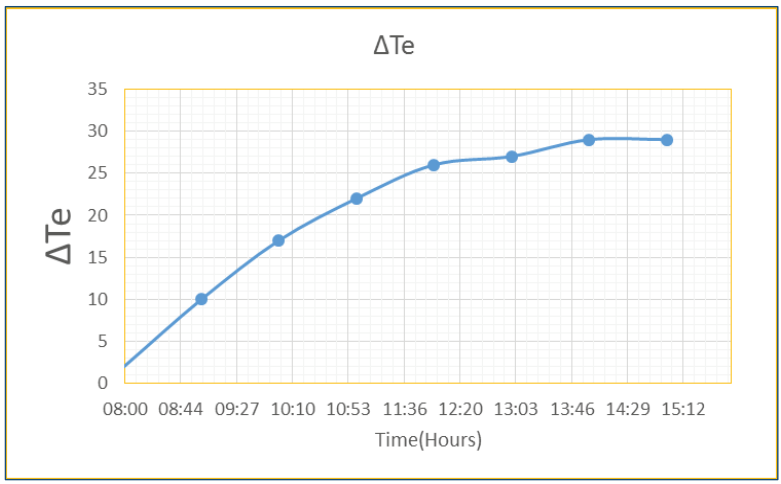


**Fig. (5.15). Measured variation of evaporator temperature with time at 21th of June 2016**

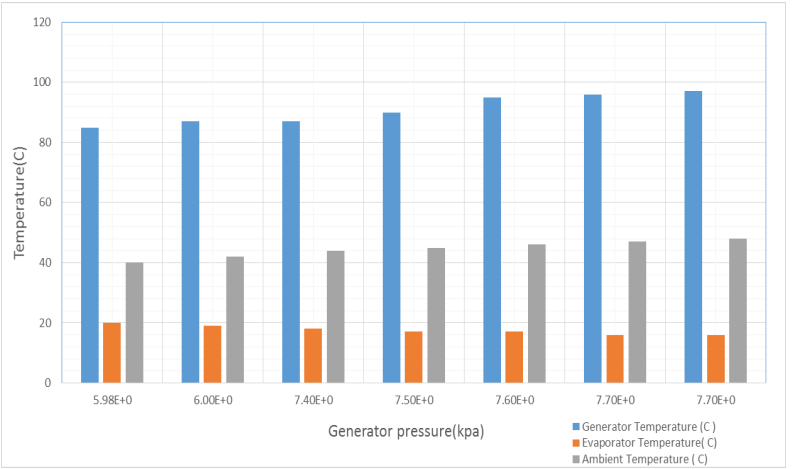


**Fig. (5.16). Measured variation of generator, evaporator and ambient temperature with generator pressure at June month, 2016**

### 5.1.3.1.2 Coefficient of Performance (COP)

The coefficient of performance of solar-powered absorption cooling system (COP) depends on the amount and the state of refrigerant (water) collected. The range of COP is (0.31-0.72) for concentration 50% (water-lithium bromide). The high concentration releases more water vapor as well as the high pressure difference between evaporator and condenser since at any refrigeration system the coefficient of performance increases with increasing the pressure difference between evaporator and condenser (or generator).

**Figures (5.17& 5.18)** show the relationship between the coefficient of performance and the temperature of the generator on 21$^{st}$June and 21$^{st}$October. These figures show the coefficient of performance increases by increasing the temperature in the generator. Note that the performance coefficient reaches its maximum value at 0.72 a temperature of 90°C on 21$^{st}$June and the performance coefficient is slightly lower than that on 21$^{st}$October 0.68. This is because of the intensity of solar radiation in October month lower than June month. The temperature must be

maintained in condenser and absorber the index to reach a high performance coefficient. Also, discussed the overall performance coefficient with the temperature of the generator and note that the overall coefficient of performance at a temperature of 90°C on 21-June is 0.42 while, on 21-October is 0.41.

The reason for increasing the coefficient of performance with high temperature of generator is to increase the evaporation rate of water vapor in generator unit.

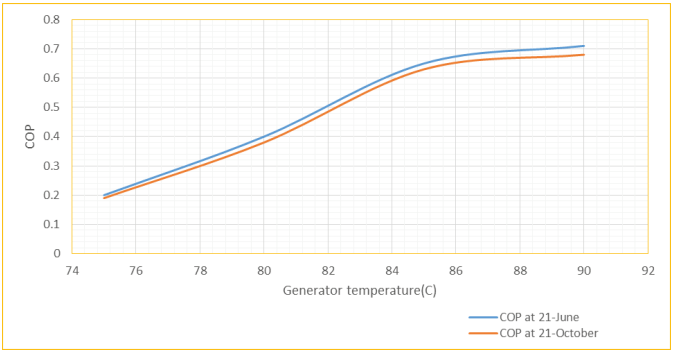


**Fig. (5.17). Experimental COP with generator temperature at 21th of June and October 2016**

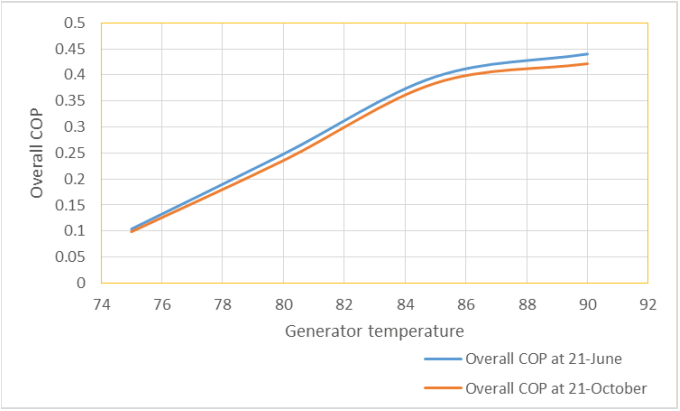


**Fig. (5.18). Experimental overall COP with generator temperature at 21th of June and October 2016**

### 5.1.3.2 Diethyl Ether-Ethanol Solution Performance

The second part of the solar absorption cooling system test is the results of the Diethyl Ether-Ethanol pair test result. The same system is cleaned and flashed by clean water from the LiBr-water solution and recharged with the new solution. The diethyl ether acts as the refrigerant, while ethanol acts as absorbent. Three mixture concentration are tested, namely 40%, 50%, 60% by volume, which means 40%, 50%, 60% of the mixture is diethyl ether. The physical properties of diethyl ether and ethanol are shown in the table below

**Table (5.1) Physical properties of diethyl ether and ethanol**

| Diethyl Ether | | Ethanol |
|---|---|---|
| Formula | $(C_2H_5)_2O$ | $C_2H_6O$ |
| Molar mass | 74.12 g/mole | 46.06844 g/mole |
| Density | 713 kg/m$^3$ | 789 kg/m$^3$ |
| Normal boiling point | 34.6°C | 78.37°C |
| Normal melting point | -116.3°C | -114.1°C |
| Enthalpy change of vaporization | 27.530 kJ/mol at 11.85°C<br>27.247 kJ/mol at 22.48°C | +38.56 kJ/mol |

The diethyl ether-ethanol is prepared in the laboratory. The boiling temperature of diethyl ether is 34 ºC.to prevent evaporation the diethyl ether in lab temperature put the diethyl ether bottles in ice box to drop the temperature. Also, drop the temperature the unit of absorption system. After the temperature is lowered mixing with ethanol according to concentration is selected. The quantity of solution required in absorption cooling system is 16 liters.

After reach the cooling temperature of diethyl ether to 14ºC mixing with ethanol and continuous stirring in order to give homogenous solution according to concentration is selected. The quantity of solution required in absorption cooling system is 16 liters.

**5.1.3.2.1 Variation of Temperatures, Pressures and Coefficient of Performance (COP)**

**Figs. (5.19-5.20**) show diethyl ether vapor temperature and pressure increases with increment of the solar radiation during 21-July. The maximum pressure and temperature reaches to over 3.1 bar and 71$^{o}$C respectively during summer season. For the summer test days of the experimental part, higher temperatures are observed during the daytime occurs between 10:30 am and 12:30 pm. An increasing in outlet vapor temperature is noticed during early hours of the day until it reaches maximum values around solar noon when total solar radiation values are the highest. After that at the afternoon, outlet vapor temperature decreases due to the increase in the incident angle which causes a decreasing in solar incident on the module. The temperature of the generator reaches 71$^{o}$C in June, July, August day, where the maximum registered ambient temperature is 43$^{o}$C during the test.

**Fig (5.21)** shows the generation temperature of released diethyl ether vapor is low due to the high amount of the diethyl ether vapor released at high concentration, while the low concentration needs more temperature to begin releasing diethyl ether vapor due to the high amount of ethanol in the low concentration solution. The increase of ethanol concentration in the solution leads to high boiling temperature for the solution.

**Fig (5.22)** shows that high pressure at high concentration and vice versa, since the high amount of diethyl ether vapor released at high concentration. The different in pressure and temperature for the same concentration depends on weather conditions due to the different days in July for tests.

**Fig (5.23)** shows the (COP) for the solar continuous absorption system operating with diethyl ether-ethanol solution for different solution concentrations (40%, 50%, and 60%). It can be observed that high performance is obtained at high concentration due to large amount of

diethyl ether vapor produced. The range of COP is 0.57-0.81. The high concentration gives more released diethyl ether as well as large pressure difference between evaporator and condenser, since at any refrigeration system the coefficient of performance increases with increasing the pressure difference between evaporator and condenser (or generator). The evaporator pressure from (0.37-0.7) bar, the evaporator temperate range (20 -9) °C

**Fig (5.24)** shows the variation of evaporator temperature with daytime for the 21-July note that the process of evaporation gradually increases until it reaches its highest value at afternoon when the intensity of solar radiation increases and lead to raising the temperature of hot water into the generator, which leads to an increase in cooling rate**.**

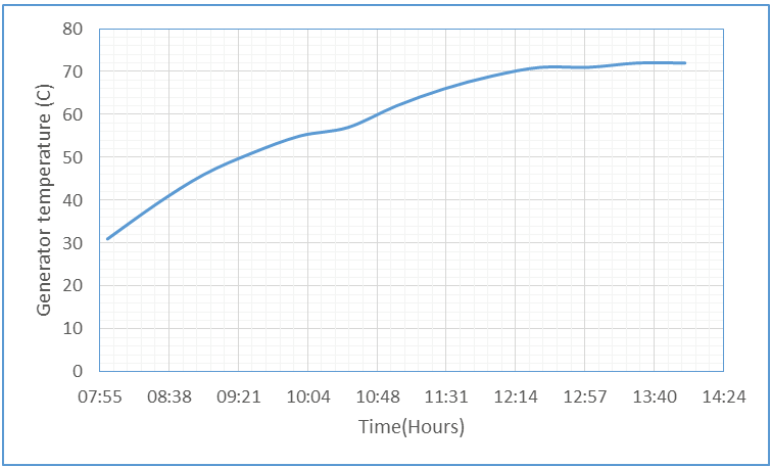


**.Fig. (5.19). Experimental generator temperature with time at 21th of July 2016**

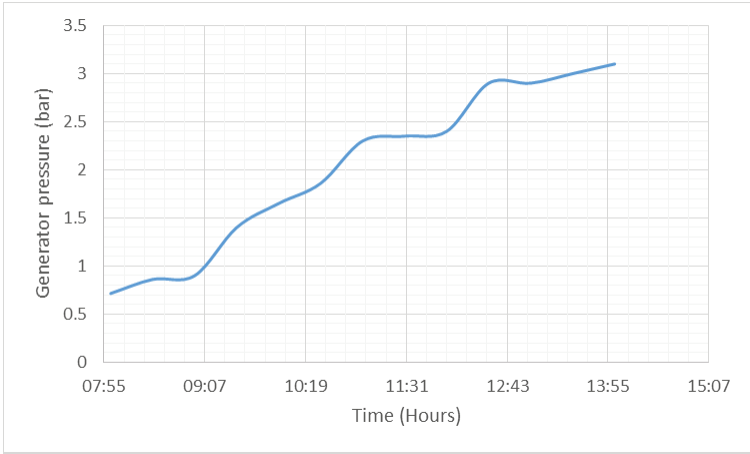


**Fig. (5.20). Experimental generator pressure with time at 21th of July 2016**

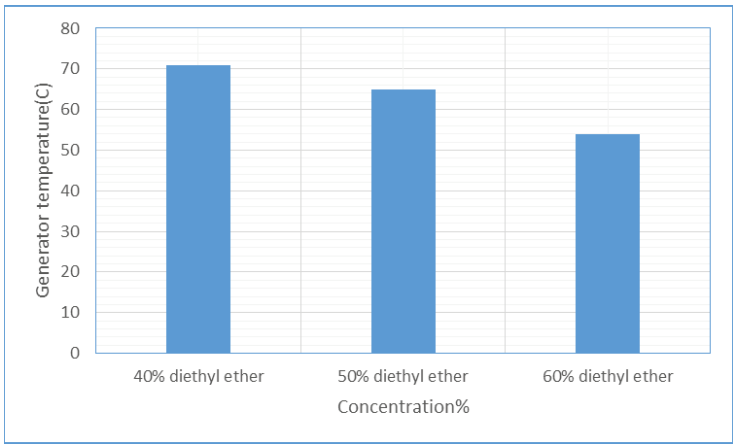


**Fig. (5.21). Measured generator temperature with different concentration of diethyl ether (July 2016)**

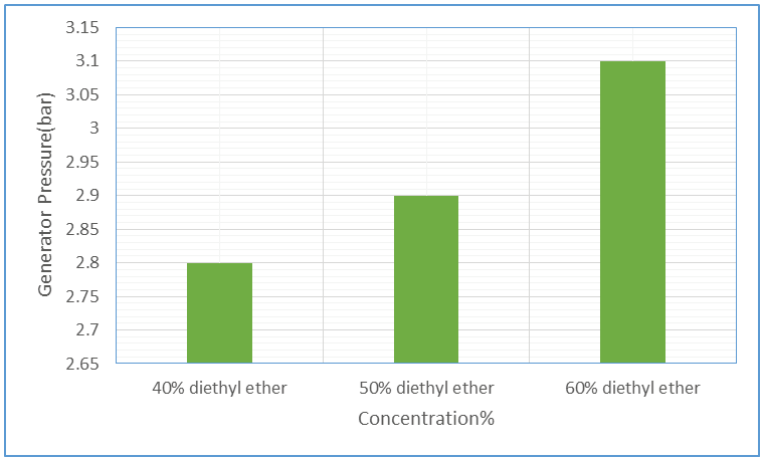


**Fig. (5.22). Measured generator pressure with different concentration of diethyl ether (July 2016)**

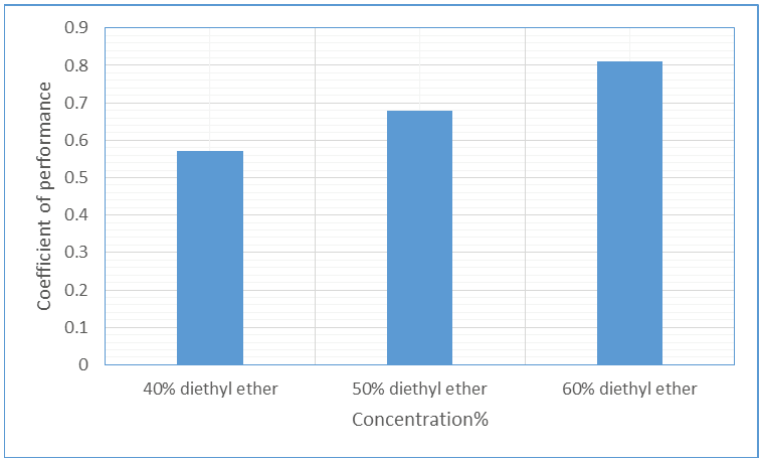


**Fig. (5.23). Measured coefficient of performance with different concentration of diethyl ether (July 2016)**

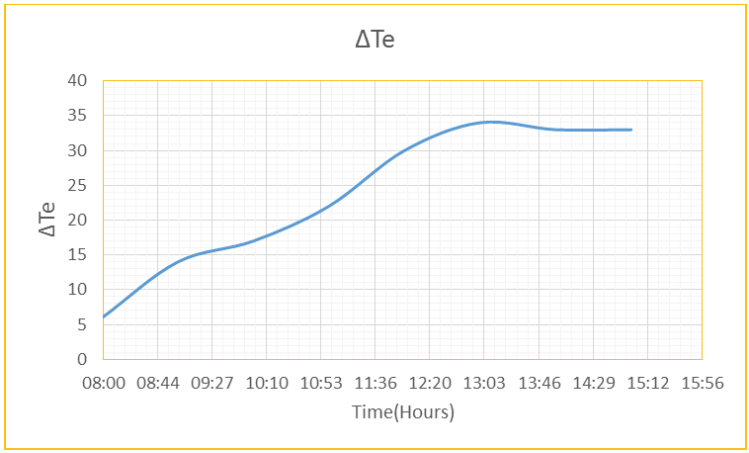


**Fig. (5.24). Measured variation of evaporator temperature with time at 21th of July 2016**

## 5.2 Theoretical Results.

The theoretical results include the prediction of total incident solar radiation, the solar angle, the collector loop performance and the solar absorption cooling system performance. The prediction of performance involved the solution of the governing equation (mass and energy conservation) for each system component. The results are validated and compared with corresponding measured results.

### 5.2.1. Total Solar Radiation

**Fig. (5.25)** shows the predicted annual maximum daily solar radiation. Fig. shows that the maximum annual daily solar radiation is obtained during summer months since solar radiation is incident at month normally on earth surface. The fig. also shows comparison between measured and predicted annual maximum daily solar radiation. The comparison indicates good agreement which also proves the validation of the predicated results. The maximum solar radiation occurs in 21-June is (983.182W/$m^2$) and minimum solar radiation in 21-December is (370.057 W/$m^2$). The predicted and measured total solar radiation for the 21st day of June month are (983.182

W/m$^2$ and 927 W/m$^2$) respectively. The calculated solar radiation value is slightly higher than the radiation measured by 5.7%.

**Fig (5.26)** presents the daily variation of direct normal solar radiation for the 21$^{st}$ day of each month during year 2016. The figure shows that June, July has the highest value of direct normal solar radiation which reaches 950 W/m$^2$. These results indicate that solar radiation may satisfy the power demands of the following applications: -solar heating, solar refrigeration, and conditioning, solar desalination, solar photovoltaic, etc.

**Fig. (5.27)** shows the variation total solar radiation, beam solar radiation, diffuse solar radiation and elevation angle during year for 21$^{st}$ for each month at 12:00pm. The total solar radiation increases when increasing the elevation angle. Also, the diffuse radiation and beam solar radiation increased. The maximum value of elevation angle at 21-June (80.99°) and total solar radiation, beam solar radiation and diffuse solar radiation (983.182 W/m$^2$,861.912 W/m$^2$ and 127.27 W/m$^2$) respectively. The minimum values of elevation angle, total solar radiation, beam solar radiation and diffuse solar radiation occur on 21-December (34.146°, 370.057 W/m$^2$, 307.78 W/m$^2$ and 62.277 W/m$^2$) respectively.

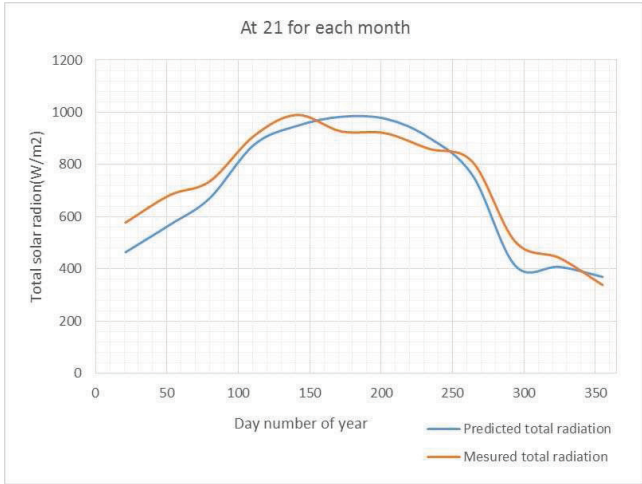


**Fig. (5.25). Annual max. Daily radiation the measured total solar radiation and predicted at 21th of each month**

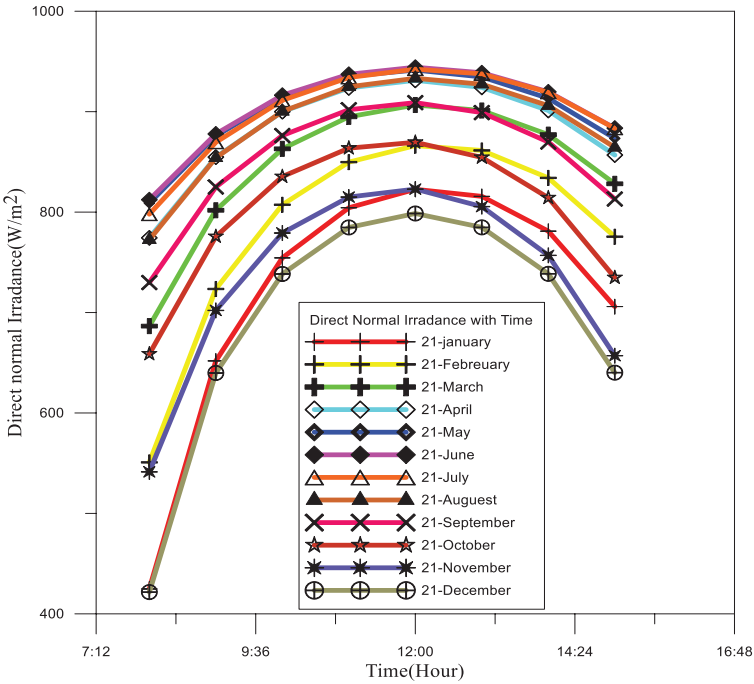


**Fig. (5.26) Variation Direct Normal solar radiation for the 21th day of each month, year 2016**

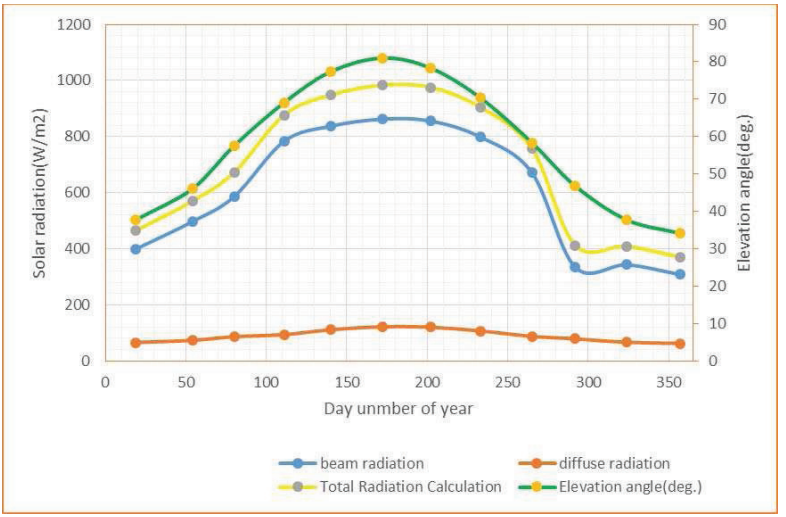


**Fig. (5.27) Total solar radiation, beam solar radiation, diffuse solar radiation and elevation angle for the 21th day of each month at 12:00pm, year 2016**

### 5.2.2. Solar Angles

The sun location varies in the sky from day to day and from hour to another. The earth rotates every 24 hours about its axis, which is tilted at an angle various from (-23.45 to +23.45) degree to the plane of the ecliptic. The earth moves around the sun in the elliptical shape, and the earth makes a revolution around the sun yearly. It is well known that the sun is at its high position in summer than in winter. All the above facts make the relative motions of the sun and earth are not simple, but predictable. The solar azimuth angle is the compass direction from which the sunlight is coming or is the angle of the sun rays measured in the horizontal plane from the south for the Northern Hemisphere or from the north for the Southern Hemisphere (Negative in the morning and positive afternoon). The daily variation of azimuth angle is shown in **Figs (5.28-5.31)**. The value of solar azimuth angle varies from 76.285° to 282° (deg. CW from N) during 21-June month, while the values of 21-December are from 117.51° to 242.31° (deg. CW from N) depends on the length of the day and local time. Also, the figs show the

elevation angle and the zenith angle Also, the figures show the sunrise, sunset and solar noon (5.45 am, 11.54 am and 5.51 pm) for 21/9/2016 as a sample.

Another important angle in the design of a solar system is the maximum elevation angle (α), which is, the maximum height of the sun in the sky at a particular time of the year. The maximum elevation angle occurs at solar noon and depends on the latitude angle (Φ) and declination angle (δ), as shown in the **Fig. (5.32)**. The figure indicates that the maximum elevation angle varies from 34.146$^{o}$ in 21-December to 80.99$^{o}$ in 21-June. The elevation angle increases directly with declination angle.

The zenith angle ($\theta_z$) is the angle between the solar ray and the vertical normal to the horizontal plane. The zenith angle is related to the elevation angle, but it is measured from the vertical rather than from the horizontal, thus making the zenith angle = 90° - elevation.

Also, the **fig. (5.32)** shows that as the season changes from Winter to Spring and then to Summer, the sunrise and sunset points move gradually northward along the horizon. In summer season especially May, June, July, August, the day gets longer as the sun rises earlier and sets later. The solar azimuth angle, elevation angle, and zenith angle describe the sun position in the sky fully.

**Figs (5.32, 5.33)** show the maximum elevation angles at June and July with minimum zenith angle for the same months. Also, the above figures show that December and February have the minimum elevation angle. So, it is essential for any solar study to know the location of peak solar radiation and time during the day.

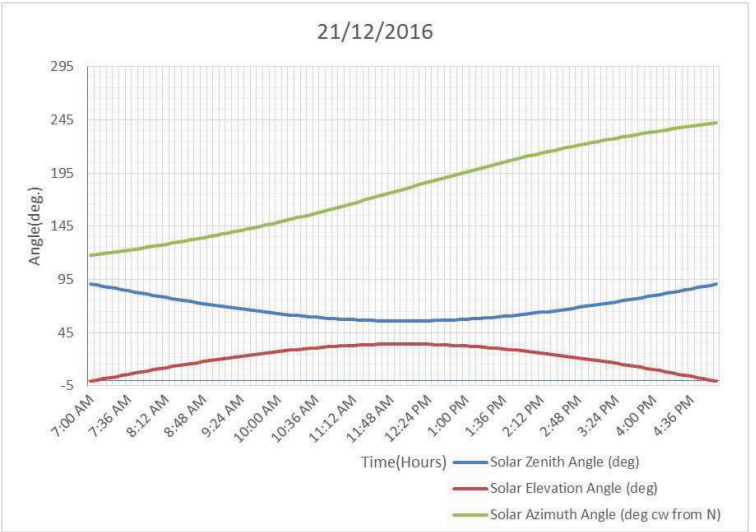


**Fig. (5.28) Azimuth angle, zenith angle and elevation angle calculation for 21-December year 2016**

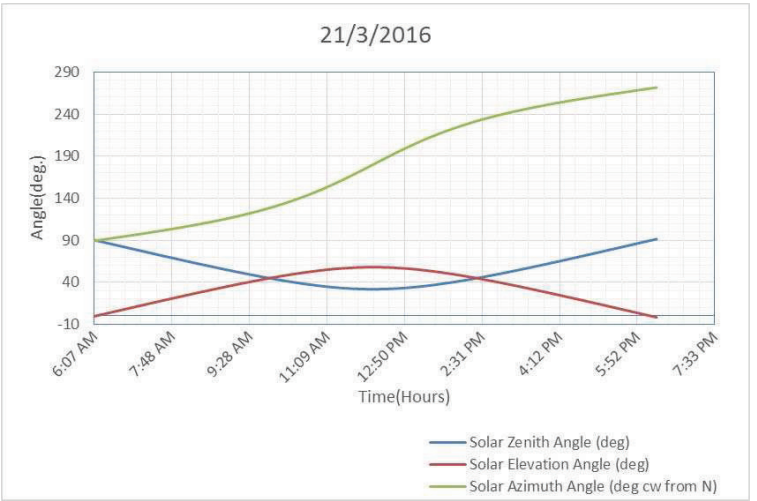


**Fig. (5.29) Azimuth angle, zenith angle and elevation angle calculation for 21-March year 2016**

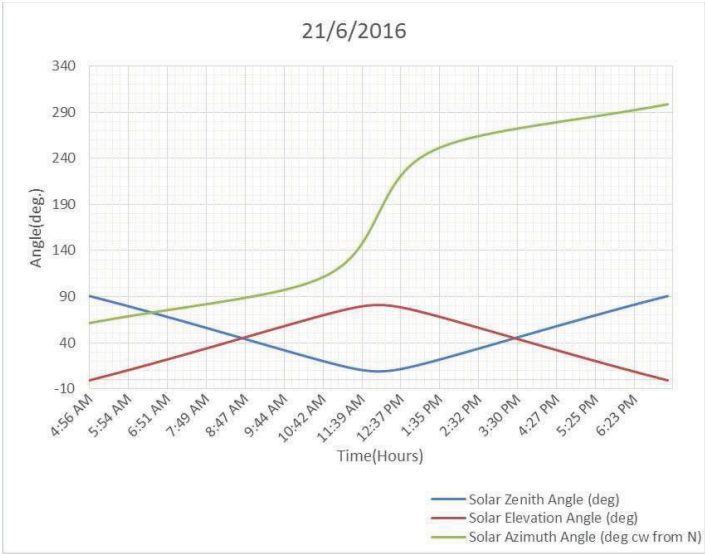


**Fig. (5.30) Azimuth angle, zenith angle and elevation angle calculation for June 21 year 2016**

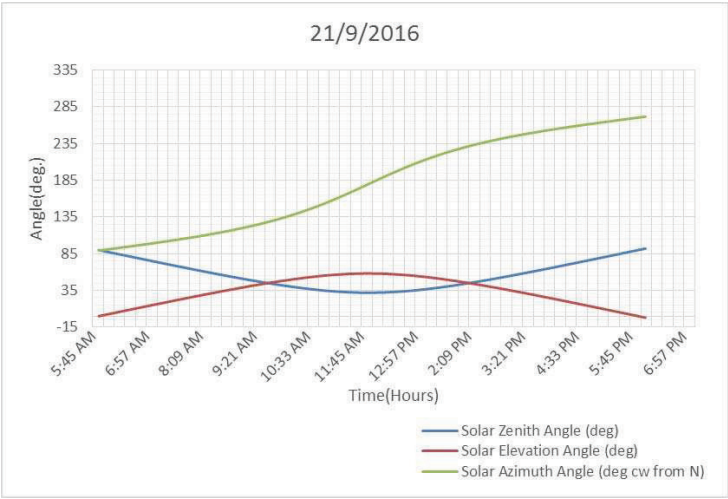


**Fig. (5.31) Azimuth angle, zenith angle and elevation angle calculation for 21-September year 2016**

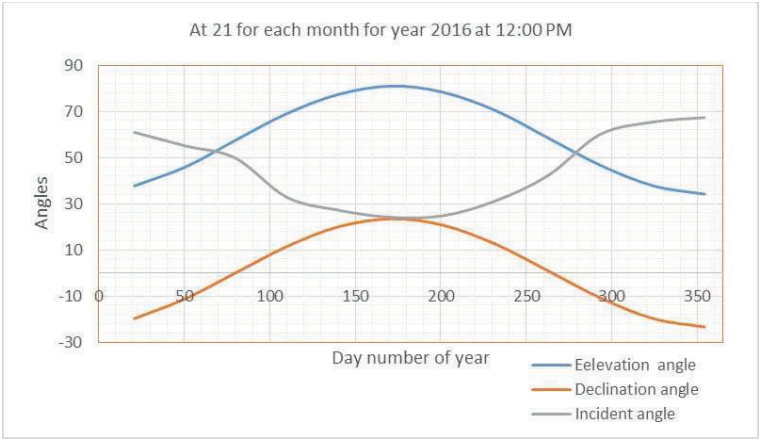


**Fig. (5.32) Incident angle, Declination angle and elevation angle calculation at 21st for each month for year 2016**

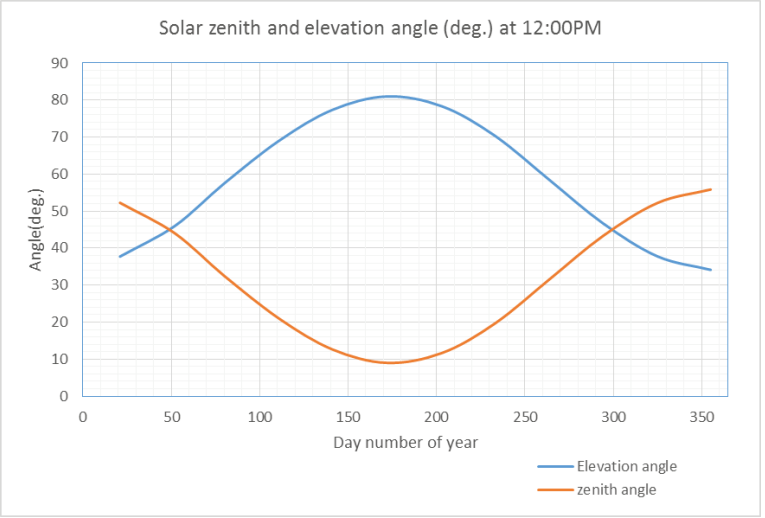


**Fig. (5.33) Zenith and elevation angle calculation at 12:00pm for year 2016**

### 5.2.3 Collector Loop Performance

The performance of the solar collector is analyzed theoretically. **Fig. (5.34)** shows the total solar radiation, useful heat and absorbed radiation during the year 2016 at 21st.The absorptivity of receiver, effective transmissivity and transmissivity of the cover are effected parameters on the absorbed radiation. At 21-June the total solar radiation is (983.182W/$m^2$) and absorbed radiation (694.14W/$m^2$). **Fig. (5.35)** shows the fraction of useful heat from total solar radiation. The higher fraction at noon (0.642). **Fig. (5.36)** illustrates the variation of mean temperature with useful heat at a different mass flow rate. The figure shows increasing mass flow rate refers to increasing useful heat and decreasing mean temperature. **Fig. (5.37**) shows comparison between theoretical and experimental efficiency of the collector at mass flow rate 0.0277 kg/s. The figure shows the theoretical efficiency range from (0.68 to .72) and experimental efficiency form (0.48 to 0.68). **Fig (5.38)** shows the predicted and measured with useful heat at different mass flow rate at 21st of each month year 2016. **Fig (5.39)** shows the predicted solar radiation with hot water temperature with time at 21-July, the year 2016.The fig. shows when increasing total solar radiation increase hot water temperature refers to increasing absorbed solar radiation. Also, the figure shows the hot water temperature variation for the solar-powered absorption cooling system for the day 21th of June. It can be observed that the maximum temperature of hot water reaches to (371 K)). The figure also shows that the maximum total solar radiation and absorbed radiation at 11:00 A.M are 983.182W/$m^2$ and 694.14W/$m^2$, respectively. The predicted and measured total solar radiation are 983.18 W/$m^2$ and 927W/$m^2$ respectively at the same day (21th June) with error percentage 4.6%. The reason for the difference in early hours of the day, since the solar refrigeration system works under real conditions such as wind, dust, variation in solar radiation as well as a change in environment temperature.

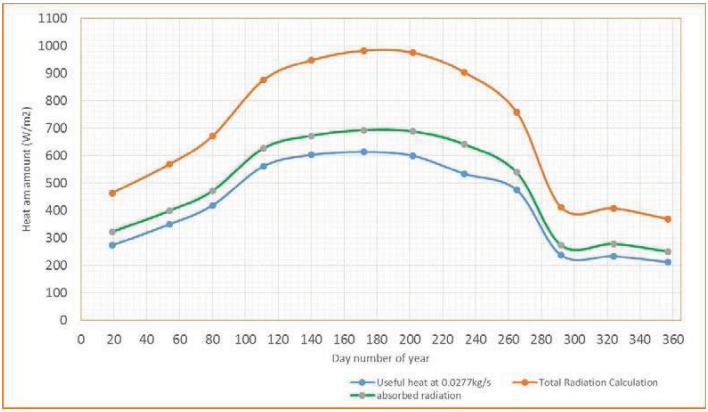


**Fig. (5.34) Total solar radiation, absorbed radiation and useful heat at different mass flow rate at 12:00pm for year 2016**

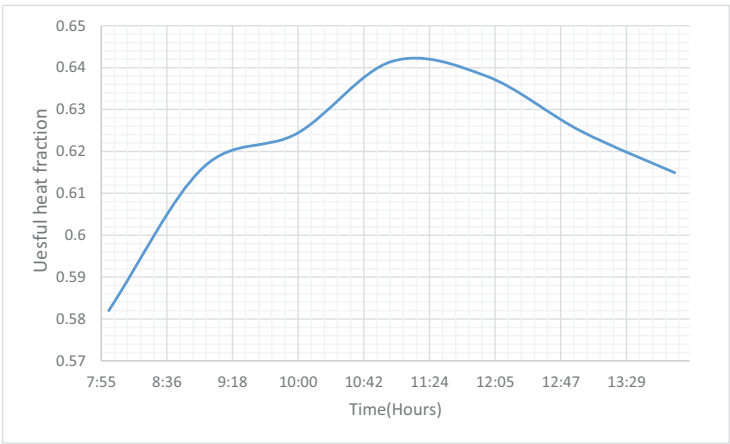


**Fig. (5.35). Useful heat fraction from total solar radiation during June month year 2016**

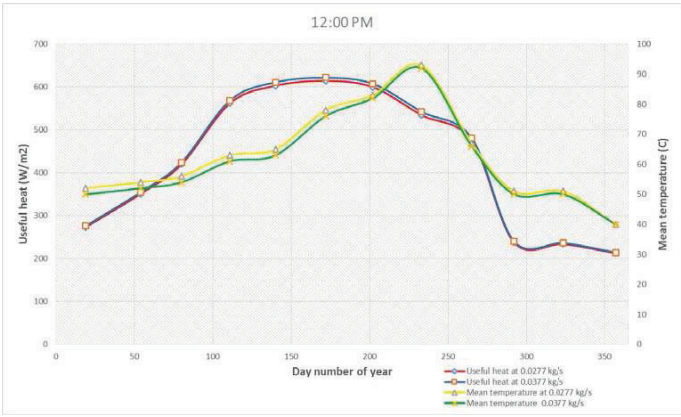


**Fig. (5.36). Useful heat and mean temperature during year 2016 at 21st for each month.**

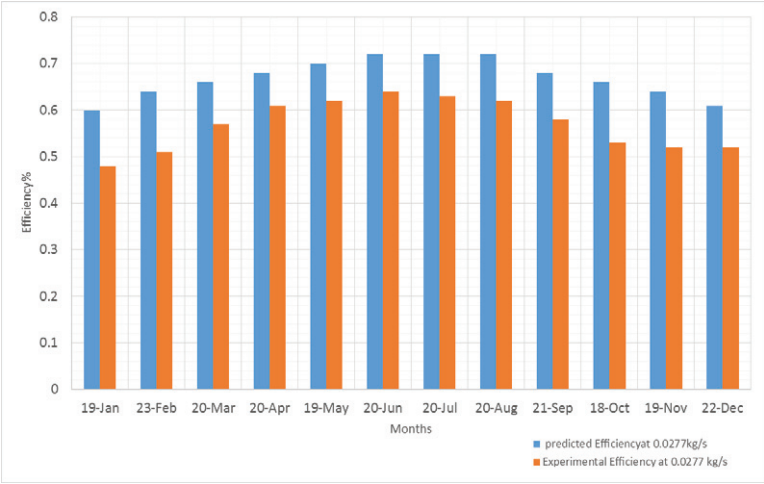


**Fig. (5.37). The theoretical and experimental efficiency of collector at mass flow rate 0.0277kg/s.**

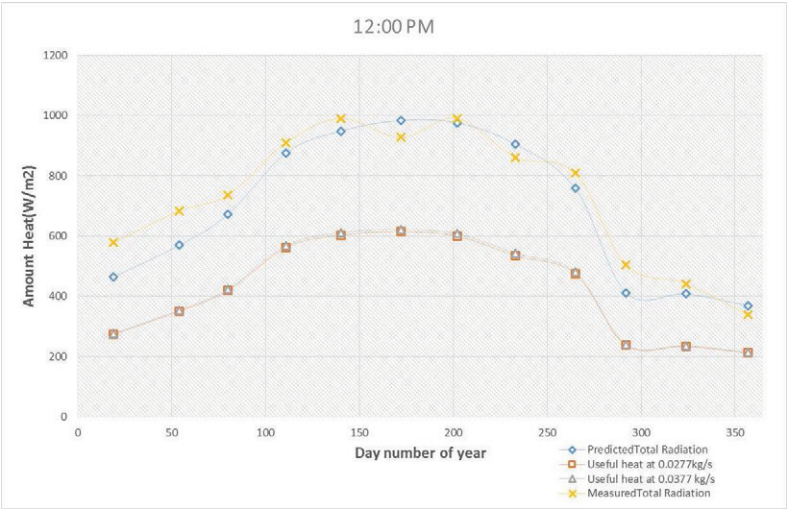


**Fig. (5.38). The total radiation measured and predicted with useful heat at different mass flow rate at 21th of each month, year 2016**

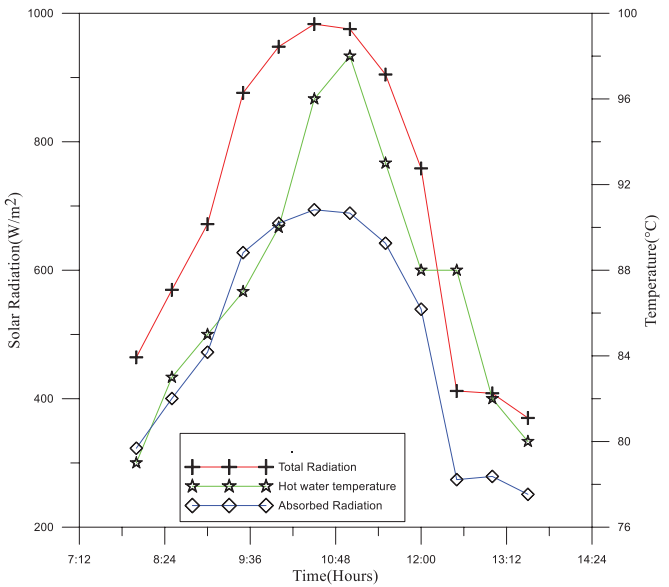


**Fig. (5.39). Predicted solar radiation and hot water temperature with Time at 21th of June 2016**

### 5.2.4 Absorption cooling system performance

**Fig. (5.40)** shows the COP and circulation ratio (mass flow rate of refrigerant/mass flow rate of strong solution) with absorber temperature. The figure shows that as the absorber temperature increases the COP decreasing which the circulation ratio increases because when the temperature of absorber increases the absorption process in absorber unit is incomplete (small heat rejected from absorber unit). In the absorber, the concentrated solution is brought into contact with the vapor supplied by the absorption process occurs if the absorber is cooled by an external sink.

**Fig. (5.41)** shows the effect of absorber temperature on heat rejected from absorber and lithium bromide concentration in the absorber. When the absorber temperature increases the concentration of lithium bromide increases because incomplete absorption process occurs in absorber while the heat rejected is decreased. When the absorber temperature increases, the generator thermal load increase with a constant evaporator thermal load, therefore the COP decreases. It is shown that the decreasing of the absorber temperature causes significant increasing in COP.

**Fig. (5.42)** shows the effect absorber temperature on the heat amount from generator, condenser, evaporator and heat exchanger. When the temperature of absorber increases the absorption process inside absorber is incomplete. The increasing in the temperature of the absorber unit refers to increase the temperature of the solution lithium bromide- water inside the absorption unit and thus affects the absorption process between the evaporator unit and the absorber unit. The amount of solution that goes into the generator has a strong solution, and thus the amount of transfer heat to the solution is small, which affects the process of evaporation.

**Fig. (5.43)** shows the effect of the temperature condenser on the coefficient of performance and circulation ratio. The high temperature of

condenser lead to the exchange of heat between the cooled water and steam is a little, and thus the process of condensation is incomplete. Which leads to a low coefficient of performance. **Fig. (5.44)** shows the relationship between the pressure and the temperature in the generator for the diethyl ether. The high temperature in the generator leads to the generation of steam, and the temperature of the boiling point of Diethyl ether is low, so the steam pressure is high by evaporating a high quantity of steam inside the generator unit.

**Fig. (5.45)** shows the variation of the exergy loss rate of the different components. As shown in the figure, the absorber has highest exergy loss rate among the different components. The worst component from the viewpoint of the exergy loss rate in the single- effect system is the absorber followed by the condenser, evaporator, solution heat exchanger and the generator. That shows the absorber is the component needs the maximum improvement in design to reduce the exergy loss rate and so reduces the irreversibility.

**Fig. (5.46)** shows generator temperature effects the ECOP. It can be seen that the trend of the ECOP is not similar to that of the COP. The ECOP increases first and then decreases with a further increasing in the generator temperature. By expanding the generator temperature, the amount of exergy entering the system is increased. This causes more steam to separate from the LiBr-water solution. This increases the refrigerant flowrate, and exergy leaves the system. Although this has a positive effect on the system, the temperatures of the condenser and absorber are increased with this effect. The results of this effect cause the destruction of exergy in the cycle and decrease the ECOP. Therefore, at the beginning of the cycle, ECOP increases with the increasing in generator temperature, but gradual destruction of exergy causes the ECOP to decrease.

**Fig. (5.47)** shows the difference of lower temperature in evaporator unit with time during June 2016.Also, the figure explains different working fluid pairs, i.e. (Diethyl ether–ethanol and lithium bromide-water). The difference of lower temperature in Diethyl ether-water is higher than lithium bromide-water at the same concentration 50%. The duration of evaporation of diethyl-ether is less than the period of evaporation of pure water because the degree of boiling diethyl- ether is 34 while the boiling water level is less than 100. The system in the case of lithium-bromide-water operating under vacuum pressure so that the amount of steam released in case diethyl-ether is higher than water and therefore the cooling rate is higher, also higher the coefficient of performance is shown in **fig. (5.48)**

**Fig. (5.49-5.50)** show the comparison between theoretical and experimental the coefficient of performance for solar powered absorption cooling system. The comparison is achieved for different days of June with 16 liters of lithium bromide-water. The experimental COP is between "0.35 to 0.72" while the theoretical COP is between "0.39 to 0.76". The experimental performance for the present study satisfies the results of another researcher such as **[20] and [73]** who built and tested a purpose designed solar diffusion absorption refrigerator. The COP of **[13]** is lower than another researcher because the system is intermittent solar absorption system and a small quantity of ammonia.

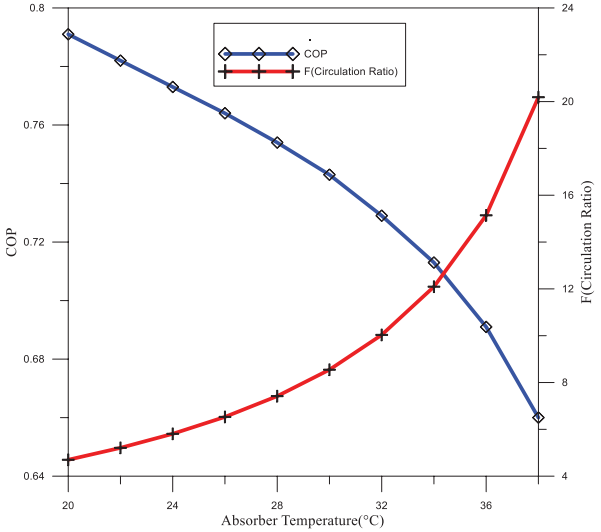


**Fig. (5.40). COP of the absorption cooling system and the circulation ratio with absorber temperatures**

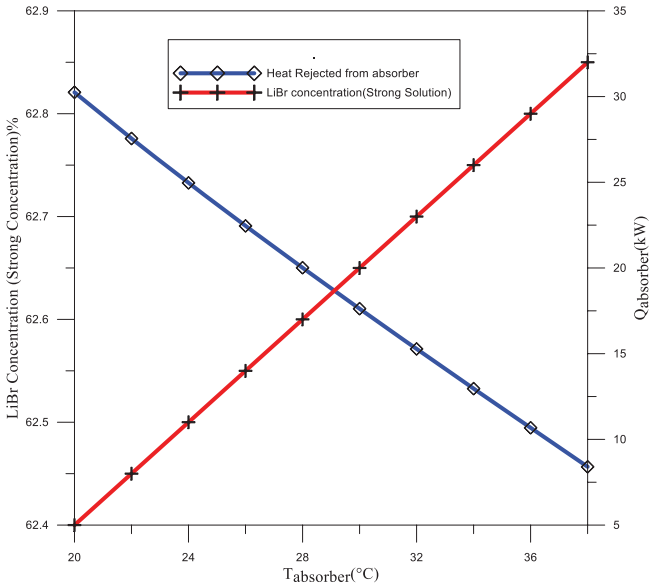


**Fig. (541). Heat rejected from absorber unit and LiBr concentration (strong solution) with absorber temperatures**

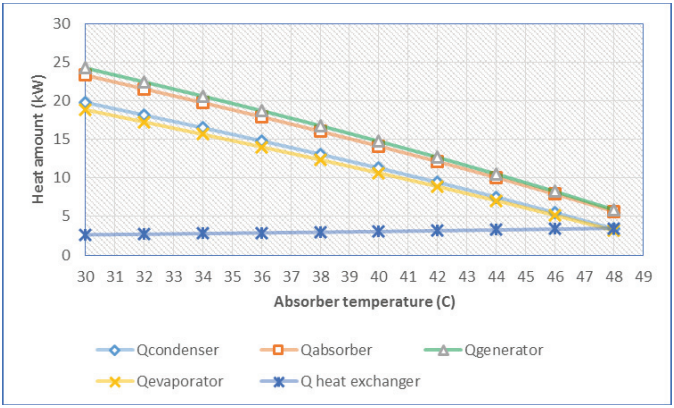


**Fig. (5.42). Heat amount with absorber temperatures**

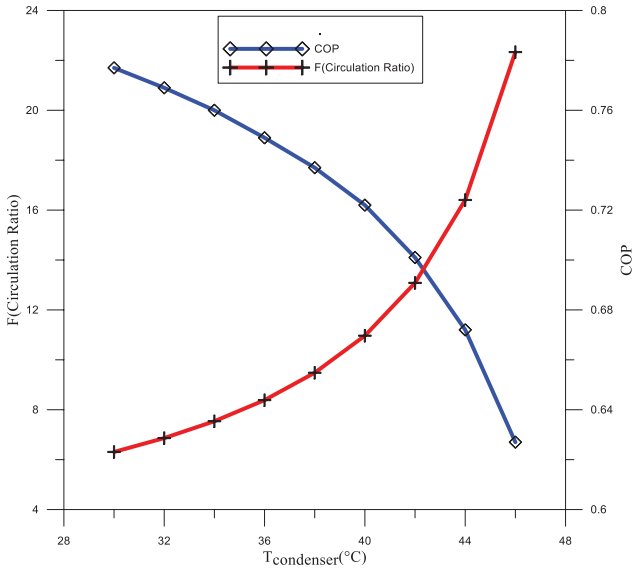


**Fig. (5.43). COP of the absorption cooling system and the circulation ratio with condenser temperatures**

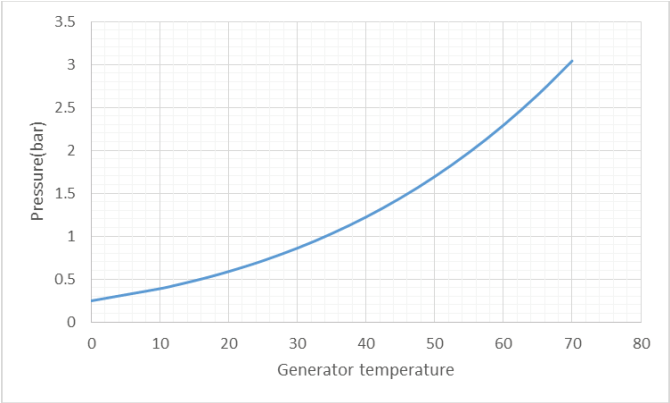


**Fig. (5.44). Generator pressure vs generator temperature for Diethyl ether**

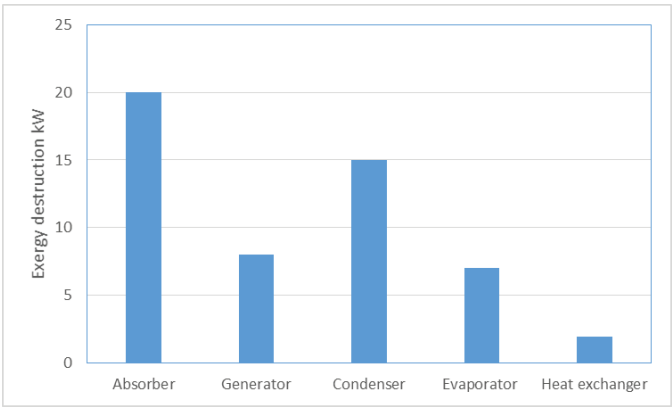


**Fig. (5.45) Exergy losses in components**

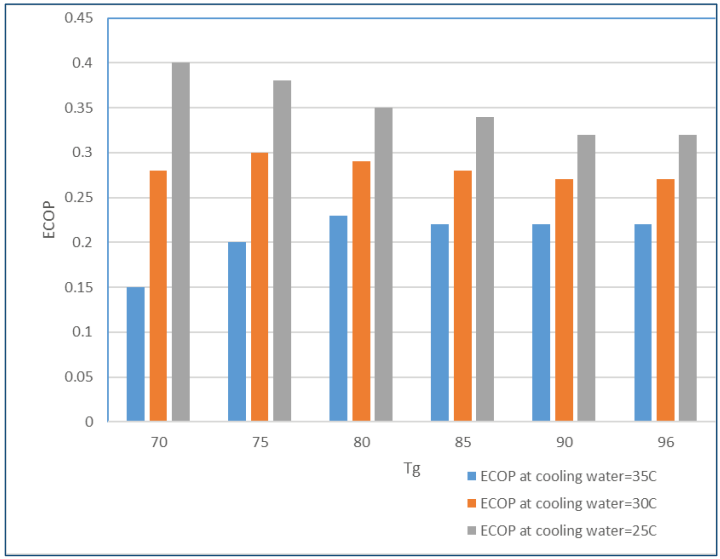


**Fig. (5.46) Exergy efficiency of the absorption refrigeration system with the generator temperature for different cooling water temperatures**

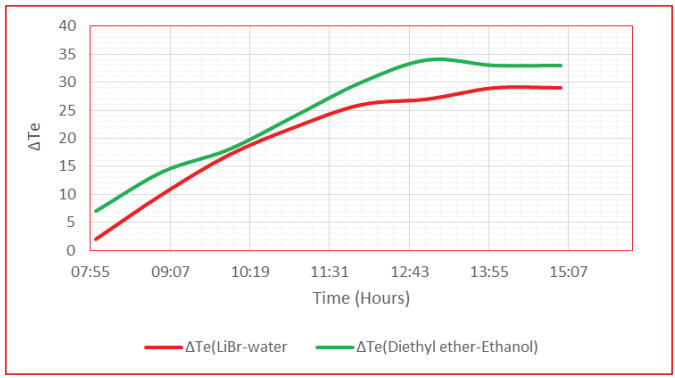


**Fig. (5.47) Comparison between evaporator temperature difference with time for (Diethyl ether-ethanol) and (Lithium bromide-water) at same concentration 50% for June 2016**

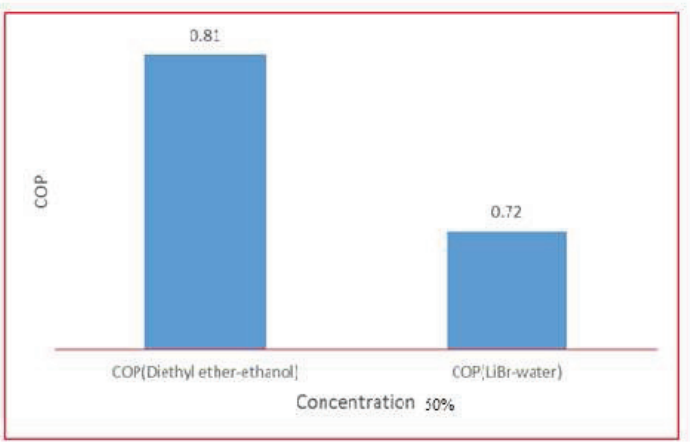


**Fig. (5.48) Comparison between COP with concentration (Diethyl ether-ethanol) and (Lithium bromide-water)**

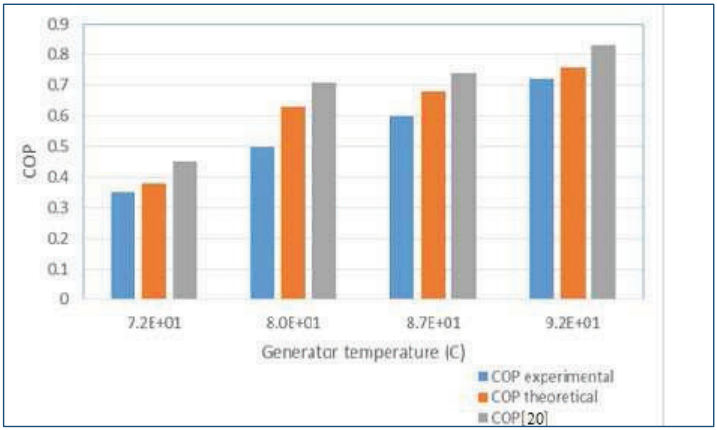


**Fig. (5.49). Comparison between experimental, theoretical and reference [20] with generator temperature**

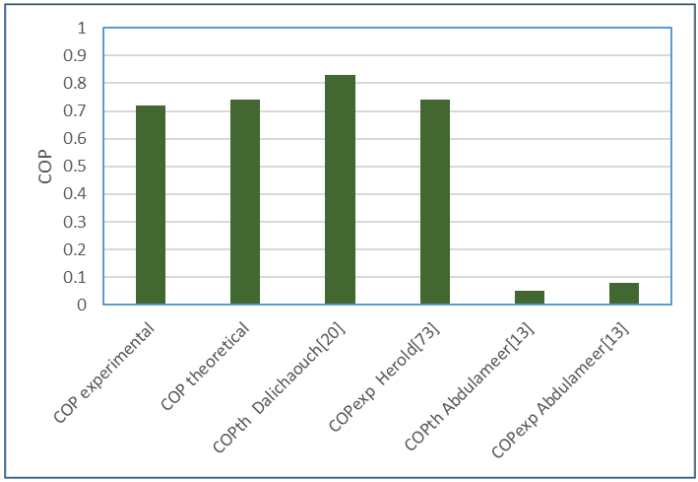


**Fig. (5.50). Comparison between experimental, theoretical COP for lithium bromide-water and references [20], [73] and [13]**

# CHAPTER SIX
# CONCLUSIONS AND SUGGESTIONS FOR FUTURE WORK

## 6.1 Conclusions

The solar energy uses for cooling purposes is an attractive prospect; the key factor for this application is the availability of solar energy for a specific location and climate and suitable cooling technology. Currently, flat plate or compound parabolic concentrator collectors with absorption cooling technology could be used for solar cooling systems, as an alternative to fossil fuel-based conventional electrical powered cooling systems. For hot climates like Iraq, a solar cooling system could be a sustainable, clean, and viable system to meet cooling energy demand. The following conclusions have been drawn from the results of the present study:

1. The compound parabolic concentrator (CPC) is efficient for solar powered absorption cooling system working in conditions as Iraq weather during summer and winter seasons.

2. The continues absorption cooling system using two pairs as a working fluid (lithium bromide –water and diethyl ether-ethanol) with the high, released amount of (water or diethyl ether) vapor is possible to satisfy the home requirement in the rural area.

3. The increasing in the amount of (water and diethyl ether) vapor released for the new amount of working pair fluids is possible at current weather conditions due to high temperature and pressure.

4. The increasing in the refrigerant concentration in solution leads to release more (water and diethyl ether) vapor at the generator supports refer to the increasing in the coefficient of performance by increasing the pressure difference between condenser and evaporator.

5. The absorption cooling system work at the range of temperature (65-95) °C is suitable in the hot area

6. The proposed working pair (Diethyl ether –Ethanol) can act as a working pair for absorption refrigerator.

7. When employing the recommended pair, an absorption refrigeration system has the requirements of mild pressure and a low-temperature heat source

8. The new couple (Diethyl Ether –Ethanol) can provide cooling at temperatures lower than that be supplied by LiBr-$H_2O$, i.e. (9°C for Diethyl ether-ethanol and 16°C for LiBr-$H_2O$)

9. (Diethyl Ether –Ethanol) No vacuum is needed as in the case of water-lithium bromide

10. The low pressure is 1 atm, and the high pressure is 5 atm (moderate pressure) for (Diethyl Ether –Ethanol).

11. The cooling of condenser can be carried out using ambient air, as with water (Diethyl Ether –Ethanol) pair.

12. The COP is found (0.31-0.72) for absorption refrigeration system using lithium bromide-water while (0.6-0.82) for (Diethyl Ether –Ethanol).

13. For generator temperature from 65°C to 80°C, the absorption system work efficiently.

## 6.2 Suggestions for Future Work

The following recommendations are suggested for future works:

1-Using new working fluid pair (n-butane–ethanol) and study the performance of the system experimentally.

2-Design and fabrication absorption cooling system uses the bubble pump to circulate the solution from the absorber to the generator.

3-Setup tracking system on the Compound Parabolic Concentrator to increase the range for capture the solar radiation for a long period.

4- Using helical coil as absorber unite in solar collector

5- Studying the use of automatic devices for throttling process, opening and closing process.

6. Studying to improve the performance of solar absorption cooling system by using Nano refrigerant.

# Bibliography

**[1]**- Hassan HZ, Mohamad AA.” A review on solar-powered closed physic-sorption cooling systems”. Renewable and Sustainable Energy Reviews 16: pp.2516–38; 2012.

**[2]**-Lucas T, Raoult-Wack AL. “Immersion chilling and freezing in aqueous refrigerating media: review and future trends: Refrigeration congelation par immersion dans des milieu refrigerants: revue et ten dances futures”. International Journal of Refrigeration 21:419–29; 1998.

**[3**]-Balaras CA, Grossman G, Henning H-M, Infante Ferreira CA, Podesser E, Wang L, et al. “Solar air conditioning in Europe—an overview”. Renewable and Sustainable Energy Reviews 11:pp.299–314; 2007.

**[4]-**Abu Hamdeh NH, Al-Muhtaseb MtA. “Optimization of solar adsorption refrigeration system using experimental and statistical techniques”. Energy Conversion and Management 51:pp.1610–5; 2010.

**[5]-**Afshar O, Saidur R, Hasanuzzaman M, Jameel M. “A review of thermodynamics and heat transfer in solar refrigeration system”. Renewable and Sustainable Energy Reviews 16:pp.5639–48; 2012.

**[6**]- Mirasgedis S, Diakoulaki D, Papagiannakis L, Zervos A. “Impact of social costing on the competitiveness of renewable energies: the case of Crete”. Energy licy 28:pp.65–73; 2000.

**[7].** Wikipedia contributors. "Solar thermal energy", (October). Retrievedfrom http://en.wikipedia.org/w/index.php?title=Solar_thermal_energy&oldid=507809338; (2012)

**[8].** Choudhury B, Chatterjee PK, Sarkar JP. "Review paper on solar-powered air-conditioning through adsorption route". Renewable and Sustainable Energy Reviews; 14:pp.2189–95, 2010.

[9]. Turanjanin V., Bakić, V., Jovanović, M., Pezo, M.: "Fossil fuels substitution by the solar energy utilization for the hot water production in the heating plant Cerak in Belgrade", International Journal of Hydrogen Energy, 34, 7075-7080.ISSN: 0360-3199, 2009.

[10]. Kalkan N, Young EA, Celiktas A. "Solar thermal air conditioning technology reducing the footprint of solar thermal air conditioning". Renewable and Sustainable Energy Reviews; 16:6352–83, 2012.

[11]. Winston R., Minano J.C. and Benitez P. "Non imaging Optics", Elsevier Academic Press, Burlington (2005).

[12]. Mansi G., Sheth, Dr.P.K.Shah. "Design and development of compound parabolic concentrating solar collector with flat plate absorber", International Journal of Innovative Research in Science – Engineering and Technology,Vol.2, Issue 8; (2013)

[13]. Abdulameer D, Hamza, Shahad HAK "Investigation of Solar Powered Intermittent Absorption and Adsorption Refrigeration System".Thesis ;2016

[14].Auda S, Ameer A, Shahad HAK. "Characteristics Review of Optical Concentrators".7(1):168–82; 2017.

[15]. Soteris Kalogirou, "The potential of solar energy in food-industry process heat applications", 25th National Renewable Energy Convention. Warangal, India, 2001.

[16]. David Appleyard, "Chilling out in the sun: solar cooling", Renewable Energy World International Magazine. 13 Issue 3 (2010).

[17].Muhumuza R and Strachan P.master thesis of "Modelling , Implementation and Simulation of a Single-Effect Absorption Chiller in MERIT. 2010.

[18]. Thirugnanasambandam M, IniyanS, GoicR. "A review of solar thermal technologies". Renewable and Sustainable Energy Reviews 14:312–22; 2010.

[19]. Saidur R, MasjukiH, Hasan uzzaman M, Mahlia T, TanC, OoiJ, etal. "Performance investigation of a solar powered thermoelectric refrigerator". International Journal of Mechanical and Materials Engineering, 3:7–16; 2008.

[20]. Dalichaouch M. A "Theoretical and Experimental Investigation of an Absorption Refrigeration System for Application with Solar Energy Units". Ph.D thesis,(July), 1989.

[21]. Srikhirin, P., Aphornratana, S. and Chungpaibulpatana, S. "A review of absorption refrigeration technologies". Renewable & Sustainable Energy Reviews, vol. 5, pp. 343_372. (2001).

[22]. Labus, J., Bruno, J. and Coronas, A. "Review on absorption technology with emphasis on small capacity absorption machines". Thermal Science, vol. 17, no. 3, pp. 739_762. (2013).

[23]. Gosney W B: "Principles of refrigeration", Cambridge University Press, ch 6; 1982

[24]. Marsh, R.W. and Olivo, C.T. "Basics of Refrigeration". Litton Educational Publishing. (1979)

[25]. Electrolux. Electrolux history 1920-1929.Available at: http://group.electrolux.com/en/history-1920-1929-737/;( 2011)

[26]. Grant, T. (Ed.). "International Directory of Company Histories", vol. 53. St.James Press; (2003)

[27]. Einstein, A. and Szilard, L. (1930 November 11). Refrigeration. US Patent1,781,541.Availableat: http://www.google.com/patents/US1781541

[28]. Jordan, R. and Priester, G."Refrigeration and Air Conditioning". Constable and Company. (1949)

[29]. Garland, P.W., DeVault, R.C. and Zaltash, A. "Large commercial absorption chiller development program". Tech. Rep., United States department of energy. (1998)

[30]. King, G. "Modern Refrigeration Practice". McGraw-Hill. (1971)

[31]. Ziegler, F. 'Recent developments and future prospects of sorption heat pump systems". International Journal of Thermal Sciences, vol. 38, pp. 191_208. (1999)

[32]. Dawood Jeggels"Transient simulation of a Lithum bromide-Water Vapour Absorption Refrigeration System" Thesis presented in partial fullment of the requirements for Ms.c. (December); 2015.

[33].Sury R. K., Al Madani K., Ayyash S., "Choice of thermal energy system for solar absorption cooling", Solar Energy, Vol. 32, N°2, pp. 181-187,1984.

[34]. Darkwa J., Fraser S., Cow D.H.C., "Theoretical and practical analysis of an integrated solar hot water-powered absorption cooling system, Energy", vol.39, Issue1, pp. 395-402, 2012.

[35] Florides G. A., Kalogiro S.A., Tassou S. AWrobel., L.C., "Modeling and simulation of an absorption solar cooling system for Cyprus", Solar Energy, Vol. 72, N°1, pp. 43-51 2002.

[36] Gomri R., "Simulation study of the performance of solar/natural gas absorption cooling chillers" ,Energy Conversion and Management, Vol.65, pp-675-681, 2013.

[37]. R Lazzarin, E Rizzon, M Sourano, B Boldrin, G Scalabrin : "Performance predictions of a lithium bromide utilizing solar energy", Sun, proceedings of **the international solar energy congress, New** Delhi, India, January.Vol 3, p 1572-1580 Pergamon. 1978.

[38]. ASHRAE handbook and product directory, "Fundamentals volume".1977

[39]. W. F Stoecker and J.W Jones: "Refrigeration and air conditioning ", 2nd edition, Mc Craw-Hill Book company, ch 7, 12, 17. 1982

[40]. J L Threlkeld: "Thermal environmental engineering, 2nd edition Prentice-Hall, Inc, and pp 103-115. 1970

[41]. D Van Hatten and P Actis Dato: "Description and performance of an active solar cooling system using a lithium bromide-water absorption machine", Energy and *Buildings,* vol 3, pp 169-196. 1981.

[42]. R H Perry and CH Chilton: "Chemical engineer's Handbook", 5th edition,Mc Craw-Hill Book cie, 1973, ch 12.

[43]. L M Rozenfeld and M S Karnaukh : "Analysis of actual processes in a lithium bromide absorption machine", Proceedings of the 11th International Congress of Refrigeration , Munich.P 653-657.

[44]. L A Mc Neely: "Thermodynamic properties of aqueous solutions of lithium bromide", *ASHRAE Transactions,* part 1, p 413-434. 1979

[45]. N G Schmuilov and L M Rozenfeld: "Typical features of the design and optimization of *LiB,.* absorption refrigerating machines", *Chem Pet Eng* vol 19 n 11-12 Nov-Dec 1983 p 514-519 Plenum Publishing corporation, pp. 514-518. 1984

[46]. S B Gosh and G P Gupta: "Design of a solar energy operated LiBr-water absorption refrigeration system for refrigeration storage", *Sun,*

*proceedings of the international solar* energy *congress,* New Delhi, India. Vol 3 January 1978 pp. 1997-2000.

[47]. V Y Nakoryakov and N I Girgor'yeva: "Combined heat and mass transfer in film absorption", *Heat Transfer-Soviet Research,* vol 12 n 3 pp. 111-117. 1980

[48]. V Y Nakoryakov, N S Bufetov, N I Grigor'yeva : "Heat and mass transfer in film absorption", *Fluid Mechanics-Soviet Research,* vol 11 n 3 May-June pp. 97-115. 1982

[49]. R Chang, J A Duffie and G 0 G LOF: "A study of a solar air conditioner", *Mech Eng,* n 85 pp31. 1963

[50]. N R Sheridan: "Performance of the Brisbane solar house", it Solar energy, n 12 p 395. 1952

[51]. C F Kettleborough: "Solar-assisted comfort conditioning", *Mech Eng,* vol 105 n 12 Dec pp 48-55. 1983

[52]. W C Dickinson and P N Cheremisinoff, editors : "Solar energy technology handbook", part B Applications, Systems Design, and Economics Marcel Dekker, Inc. ch 30, 42. 1980

[53]. J C V Chinnappa : "Utilization of solar energy for space cooling : a review",*Int solar building Technology conference,* Royal Institute of British Architects, 25th-29th July, , London. 1977

[54]. - S A Klein, P I Cooper, T L Freeman, D M Beeckman, W A Beckman, J A Duffle: TRNSYS: "A transient simulation program", *Solar* energy, vol 17 pp 29. 1975

[55]. C .B Winn, G. R Johnson, T .E Corder : SIMSHAC : "A Simulation programme for solar heating and cooling of buildings", *Journal of simulation* ,n 165 1976.

[56]. Holm stead Solsem and Martine Marietta "Interactive thermal analysis system-user manual", Engin. Dept technical manual, Martin Marietta corp., Denver, 1976.

[57]. "An introduction to SOLCOST", ERDA, Division of solar energy technology transfer, Washington DC, June 1977.

[58]. S .A. Klein and W. A Beckman: "A general design method for closed-loop solar energy systems", *Sol energy* vol 22 p 269-282. 1979

[59]. J .A Duffle and W.A Beckman: "Solar engineering of thermal processes", Wiley interscience, 1980.

[60]. M. M .El Sayed, I .S Taha, M .A Darwish : "Computer simulation of solar cooling", Fundamentals and application of solar energy, AIChE Symposium series, part 2 n 210 vol 77 pp. 86-96. Ch 2.33. D .C. 1981 Anand, R. W Allen, B Kumar: "Transient simulation of absorption machines", J sol energy engin, vol 104 August pp.197-203. 1982

[61]. D K Anand et al. : "Second law analysis of solar powered absorption cooling cycles and systems", *J sol* energy engin , vol 106 p291-298. August 1984

[62]. Wilbur, P.J., and Mitchell, C.E., “Solar absorption air conditioning alternatives”, Solar Energy, vol. 17, no. 3, pp. 193-199, 1975.

[63]. Li, Z.F., and Sumathy, K., “Simulation of a solar absorption air conditioning system”, Energy Conversion and Management, vol. 42, no. 3, pp. 313-327, 2001.

[64]. Li, Z.F., and Sumathy, K., “Experimental studies on a solar powered air conditioning system with partitioned hot water storage tank”, Solar Energy, vol. 71, no. 5, pp. 285-297, 2001.

[65]. Florides, G.A., Kalogirou, S.A., Tassou, S.A., and Wrobel, L.C., "Modelling and simulation of an absorption solar cooling system for Cyprus", Solar Energy, vol. 72, no. 1, pp. 43-51, 2002.

[66] .Atmaca, I., and Yigit, A., "Simulation of solar-powered absorption cooling system", Renewable Energy, vol. 28, no. 8, pp.1277-1293, 2003.

[67]. Florides, G.A., Kalogirou, S.A., Tassou, S.A., and Wrobel, L.C., "Design and construction of LiBr-water absorption machine", Energy Conversion & Management, vol. 44, no. 15, pp. 2483-2508, 2003.

[68]. Assilzadeh, F., Kalogirou, S.A., Ali, Y., and Sopian, K., "Simulation and optimization of a LiBr solar absorption cooling system with evacuated tube collectors", Renewable Energy, vol. 30, no. 8, pp. 1143-1159, 2005.

[69]. Mittal, V., Kasana, K.S., and Thakur, N.S., "Performance evaluation of solar absorption cooling system of Bahal (Hatyana)", Journal of the Indian Institute of Science, vol. 85, pp. 295-305, 2005.

[70]. Sayegh, M.A., "The solar contribution to air conditioning systems for residential buildings", Desalination, vol. 209, vol. 1-3, pp. 171-176, 2007.

[71]. Balghouthi, M., Chahbani, M.H., and Guizani, A., "Feasibility of solar absorption air condition in Tunisia", Building and Environment, vol. 43, no. 9, pp. 1459- 1470, 72. 2008.

[72]. Mateus, T., and Oliveira, A.C., "Energy and economic analysis of an integrated solar absorption cooling and heating system in different building types and climates", Applied Energy, vol. 86, no. 6, pp. 949-957, 2009.

[73]. Herold, K.E., Radermacher, R. and Klein, S.A. "Absorption Chillers and Heat Pumps". CRC Press. (1996).

[74]. Agrawal, A. and Hindin, B. "Corrosion inhibition of ammonia water absorption chillers". US Patent 5,342,578.Available at:

http://www.google.com/patents/US5342578; (1994 August 30)

[75]. Mansfeld, F. and Sun, Z. "Corrosion protection of steel in ammonia/water heat pumps". US Patent 6,632,294.Available at

http://www.google.com/patents/US6632294; (2003 October 14)

[76]. Kulankara, S. and Herold, K.E. "Theory of heat and mass transfer additives in absorption chillers". HVAC&R Research, vol. 6, pp. 369_380. (2000)

[77]. Möller, R. and Knoche, K. "Surfactants with NH3_H2O. International Journal of Refrigeration", vol. 19, no. 5, pp. 317_ 321. (1996).

[78]. Wang, X. and Chua, H.T. "bsorption cooling-a review of lithium bromide water cooling technologies". Recent Patents on Mechanical Engineering, vol. 2, pp.193_213. (2009).

[79]. Wang, K., Abdelaziz, O., Kisari, P. and Vineyard, E.A. State-of-the-art review on crystallization control technologies for water/LiBr absorption heat pumps. International Journal of Refrigeration, vol. 34, pp. 1325_1337, (2011).

[80]. Grossman, G. and Zaltash, A. "ABSIM-modular simulation of advanced absorption systems. International Journal of Refrigeration", vol. 24, pp. 531_543. (2001).

[81]. Somers, C., Mortazavi, A., Hwang, Y., Radermacher, R., Rodgers, P. and Al-Hashimi, S. "Modeling water/lithium bromide absorption

chillers in aspen plus". Applied Energy, ,vol.88, pp.4197-4205. (2011).

[82]. Bakhtiari, B., Fradette, L., Legros, R. and Paris, J. "A model for analysis and design of h2o-libr absorption heat pumps". Energy Conversion and Management,vol. 52, pp. 1439_1448. (2011).

[83]. Kohlenbach, P. and Ziegler, F."A dynamic simulation model for transient absorption chiller performance". Part I: The model. International Journal of Re- frigeration, (2008), vol. 31, pp. 217_225.

[84]. Kim, B. and Park, J. "Dynamic simulation of a single-effect ammonia-water absorption chiller". International Journal of Refrigeration, , vol. 30, pp. 535_545. (2007).

[85]. Agyenim, F., Knight, I. and Rhodes, M. "Design and experimental testing of the performance of an outdoor LiBr-$H_2O$ solar thermal absorption cooling system with a cold store". Solar Energy,vol. 84, pp. 735_744. (2010).

[86]. Kalogirou, S., Florides, G., Tassou, S. and Wrobel, L. "Design and construction of a lithium bromide water absorption refrigerator". In:,Clima 2000. (2001)

[87]. Winston R., "Principles of Solar Concentrators of a Novel Design", *Solar Energy*, 16, pp. 89-95. (1974)

[88]. A. Rabl. "Optical and thermal properties of compound parabolic concentrators". *Solar Energy*, 18:497–511, 1976.

[89]. Fujita, I. and Hihara, E."Heat and mass transfer coefficients of falling film absorption process". International Journal of Heat and Mass Transfer,vol. 48, pp.2779_2789. (2005).

[90]- A .J Chapman : "Heat transfer", 3rd edition, Mc Millan publishing co,Inc ch 8, 12. 1974

[91]- J. J Lorenz and D Yung : "A note on combined boiling and evaporation of liquid films on horizontal tubes", *J heat tran.,fer,* vol 101 p178-180. Feb 1979

[92]-J.P.Holman,"Heat Transfer",4th edition,McGraw hill Kogakusha,1976.

[93]- Sahoo. K. C, Das. S. N "Theoretical Design of adiabatic capillary tube of a domestic refrigerator using refrigerant R-600a" American Journal of Engineering Research (AJER) e-ISSN : 2320-0847 p-ISSN : 2320-0936 Volume-03, Issue-05,306-314 www.ajer.org,2014.

[94]-Asim M. "Simulation of Solar Powered Absorption Cooling System for Buildings in Pakistan".Thesis; 2016.

[95]. H. P. Gary and J. Prakash "Solar Energy Fundamentals and Applications", New Delhi, www.Tata McGraw-Hill. Com, 2005.

[96]. Norton B, Eames PC, Yadav YP and Griffiths PW, "Inverted Absorber solar Concentrators for Rural Applications". Ambient Energy, Vol. 18, No. 3, pp 115-120, 1997.

[97]. N De Nevers and J Seader: "Lost work: A measure of thermodynamic efficiency", *Energy,* Pergamon Press Ltd vol 5, pp. 757-768. 1980.

[98]- Mehrabian,M.A.,and Shahbeik,A.E.,"thermodynamic modeling of a single-effect LiBr-$H_2O$ absorption refrigeration cycle",Proc. MechE Part E,Vol.219,pp.261-273,2004

# Appendix (A)

## Vapor Compression Vs Vapor Absorption

Introducing the concept of refrigeration through vapor absorption can be approached by examining a basic representation of a generalized refrigeration cycle as shown in Figure A.1. This refrigeration cycle provides for refrigeration through the evaporation of a low temperature liquid refrigerant. The condition of the evaporated refrigerant has to be elevated in pressure and temperature to the high pressure portion of the cycle. Once at a higher pressure it is now possible to condense the refrigerant by exposing it to a temperature that is lower than the high pressure vapor, but higher than the evaporator temperature. The liquid refrigerant can then return to the evaporator through a throttling device and the cycle can repeat itself. The relevance of this example is that the encompassing principles of the more commonly known vapor compression cycle and the vapor absorption cycle both make use of this generalized component configuration. However, what defines the difference between these two technologies is the manner in which the condition of the refrigerant vapor is raised from the low pressure evaporator section to the high pressure condenser section. Figure A.2 shows the fundamental components that these two different methods require to facilitate the process that will raise the pressure and temperature of a stream of refrigerant vapor. In the case of the vapor compression process, Figure A.2a, an electrical motor is used to drive a compressor. This compressor mechanically raises the pressure and temperature of the evaporated refrigerant to a higher state where it is suitable for condensation. In contrast

to this, the driving energy that powers the vapor absorption components, Figure A.2b, is a source of heat and while this thermal energy can be

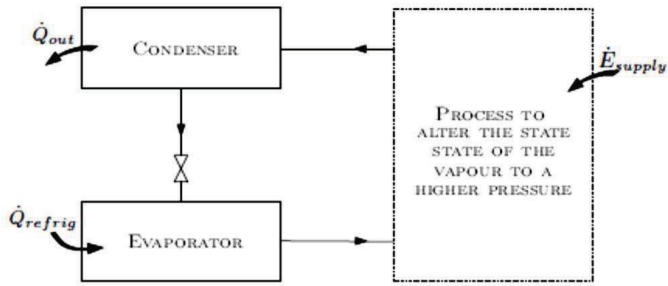


Figure A.1: Generalized refrigeration cycle

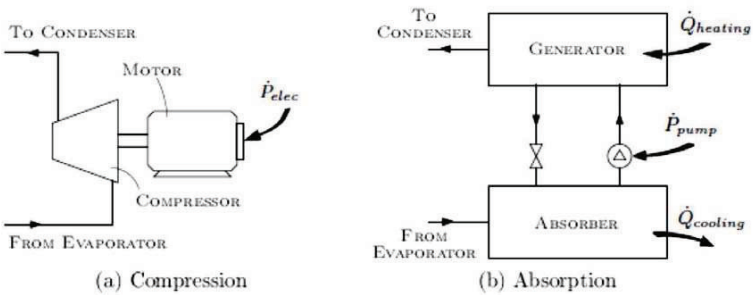


Figure A.2: Comparison of components used for the conditioning of refrigerant vapor through a compression and absorption process

supplied through electrical heaters there is a wide variety of possible sources for heat that can used to fuel the vapor absorption components. Emphasis has been placed on the thermal energy used to drive the vapor absorption components, but the vapor absorption components require additional external interfaces in order to operate. These two external interfaces are the cooling required in the absorber component, at a similar temperature to that used in the condenser component, and the electrical energy requirement of a small pump.

This pump is referred to as being small due to the relative energy requirements of the generator and condenser when compared with the pumping requirements. A more detailed explanation into the operation of a vapor absorption cycle will be discussed in the remainder of this chapter.

# Appendix (B)
# The Published Papers

1- The paper entitled" **Characteristics Review of Optical concentrators** "published in International Journal of Current Engineering and Technology

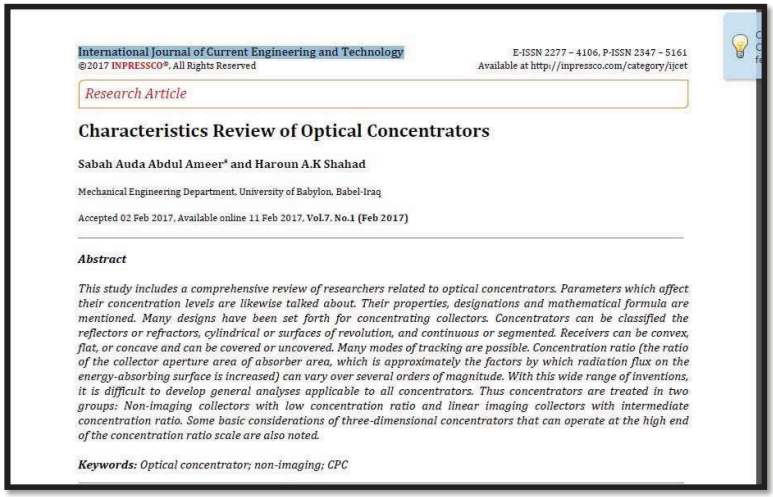

International Journal of Current Engineering and Technology
©2017 INPRESSCO®, All Rights Reserved

E-ISSN 2277 – 4106, P-ISSN 2347 – 5161
Available at http://inpressco.com/category/ijcet

*Research Article*

## Characteristics Review of Optical Concentrators

**Sabah Auda Abdul Ameer[a] and Haroun A.K Shahad**

Mechanical Engineering Department, University of Babylon, Babel-Iraq

Accepted 02 Feb 2017, Available online 11 Feb 2017, **Vol.7, No.1 (Feb 2017)**

***Abstract***

*This study includes a comprehensive review of researchers related to optical concentrators. Parameters which affect their concentration levels are likewise talked about. Their properties, designations and mathematical formula are mentioned. Many designs have been set forth for concentrating collectors. Concentrators can be classified the reflectors or refractors, cylindrical or surfaces of revolution, and continuous or segmented. Receivers can be convex, flat, or concave and can be covered or uncovered. Many modes of tracking are possible. Concentration ratio (the ratio of the collector aperture area of absorber area, which is approximately the factors by which radiation flux on the energy-absorbing surface is increased) can vary over several orders of magnitude. With this wide range of inventions, it is difficult to develop general analyses applicable to all concentrators. Thus concentrators are treated in two groups: Non-imaging collectors with low concentration ratio and linear imaging collectors with intermediate concentration ratio. Some basic considerations of three-dimensional concentrators that can operate at the high end of the concentration ratio scale are also noted.*

***Keywords:*** *Optical concentrator; non-imaging; CPC*

2- The paper entitled" **State of the Art of Solar Absorption Cooling Technologies** "published in International Journal for Research in Applied Science & Engineering

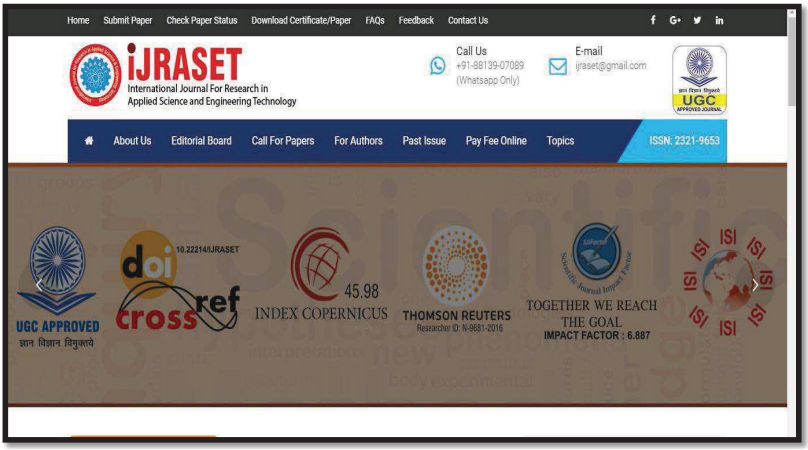


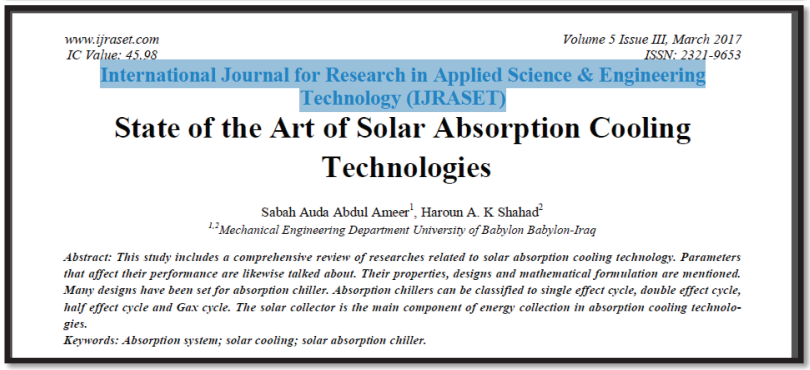

www.ijraset.com
IC Value: 45.98

Volume 5 Issue III, March 2017
ISSN: 2321-9653

International Journal for Research in Applied Science & Engineering Technology (IJRASET)

# State of the Art of Solar Absorption Cooling Technologies

Sabah Auda Abdul Ameer[1], Haroun A. K Shahad[2]
[1,2]Mechanical Engineering Department University of Babylon Babylon-Iraq

***Abstract:*** *This study includes a comprehensive review of researches related to solar absorption cooling technology. Parameters that affect their performance are likewise talked about. Their properties, designs and mathematical formulation are mentioned. Many designs have been set for absorption chiller. Absorption chillers can be classified to single effect cycle, double effect cycle, half effect cycle and Gax cycle. The solar collector is the main component of energy collection in absorption cooling technologies.*

***Keywords:*** *Absorption system; solar cooling; solar absorption chiller.*

3-The paper entitled" **Design and Fabrication of Two Dimension Compound Parabolic Concentrator for Iraqi Climate** "published in International Journal for Research in Applied Science & Engineering


*www.ijraset.com* *Volume 5 Issue V, May 2017*
*IC Value: 45.98* *ISSN: 2321-9653*
**International Journal for Research in Applied Science & Engineering Technology (IJRASET)**

# Design and Fabrication of Two Dimension Compound Parabolic Concentrator for Iraqi Climate

Sabah Auda Abdul Ameer[1], Haroun A. K Shahad[2]
[1,2]*Mechanical Engineering Department, University of Babylon, Babylon-Iraq*

***Abstract:*** *The collectors are employed, when the temperature prerequisite is more than 100°C. In this work a two-dimension compound parabolic concentrator solar collector constructed of mild steel sheet with serpentine copper tube fixed on a flat plate absorber, has been designed for Iraqi climate. This compound parabolic concentrator consists of two stainless-steel parabolas. The concentrator is closed from the top and sides with 4mm glass sheets. The two parabolas are truncated at the top to reduce the apparatus height and the effect of shading. This two dimensional compound parabolic concentrator is designed to have a concentration ratio of 5. The serpentine copper tube is fixed on flat mild steel absorber plate. The copper tube and flat plate are black coated. The collector is tested in Iraqi weather during the months of August, September and October. Initial results show that the maximum absorber temperature is recorded in August which 120 °C with a reflector temperature of 69 °C and aperture cover glass temperature 43°C.*
***Keywords:*** *Two Dimension, Compound Parabolic Concentrator, Non-Imaging Collector, Serpentine Absorber.*

## I. INTRODUCTION

The collectors are classified as either reflectors or refractors. In the present work the reflector type is used which is a compound parabolic concentrator (CPC). Concentrating collectors can increase the solar radiation intensity to about 10000 folds [1]. The

4-The paper entitled" **Analysis of the Experimental and Theoretical Performance of the Non-Imaging Compound Parabolic Solar Collector".** "published in Indian journal of Science & Technology

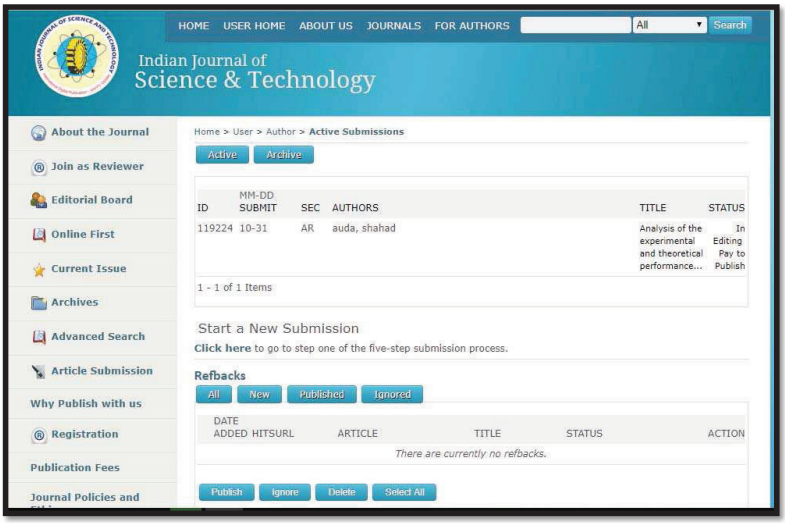


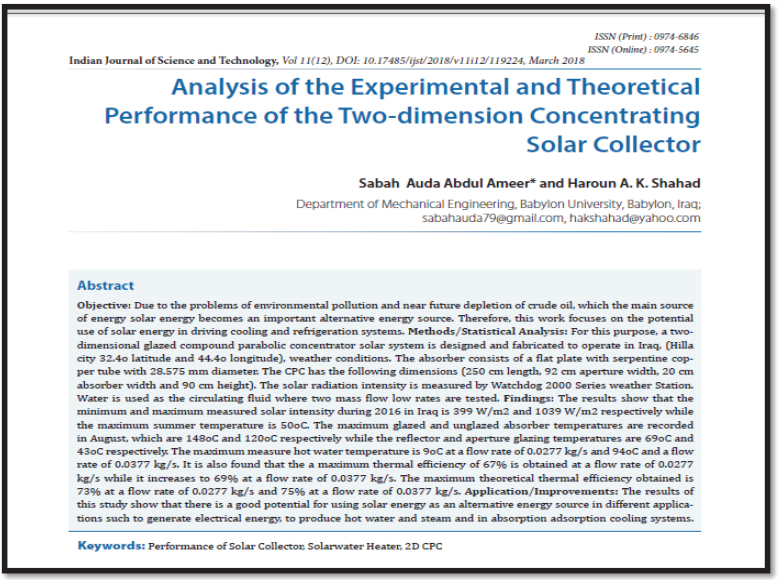

# الخلاصة

تم إجراء دراسة شاملة بما في ذلك التصميم والبناء والاختبار مع النمذجة والتحقيقات النظرية لنظام التبريد الامتصاصي ذات التدفق المستمر بالطاقة الشمسية. تم اختبار النظام التجريبي تحت ظروف الطقس العراقية في محافظة بابل عند 33.4° خط عرض و 44.4° خط طول.

ويتكون النظام من مجمع الطاقة الشمسية ذات قطع مكافئ (CPC)، وحدة المولد، وحدة المكثف، وحدة الامتصاص، وحدة المبخر، خزان للخزن، ومجموعة من المضخات. وقد تم حساب كمية الإشعاع الشمسي المباشر والإشعاع الشمسي المنتشر والإشعاع الشمسي الكلي على سطح ثابت مائل خلال العام ومقارنته بقياسات مقياس البيرانومتر.

وبلغت القيمة القصوى المحسوبة للإشعاع الشمسي المباشر الطبيعي( 944-894) واط / متر مربع في موسم الصيف في الساعة 12:00 ظهرا وكان القياس الشمسي العالمي لقياس البيرانومتر 1031 واط / متر مربع. تم حساب الزوايا الشمسية مثل زاوية الارتفاع وزاوية السمت الشمس وزاوية الذروة. وكانت زاوية الارتفاع القصوى 80.99° في 21 يونيو في الساعة 12:00 مساء و 34.1° في 21 ديسمبر في الساعة 12:00 مساء.و قيمة زاوية السمت الشمسية (درجة من الشمال) ما بين 76.285° في 7:00 صباحا و 282.75° في 17:00مساءا في 21 يونيو، في حين أن زاوية السمت في ديسمبر يبدأ عند 117.5° في 7:00 صباحا وينتهي 242.3° في 17:00 مساءا.

يجب أن تأخذ زاوية السقوط القيمة المثلى لأقصى قدر من الإشعاع التي يمكن الحصول عليها من الإشعاع الشمسي العادي المباشر. ويجب أن يكون مقدار زاوية السقوط صغيرا بما فيه الكفاية لجعل قيم زاوية السقوط جيب التمام كافية بدرجة كافية لمزيد من حالات الإشعاع على سطح الاستقبال. قيمة زاوية السقوط الشمسية هي 24.1° - 32° في 21 أبريل ومايو ويونيو ويوليو وأغسطس من 12:00 مساء، في حين أنه هو 42° - 67.35°في 21 سبتمبر، أكتوبر تشرين الثاني، ديسمبر ، يناير، فبراير، ومارس. أدت الزيادة في زاوية السقوط الشمسية إلى زيادة في خسائر الإشعاع الشمسي بسبب انخفاض جيب التمام لزاوية الحادث. و يتكون (CPC) من لوحة امتصاص الاشعاع (0.2 * 2.5)مترمربع و مساحة فتحة الدخول (0.9 * 2.5) متر مربع. والمرآة (العاكس) ل(CPC) مصنوعة من الفولاذ المقاوم للصدأ لتعكس الإشعاع الشمسي على وحدة الامتصاص. يتم تثبيت أنبوب النحاس الملتوي على لوحة الامتصاص والمغلفة مع الطلاء الأسود الانتقائي. وتسجل درجة الحرارة القصوى للمستقبل في آب والتي تبلغ 148 درجه مئويه و 120

درجه مئويه مع أو بدون تزجيج المجمع الشمسي بينما تكون درجة حرارة العاكس 69 درجه مئويه وتكون درجة حرارة زجاج الفتحة 43 درجه مئويه .

وأظهرت النتائج التجريبية أن الحد الأقصى للكفاءة الحرارية عند الساعة 12:00 ظهرا عند الساعة 21 من كل شهر من (0.67-0.48) عندما يكون معدل التدفق 0.0277 كغم / ثانية في حين أن الكفاءة الحرارية تصبح (0.69-0.5) عندما يكون معدل تدفق الكتلة من الماء 0.0377 كغم / ثانية. و درجة حرارة الماء الساخن في معدل التدفق الشامل 0.0277كغم/ثا هو 98 درجه مئويه بينما في معدل التدفق الشامل 0.0377كغم/ثا هو 94 درجه مئويه. تم تصميم واختبار النموذج النظري للمجمع الشمسي تحت ظروف الطقس نفسها. يتم الحصول على الكفاءة الحرارية للمجمع الشمسي بواسطه برنامج الماتلاب 2017. الكفاءة الحرارية (0.73-0.67) في معدل التدفق الكلي (0.0277 كغم /ثا) مع نسبه التركيز 4.5 في 12:00 م في 21 من كل شهر. يتم اختبار اثنين من نوعين من السوائل العاملة وهي ليثيوم بروميد- ماء و ديثيل الأثير - الإيثانول. يتم شحن النظام بـ 16 لتر محلول بروميد الليثيوم مع تركيز 50٪ في الجزء الأول من البرنامج التجريبي. في الجزء الثاني من البرنامج يتم شحن النظام مع 16 لتر من ديثيل الأثير-الإيثانول مع تركيزات مختلفة (40٪، 50٪، و 60٪). درجات الحرارة المقاسة للمولد هي 98 درجه مئويه ، درجه مئويه 70لـ الماء-بروميد الليثيوم وأنظمة امتصاص ديثيل الأثير- الإيثانول على التوالي في موسم الصيف.

إن الضغط المقاس (العالي والمنخفض) لنظام الامتصاص ل (ليثيوم بروميد-الماء و ديثيل الأثير-إيثانول) هو (7 كيلو باسكال و 1.45 كيلو باسكال) و (300 كيلو باسكال و 37.5 كيلو باسكال) على التوالي. إن الضغط المتنبأ (العالي والمنخفض) لنظام الامتصاص ل (ليثيوم بروميد-الماء و ديثيل الأثير الإيثانول) هو (7.54 كيلو باسكال و 0.72 كيلو باسكال) و (347 كيلو باسكال و 29.8 كيلو باسكال) على التوالي.

تم قياس درجة الحرارة (العالية والمنخفضة) لنظام الامتصاص ل (بروميد الليثيوم و ديثيل الأثير الإيثانول) (92 درجة مئوية و 67 درجة مئوية) على التوالي، ويقاس معامل أداء نظام الامتصاص نظريا وتجريبيا لنوعين من السوائل العامله في تركيزات حل مختلفة. يتم تحليل نموذج الحالة الثابتة والنموذج الديناميكي باستخدام الربط بين برنامج Matlab2017 وبرنامج EES. توازن الطاقة والكتلة التي تحققت على نظام الامتصاص للتنبؤ ببعض المعلمات مثل درجة الحرارة والضغط ,(ECOP ) و (COP) لمقارنتها مع الجانب المقاس. وقد حققت نتائج النموذج التجريبية لدرجات الحرارة والضغط وكذلك معامل الأداء.

**الجمهورية العراقية**
**وزارة التعليم العالي و البحث العلمي**
**جامعة بابل/كلية الهندسة**
**قسم الهندسة الميكانيكية**

# دراسة عملية ونظرية لمنظومة تبريد امتصاصية مدمجة بمجمع شمسي مركز

أطروحه مقدمة الى قسم الهندسة الميكانيكة-كليه الهندسة -جامعة بابل
كجزء من متطلبات نيل درجة دكتوراه فلسفة في الهندسة الميكانيكية
هندسة القدرة)

**من قبل**
**صباح عودة عبد الأمير**
**ماجستير هندسة ميكانيكية، 2007**

**باشراف**
**الاستاذ الدكتور هارون عبد الكاظم شهد**

1439 هـ 2018 م